# Development of Nanoparticle Based Nicotine Vaccines for Smoking Cessation

Yun Hu

Dissertation submitted to the faculty of Virginia Polytechnic Institute and State University in partial fulfillment of the requirements for the degree of

Doctor of Philosophy

In

Biological Systems Engineering

Chenming Zhang, Chair

Marion F. Ehrich

Xiang-Jin Meng

Ryan S. Senger

April 29th, 2015

Blacksburg, VA

Keywords: nicotine vaccine, nanoparticle, smoking cessation, liposome, humoral response

# Development of Nanoparticle Based Nicotine Vaccines for Smoking Cessation

Yun Hu

## Abstract

Cigarette smoking is prevalent worldwide and has consistently been the top preventable cause of many serious diseases. In recent years, nicotine vaccines that can induce production of nicotine specific antibodies in human have emerged as a promising medicine to treat tobacco addiction. However, traditional nicotine vaccine designs have many disadvantages, including low immunogenicity, low specificity, and short immune response persistence. To overcome the above limitations, in this study, various nanoparticle-based vaccine delivery systems have been developed and evaluated as potential delivery vehicles for vaccines against nicotine addiction.

Firstly, a nicotine vaccine was synthesized by conjugating bovine serum albumin (BSA)-nicotine complex to the surface of nano-sized cationic liposome. Significantly higher anti-nicotine antibody titer was achieved in mice by liposome delivered nicotine vaccine compared with nicotine-BSA vaccine.

Secondly, a novel nanoparticle (NP)-based delivery platform was constructed by incorporating a negatively charged nanohorn into cationic liposome. Marked improvement in stability *in vitro* and significant increase in titer of anti-nicotine antibodies were detected in nanohorn supported liposome (NsL) delivered vaccine than liposome delivered vaccine.

Thirdly, lipid- poly(lactic-co-glycolic acid) (PLGA) hybrid NPs were constructed as vaccine delivery system. Preliminary results showed that PLGA-lipid hybrid NPs exhibited improved stability, better controlled release of antigens, as well as enhanced uptake by dendritic cell (DC). A lipid-PLGA hybrid NP was also developed that was structurally responsive to low pH challenge. The lipid shell of the hybrid

nanoparticle was rapidly disintegrated under a low pH challenge, which resembles the acidic environment of endosomes in DCs.

In the final study, hybrid NPs with various cholesterol concentrations were constructed. Slower and more controlled release of antigens in both human serum and phosphate buffered saline were detected in nanoparticles with higher cholesterol content. However, nanoparticles containing higher cholesterol showed poorer stability due to increase fusion among NPs. It was later found that PEGylation of NPs can effectively minimize fusion caused size increase after long term storage, leading to improved cellular uptake.

The findings from this study on the nanohorn-lipids based nicotine vaccine as well as lipid-PLGA hybrid NPs may provide solid basis for future development of lipid-PLGA based nicotine vaccine.

## Dedication

I dedicate this dissertation to my parents: Zongyu Duan and Deyou Hu.

## Acknowledgements

I would like to give my greatest thanks to my advisor, Dr. Chenming Zhang, for the generous support and on all my research work, for his insightful and innovative ideas on nicotine vaccine development, for his excellent role as a life guide, and for the forever smile on his face.

I am grateful for my committee members, Dr. X.J. Meng, Dr. Marion Ehrich, and Dr. Ryan S. Senger for their kind guidance and support.

I enjoyed all the days working with my colleagues, Dr. Jianzhong Hu, Dr. Somayesadat Badieyan, Dr. Wei Huang, Dr. Hong Zheng, Ambika M.V. Murthy, Zongmin Zhao, Frank Gillam, Reece Hoerle, Meaghan Devine, Nolan Shen, Heather Harshbarger, Nathan Harms. I am thankful for the help provided by Dr. Mary Leigh Wolfe, Cora Chen, Amy Egan, Teresa Cox, Susan Rosebrough, Barbara Wills, Denton Yoder and Ling Li.

I am grateful for all the assistances kindly provided by Deborah Kelly, Kathy Lowe on transmission electron microscope, Dr. Justin Barone and David Roth on FTIR, Melissa Makris on flow cytometer, Fuhrman Kristel on mammalian cell culture, and Dr. Kristi DeCourcy on confocal microscope.

I also thank for the generous funding support from National Institute on Drug Abuse (R21 DA030083 and UO1DA036850).

## Declaration of work performed

I declare that the work in Chapter III and Chapter IV was contributed equally by Dr. Hong Zheng and Yun Hu. Work in other chapters was primarily performed by Yun Hu. Dr. Mike Zhang supervised all the work, participated in experiment design, coordinated the experiments, and conducted manuscript revision. Dr. Marion Ehrich participated in experimental design, and conducted manuscript revision. Dr. Harry Dorn from department of chemistry at Virginia Tech kindly provided nanohorn for construction of nanohorn supported liposome. Dr. Paul Pentel and Dr. Sabina de Villiers from Minneapolis Medical Research Foundation tested nicotine antibody affinity in Chapter IV. Melissa R. Makris from College of Veterinary Medicine at Virginia Tech performed the flow cytometry analysis. Fuhrman Kristel from Veterinary Medicine Experiment Station at Virginia Tech assisted doing part of the dendritic cell related studies. Dr. Kristi DeCourcy from Fralin Life Science Institute at Virginia tech provided assistance on confocal microscopy. Kathy Lowe from College of Veterinary Medicine at Virginia Tech provided assistance on acquiring TEM images. Dr. Justin Barone and David Roth from department of biological systems engineering helped analyze FTIR spectrum of nanoparticles.

# TABLE OF CONTENTS

## List of Figures

**CHAPTER III**



**CHAPTER IV**



**CHAPTER V**

**CHAPTER VI**



**CHAPTER VII**

## List of Tables

**CHAPTER III**



**CHAPTER IV**



**CHAPTER V**



**CHAPTER VI**

## List of Abbreviations

- 3’-AmNic: 3’-aminomethylnicotine
- AAV: adeno-associated virus
- AE: association efficiency
- APC: antigen presenting cell
- BSA: bovine serum albumin
- CHEMS: cholesteryl hemisuccinate
- CpG ODN: CpG oligodeoxynucleotide
- DC: dendritic cell
- DCM: dichloromethane
- DLS: dynamic light scattering
- DOC: deoxycholate
- DOPC: 1,2-dioleoyl-sn-glycero-3-phosphocholine
- DOPE: 1,2-dioleoyl-sn-glycero-3-phosphoethanolamine
- DOTAP: 1,2-dioleoyl-3-trimethylammonium-propane (chloride salt)
- DPM: disintegrations per minute
- DSPE-PEG(2000)-maleimide: 1,2-distearoyl-sn-glycero-3-phosphoethanolamine-N-[maleimide(polyethylene glycol)-2000] (ammonium salt)

- DSPE-PEG2000-amine: 1,2-distearoyl-sn-glycero-3-phosphoethanolamine-N-[amino(polyethylene glycol)-2000] (ammonium salt)
- EDC: 1-ethyl-3-[3-dimethylaminopropyl] carbodiimide
- ELISA: enzyme-linked immunosorbent assay
- FBS: fetal bovine serum
- FITC: fluorescein isothiocyanate isomer I
- FTIR: fourier transform infrared
- GM-CSF: granulocyte macrophage colony-stimulating factor
- HE: hematoxylin-eosin
- KLH: keyhole limpet hemocyanin
- LC: loading capacity
- LPK: liposome-PLGA-KLH
- LSM: laser scanning microscope
- MDR: multidrug resistance
- MEM: minimum essential medium
- MPLA: monophosphoryl Lipid A
- MSPC: 1-myristoyl-2-stearoyl-sn-glycero-3-phosphocholine
- nAChRs: nicotinic acetylcholine receptors

- NBD PE: 1,2-diphytanoyl-sn-glycero-3-phosphoethanolamine-N-(7-nitro-2-1,3-benzoxadiazol-4-yl) (ammonium salt)
- NBD: nitro-2-1,3-benzoxadiazole
- NBL: Nic-BSA-Liposome
- Nic: rac-trans 3'-hydroxymethylnicotine hemisuccinate
- NicAb: nicotine-specific IgG antibody
- Nic-BSA: nicotine-BSA conjugate
- Nic-BSA-LIP: liposome-based anti-nicotine vaccine
- Nic-BSA-NsL: Nanohorn-supported liposome-based anti-nicotine vaccine
- NP: nanoparticle
- NRT: nicotine replacement therapy
- NsL: nanohorn supported liposome
- NTP: National Toxicology Program
- PBMC: peripheral blood mononuclear cell
- PBS: phosphate buffered saline
- PCS: photon correlation spectroscopy
- PEG: polyethylene glycol
- PK: PLGA-KLH

- PLGA: poly(lactic-co-glycolic acid)
- pMHC: peptide-MHC
- PVA: poly(vinyl alcohol)
- rEPA: recombinant Pseudomonas aeruginosa exoprotein A
- RES: reticulo-endothelial system
- Rhod B: Rhodamine B isothiocyanate
- SD: standard deviation
- SDS: sodium dodecyl sulfate
- SEC: siebe environmental control
- SWNH: single-walled nanohorn
- TCA: trichloroacetic acid
- TEM: transmission electron microscope
- TLR: Toll like receptor
- TMB: tetramethylbenzidine
- TNBS: 2,4,6-trinitrobenzene-1-sulfonic acid
- TT: tetanus toxoid

VLP: virus-like particle

## Chapter I: Introduction

Cigarette smoking has been a leading preventable cause of many fatal diseases in the past decades, resulting in loss of more than 400,000 lives and about two hundred billion dollars in the United States each year. [1] Almost every smoker once has attempted or now is trying to quit smoking, but unfortunately, the overall success rate is less than 3% without medical treatment. [2] As the major addictive component in tobacco, nicotine can be transported to brain during smoking and can enhance dopamine release, providing euphoric feeling to smokers. Abstinence from nicotine can cause various withdrawal symptoms, including craving for tobacco, irritability, anxiety, difficulty in concentrating, and restlessness. All of these compromise attempts for quitting smoking. [3] Therefore, it is urgent to provide effective medications to alleviate such symptoms and increase the success rate of smoking cessation. Currently, numerous pharmacological medications for smoking cessation, including six types of nicotine replacement therapies (NRTs), bupropion, and varenicline are available on market to smokers. [4] These pharmacological interventions work in different ways, including substituting nicotine from cigarette with artificial nicotine sources, minimizing nicotine withdrawal-caused depression, and blocking interaction between nicotine and nicotinic receptor in the brain. [5] Although these medications prove somewhat effective in helping smokers stop smoking, the overall success rate is less than 30%, and a variety of side effects, such as skin irritation, increased risk of certain cardiovascular diseases, suicide attempts, and headache are associated with their usage. [6-8] Moreover, these medications have to be used very frequently for a long time (ranging from weeks to months) in order to achieve the desired outcome. This causes much inconvenience to patients' daily life and work. [9] In addition, the high cost of these treatments may be a big economic burden to low income users. [10]

Therefore, it is necessary to develop more effective, safer, more convenient, and less expensive medications for smoking cessation. Fulfilling these requirements, nicotine vaccine has emerged as a promising strategy against cigarette smoking in recent years. [11] Nicotine vaccine is designed to produce nicotine specific antibodies, which can bind to nicotine molecules in plasma and prevent them from crossing the blood brain barrier, thereby eliminating the rewarding effect that nicotine can elicit during smoking. [12] Nicotine with a molecular weight of 162.23 g/mol is too small to elicit an immune response. Therefore, in typical nicotine vaccine design, nicotine derivatives are usually associated with much bigger carriers to activate the immune system. [13] In the past decade, there have been a couple of nicotine vaccines tested in human clinical trials, including NicVAX®, TA-NIC®, NIC002®, Niccine®, and SEL-068®. [14] Unfortunately, right now, none of these vaccines is approved by FDA for clinical use mostly due to low efficacy. The first four belong to the first generation nicotine vaccines, which use proteins or virus-like particles as carrier for nicotine hapten presentation. These vaccines have several common disadvantages, including low specificity, low immunogenicity, short persistence of immune response, and high cost. In contrast, SEL-068®, using synthetic nanoparticle as delivery system, is considered a next generation nicotine vaccine. [15] Using nanoparticles as a vaccine delivery platform for the nicotine molecule or other drug molecules has some attractive advantages: first, the bioavailability of vaccine to immune cells is improved; second, it is possible to co-deliver both antigen and molecular adjuvants to the immune system, enhancing the immune response and minimizing potential systemic cytotoxicity of adjuvants; third, degradation of nanoparticles is slower and more controllable compared to proteins, making it possible to tune the duration of immune response; fourth, synthetic nanoparticles made from lipids, PLGA are biocompatible, and biodegradable, minimizing safety concerns; fifth, it is simpler to delivery different antigens simultaneously using nanoparticles.

In our study, we tested the performance of different types of nanoparticles for their ability to enhance immunogenicity of nicotine vaccine. In chapter III, a nicotine vaccine was constructed by

conjugating BSA-nicotine complex to liposome, and the immunogenicity as well as safety of this vaccine on mice were evaluated. In chapter IV, a negatively charged nanohorn as scaffold support was incorporated into cationic liposome to improve the stability of the delivery system. The physicochemical properties and *in vitro* stability of nicotine vaccine using negatively charged nanohorn support liposome as a delivery vehicle were characterized, and the immunogenicity and safety of this vaccine were also evaluated on mice. In chapter V, numerous lipid-PLGA hybrid nanoparticle based vaccine delivery systems of varying surface charges were constructed, and the physicochemical properties of those vaccine carriers were characterized. In addition, the uptake of these hybrid nanoparticles by dendritic cells was studied *in vitro*. In chapter VI, in order to achieve the dual goal of high stability of nanovaccine during circulation and rapid activation of immune system after internalization of vaccine by immune cells, a pH sensitive lipid-PLGA hybrid nanoparticle was devised, and its antigen release profiles were studied both in physiological environment and low pH environment *in vitro*. In chapter VII, lipid-PLGA hybrid nanoparticles containing various amount of cholesterol in a lipid layer were made, and their antigen release profiles as well as uptake by dendritic cells were studied. Chapter VIII is a general conclusion of this work.

## References


[1] Centers for Disease Control and Prevention. Current cigarette smoking among adults-United States, 2011. MMWR Morbidity and Mortality Weekly Report. 2012;61:889.

[2] Benowitz NL. Nicotine addiction. The New England Journal of Medicine. 2010;362:2295.

[3] Hughes JR, Hatsukami D. Signs and symptoms of tobacco withdrawal. Archives of General Psychiatry. 1986;43:289-94.

[4] Doggrell SA. Which is the best primary medication for long-term smoking cessation-nicotine replacement therapy, bupropion or varenicline? Expert Opinion on Pharmacotherapy. 2007;18:2903-15.

[5] Schlam TR, Baker TB. Interventions for tobacco smoking. Annual Review of Clinical Psychology. 2013;9:675-702.

[6] Silagy C, Lancaster T, Stead L, Mant D, Fowler G. Nicotine replacement therapy for smoking cessation. The Cochrane Library. 2004.

[7] Food and Drug Administration. FDA drug safety communication: safety review update of Chantix (varenicline) and risk of cardiovascular adverse events. Rockville, MD: US Food and Drug Administration. 2012.

[8] Hughes JR, Stead LF, Lancaster T. Antidepressants for smoking cessation. The Cochrane Library. 2014.

[9] Shiffman S, Brockwell SE, Pillitteri JL, Gitchell JG. Use of smoking-cessation treatments in the United States. American Journal of Preventive Medicine. 2008;34:102-11.

[10] Fiore M. Treating tobacco use and dependence: 2008 update. Clinical Practice Guideline. 2008.

[11] Escobar-Chávez JJ, Domínguez-Delgado CL, Rodríguez-Cruz IM. Targeting nicotine addiction: the possibility of a therapeutic vaccine. Drug Design, Development and Therapy. 2011;5:211.

[12] Fahim RE, Kessler PD, Fuller SA, Kalnik MW. Nicotine vaccines. CNS & Neurological Disorders Drug Targets. 2011;10:905-15.

[13] Hu Y, Zheng H, Huang W, Zhang C. A novel and efficient nicotine vaccine using nano-lipoplex as a delivery vehicle. Human Vaccines & Immunotherapeutics. 2014;10:64-72.

[14] Pentel PR, LeSage MG. New directions in nicotine vaccine design and use. Advances in Pharmacology. 2014;69:553-80.

[15] Pittet L, Altreuter D, Ilyinskii P, Fraser C, Gao Y, Baldwin S, et al. Development and preclinical evaluation of SEL-068®, a novel targeted Synthetic Vaccine Particle (tSVP™) for smoking cessation and relapse prevention that generates high titers of antibodies against nicotine. The Journal of Immunology. 2012;188:75.

## Chapter II: Literature Review

### Nicotine vaccine --- a new strategy for smoking cessation

### The negative impacts of tobacco use

Tobacco, which was initially used by the Native Americans primarily for ceremonial and religious purposes, was brought back to Europe by Columbus. [1] Since then, tobacco was widely used in Europe in the form of snuff and pipe tobacco. In the late 1800s, the modern tobacco industry was started with the invention of a cigarette-making machine in the United States. Aggressive sales of cigarettes began in the early 1900s by the American Tobacco Company, which used highly successful marketing strategies and misleading advertisements. [1, 2] Nowadays, there are approximately 1.5 billion smokers worldwide, and cigarette smoking is prevalent in almost every country on Earth, regardless of the stage of economic development. [3] Currently, in the U.S.A., an estimated 42.1 million people, or 18.1% of all adults (aged 18 years or older), smoke cigarettes. Cigarette smoking is more common among men (20.5%) than women (15.8%) in the United States. [4] In developing countries, for instance in China in 2010, estimated 301 million, or 28.1% of adults (52.9% of men and 2.4% of women) were smokers, making this country the largest consumer of tobacco in the world. [5]

At the beginning years of cigarette use, the association between smoking and diseases was overlooked, and cigarette use was considered safe, or even helpful to human health due to the deceptive advertisements of tobacco companies. [6] However, during late 1930s, it was suggested that smoking potentially caused lung cancer, and a follow-up study of families reported that smokers did not live as long as non-smokers. [7, 8] In the 1960s, authoritative government agencies both in the United States and the United Kingdom concluded that cigarette smoking was a cause of lung cancer and chronic bronchitis. [1] Later in depth studies found that the combustion of cigarettes can produce over 7000

compounds in the gaseous and particulate phases, including carbon monoxide and well known carcinogens, such as benzene, formaldehyde, and polonium. These toxic components can accumulate to remarkable levels in the human body after frequent and long term smoking. [9] The impact of smoking on promoting fatal diseases is astonishing. For example, smoking can increase the risk for coronary heart disease by 2 to 4 times, stroke by 2 to 4 times, and lung cancer by at least 25 times. [10, 11] So far, smoking has been linked to dozens of diseases, including cardiovascular diseases, cancers, respiratory diseases, mental illness, and reproductive diseases. [10, 12]

Today, it is widely known that lung cancer is one of the top preventable cancers caused by smoking. In the year 2011 alone, 207,339 people in the United States were diagnosed with lung cancer, including 110,322 men and 97,017 women, and 156,953 people in the United States died from lung cancer, including 86,736 men and 70,217 women. [13] Among these lung cancer patients, more than 7,300 non-smokers die each year from lung cancer caused by secondhand smoke. [14] Besides lung cancer, worldwide, tobacco smoking also accounts for 42% of oral and oropharyngeal cancer, 42% of esophageal cancer, 13% of stomach cancer, 14% of liver cancer, 22% of pancreatic cancer, 70% of trachea, bronchus, and lung cancers, 2% of cervical cancer, 28% of bladder cancer, and 9% of leukemia. [15, 16] The harmful impact of smoking on fecundity and reproduction has also become apparent in recent years, but does not gain enough attention. Approximately 30% of reproductive age women and 35% of reproductive age men in the United States smoke cigarettes. [17] Generally, the negative influence of smoking on reproduction can be summarized to the following points: up to 13% of infertility may be attributable to cigarette smoking; smoking may accelerate the loss of reproductive function; smoking can increase risks of spontaneous abortion and ectopic pregnancy; tobacco use is also associated with high rates of long and short term morbidity and mortality for mother and child; there is a positive correlation between maternal smoking during pregnancy and childhood obesity. [17-19] The detrimental effects of cigarette smoking on neural system have been systematically investigated. Brain-

imaging studies on the influence of smoking on neural systems show that there are alterations of both gray matter and white matter in smokers. [20-22] Strong epidemiological data suggest that there is a positive correlation between smoking and increased rates of different kinds of psychiatric disorders, including schizophrenia, cannabis use, major depressive disorder, attention deficit hyperactivity disorder, and posttraumatic stress disorder.[20, 23-25]

Overall, in the United States, tobacco use remains the single largest preventable cause of death and disease.[26] Approximately 440,000 U.S. adults die from smoking-related illnesses annually, and the economic loss caused by smoking is enormous, including $133 billion in medical expenses and $156 billion in lost productivity each year. [10, 27, 28] Worldwide, tobacco use causes more than 5 million deaths per year, and current trends show that tobacco use will cause more than 8 million deaths annually by 2030. [29]

**The mechanism underlying smoking addiction**

Though smoking is apparently detrimental to human health, more than 3,200 persons younger than 18 years of age start their first cigarette each day, and an estimated 2,100 young occasional smokers become daily cigarette smokers in the United States. [10] One question has to be asked is why cigarette smoking is so attractive and addictive to people? Substantial evidences from a wide range of studies indicate nicotine is the major addictive component that drives continued use and causes long term addiction to cigarette despite the harmful consequences. [30-32] Nicotine is an alkaloid present in tobacco leaves and in lower levels in other plants such as eggplant, tomato, potato, and green pepper, where it acts as a natural insecticide.[20] On average, each cigarette contains 10-15 mg of nicotine, and 1.5 mg of this will be inhaled into human body during smoking, enabling high levels of nicotine reach the brain in 10–20 s after a puff. [33, 34] Nicotine initiates its action by binding to nicotinic acetylcholine receptors (nAChRs), which belong to a superfamily of ligand-gated ion channels.[30, 35] The binding of

nicotine to nAChRs opens the ion channels and allows the entry of sodium or calcium into nerve cells, leading to the release of neurotransmitters. [36, 37] Among the actions that can occur subsequent to this binding, is the release of dopamine from other neurons. Dopamine signaling causes an experience of euphoria and is critical for the reinforcing effects of nicotine and other drugs of abuse.[36, 38] Meanwhile, nicotine exposure can also promote glutamate release by stimulating glutamatergic neurons, facilitating the release of dopamine, thereby increasing excitation of dopaminergic neurons and enhancing responsiveness to nicotine. [36] Other neurotransmitters such as hypocretins and neuropeptides that regulate the stimulatory effects of nicotine on reward centers in the brain are also potentially involved in nicotine addiction. [39] Abstinence from nicotine among smokers can cause withdrawal symptoms, such as irritability, depressed mood, restlessness, and anxiety, which drive smokers to maintain sufficient levels of plasma nicotine to prevent withdrawal symptoms through continued smoking. [40, 41]

**Pharmacological medications for aiding smoking cessation**

Substantial studies have shown that it is never too late to stop smoking. [42, 43] Smoking cessation can drastically reduce the death risks caused by cardiovascular and lung diseases among smokers, and the survival rate of smokers with various cancers can be significantly increased by quitting smoking.[44-48] However, quitting is always easy to say and hard to do. Most of the smokers (75%) in the United States want to quit smoking, but only 3% of them can achieve long-term abstinence without aid from smoking cessation medications. [49, 50]

**Nicotine replacement therapy (NRT)**

Since nicotine is the major component of cigarette that is responsible for smoking addition, it is reasonable to develop medications that target nicotine dependence. Currently, the most commonly used pharmacotherapy against nicotine dependence is NRT. [51] In the United States, there are six FDA

approved NRT products available to smokers, including nicotine gum, nicotine lozenges, nicotine sublingual tablets, nicotine vapor inhalers, nicotine nasal spray, and nicotine transdermal patch systems. [52, 53] Generally, the mechanisms underlying the efficacy on smoking cessation of NRT products include the following: first, they can reduce withdrawal symptoms, helping smokers feel comfortable without a cigarette; second, they can reduce the rewarding effect of cigarette-delivered nicotine; third, they can provide smokers euphoric feelings, which used to be obtained from smoking. [53]

Overall, when used alone, the success rates on smoking cessation for NRT products are around 20%, which is higher compared to smokers taking placebo. [54] The efficacy of these products is greatly influenced by how they are used. For example, chewing is important to nicotine gum efficacy. Nicotine containing saliva must be retained in mouth long enough to allowing sufficient amount of nicotine to be adsorbed across the buccal mucosa, otherwise nicotine molecules delivered by gum may be metabolized in the liver and lose their function. [55] Another example is the nicotine inhaler. The amount of nicotine that smokers can acquire from the inhaler is decided by both the depth of inhalation as well as the environmental temperature. Larger amounts of nicotine molecules can be delivered under higher ambient temperature. [56, 57] More often than not, smokers cannot get enough nicotine from one single product, and therefore, different formulations of NRT products are advised to be used in combination to increase nicotine bioavailability. Commonly, the nicotine patch is combined with other nicotine products, and such a practice has been proven more effective than any single type of NRT. [58]

Though commonly and widely recommended as an aid for smoking cessation, NRT has its own limitations. First, its success rate is moderate, and not very appealing to smokers who want to quit smoking. Second, smokers have to apply these products very frequently. For example the nicotine patch has to be used every day, and users are instructed to chew nicotine gum every 1-2 hours. [53] Smokers may think it is inconvenient or even boring to receive this treatment at such high frequency. Third, it

usually takes smokers several weeks, or even months to achieve long term abstinence. [59] It is difficult for smokers to follow the medical instruction outside clinical settings over a long period, resulting in unplanned usage of NRT or even quitting medication. Fourth, NRT is not perfectly safe for humans. There are also NRT related adverse effects. For instance, skin irritation was shown to be associated with the nicotine patch; oropharyngeal complaints were reported after using nicotine gum. [60]

**Varenicline**

Besides NRT, there are two other pharmacotherapy products for smoking cessation approved by the FDA in the United States. These are varenicline and bupropion. [61] Varenicline, developed by Pfizer, Inc. and marketed as Chantix®, is a partial agonist of the α4β2 nicotinic receptor and a synthetic analog of cytisine, which was approved as a smoking cessation drug in 2006 in Eastern Europe. [62, 63] As a partial agonist of the α4β2 nicotinic receptor, varenicline can partially block receptor stimulation by high levels of nicotine delivered by smoking, thereby lowering dopamine release and reducing the rewarding effects of nicotine. [64] Moreover, it can weakly activate the nicotinic receptor and stimulate dopamine release, thus reducing craving and withdrawal symptoms during abstinence. [65] Compared to NRT, varenicline is more successful in aiding smoking cessation in terms of long term abstinence rates. [66] A wide range of studies demonstrated that varenicline can achieve abstinence rates around 30%, which are three times higher than placebo. [67-69] Despite the significantly greater efficacy of varenicline compared to NRT, varenicline has been found to cause considerable adverse side effects. [70, 71] Some of the side effects, including nausea, abnormal dreams, and insomnia, led to some patients discontinuing treatment during clinical trials among some patients. [72] A long term (52 weeks) study on the adverse effects of varenicline found that the dropout rate of patients who were using varenicline was 28.3%, which was significantly higher than 10.3% in the placebo group. [46] In addition, varenicline is also associated with more severe adverse side effects, such as developing and worsening symptoms of cardiovascular disease, suicidal intentions, and suicide attempts. [73, 74] Due to these adverse effects,

the FDA in 2009 required varenicline to carry a black box warning, and issued a safety announcement that the use of varenicline may increase risk of certain cardiovascular adverse events in patients with cardiovascular disease. [75]

**Bupropion**

Bupropion, initially used as an antidepressant drug, was found to be effective as an aid for smoking cessation and was marketed as Zyban®. [76, 77] Although the exact mechanism underlying the efficacy of bupropion on smoking cessation is not clearly understood, it was presumed that bupropion inhibits dopamine and norepinephrine reuptake in both the mesolimbic dopaminergic system and the locus ceruleus of the brain, thereby reducing the rewarding effect of tobacco smoking. [78] It was also suggested that bupropion acts as smoking cessation aid by reducing depression during abstinence. [77] The efficacy of bupropion is dose-dependent, and it has been documented that smokers using bupropion with a daily dose of 100 mg, 150 mg, or 300 mg achieved 1.42, 1.69, and 2.84 times higher abstinence rates compared to smokers on placebo. [79] One clinical trial showed that the combination of bupropion and a nicotine patch achieved significantly higher abstinence rate (35.5%), compared to 16.4% for the nicotine patch alone, and 30.3% for bupropion alone. [80] Like other pharmacotherapy products for smoking cessation, bupropion has its own adverse effects, including dry mouth, insomnia, anxiety, nausea, headache, and even seizure risk. [77, 81] Due to the potential health risks posed by bupropion, the FDA also requires a black box warning on its label and suggests careful monitoring of adverse effects among users. [82, 83]

In conclusion, pharmacotherapies, including NRT, bupropion, and varenicline, have some innate limitations for smoking cessation. First, the abstinence rates achieved by these medications are relatively low, from 5% to 20%; second, the treatment time is too long, from several weeks to several months; third, adverse effects from moderate degree to severe degree are associated with

pharmacotherapies; fourth, the high cost (around $3500 for each treatment) of pharmacotherapies may not be acceptable to low income groups. [84] Therefore, medications with greater efficacy, better safety, and lower cost are highly demanded for smoking cessation treatment.

**Nicotine vaccines**

One promising candidate for smoking cessation is nicotine vaccine, a product designed to induce the immune system to produce highly specific antibodies against nicotine. [85] It is assumed that nicotine specific antibodies can bind to nicotine molecules, sequester them in blood stream, thus reducing the amount of nicotine that can pass brain barrier and activate the rewarding system. [86] Theoretically, nicotine vaccine will have several advantages over traditional pharmacotherapies, including persistence of antibodies over several months, ensuring long term efficacy. This means daily administration is not required, and only several injections are needed to achieve the desired effectiveness, reducing the need for adherence to a dosing regimen. Furthermore, the antibodies produced by the vaccine are less likely to be self-reactive, the vaccine components are non-toxic, and no severe adverse side effects are predicted, ensuring its good safety. In addition, the cost of nicotine vaccine is much lower than traditional medications, making it affordable to low income patients.

Nicotine is a small molecule and unable to elicit humoral immune response, and therefore nicotine haptens are always associated with carrier proteins or peptides to make previously non-immunogenic nicotine analogues visible to the immune system and generate nicotine-specific antibodies. [87] To date, several nicotine vaccine candidates have been tested in human clinical trials, including NicVAX®, TA-NIC®, NIC002®, Niccine®, and SEL-068®. [88]

**NicVAX®**

NicVAX® is constructed by linking 3’-aminomethylnicotine (3’-AmNic) to recombinant *Pseudomonas aeruginosa* exoprotein A (rEPA) via a succinyl linker.[89] This vaccine is being developed

by Nabi Pharmaceuticals and GlaxoSmithKline and has completed two Phase III studies. The Phase II clinical studies in the US showed promising result: 33% of the smokers quit smoking for at least 30 consecutive days after four injections of NicVAX® at doses of 200 μg each. Greater reduction in cigarette consumption was also observed in smokers receiving a higher dose of NicVAX® than those who received a lower dose of vaccine and placebo. In the Phase IIb study, 16% of the smokers who received 5 injections of 400 μg NicVAX® each achieved 12 months continuous abstinence. [88] Although NicVAX® exhibited acceptable safety and tolerability profile in the Phase III trials, no significant difference was observed in the abstinence rate between the vaccine and placebo (11% for both vaccine and placebo), indicating the failure of the clinical trials. [90]

**TA-NIC®**

TA-NIC®, developed by Xenova/Celtic Pharma, is a conjugate of hapten nicotine N1-butryic acid and cholera toxin B carrier protein. [91] In Phase II studies, 16 smokers in each group received 50 μg, 250 μg and 1000 μg, respectively, of TA-NIC® by intramuscular injection at 0, 2, 4, 6, 8, 12, and 32 weeks. 43% of the smokers injected with TA-NIC® reported abstinence at week 6, while 9% receiving placebo achieved abstinence. The efficacy of the vaccine was dose-dependent. 8% of the smokers receiving 50 μg doses stayed abstinent at 12 month, compared to 19% and 38% of those who received 250 μg and 1000 μg doses, respectively. Moreover, TA-NIC® appeared to encourage smokers to attempt quitting, because 95% of the smokers attempted to quit in vaccine group, while only 73% of the participants tried to quit smoking. [88]

**NIC002®**

NIC002®, developed by Cytos/Novartis in Switzerland, follows a similar design as TA-NIC® and NicVAX®, except that carrier proteins are substituted by a virus-like particles (VLPs) assembled from synthetic capsid derived from phage Qβ. [92] In the Phase I study, 100% of the participants who received

NIC002® developed a nicotine-specific antibody response by day 14, and no severe adverse effects were observed. [93] In a Phase II study, NIC002® showed high safety to users, as only mild fever and flu-like symptoms were detected. Participants were divided into low, medium, and high responders according to the antibody levels at the end of the study, and the abstinence rate of high responders was the greatest with 41.5% of the participants with high anti-nicotine antibody level achieving 12 months abstinence. [94] In another clinical study, smokers were repeatedly injected with 100 µg of NIC002® five times weekly or five times bi-weekly or five times monthly, but unfortunately, insufficient antibody levels were achieved among participants, and no significant abstinence rate increase was observed compared to the placebo group. [88]

**NICCINE®**

Niccine®, developed by Independent Pharmaceutica, is another protein hapten conjugate vaccine, in which the IP18 nicotine epitope is coupled to tetanus toxoid. [95] In a Phase II study, Niccine® was tested for its efficacy against relapse prevention. In the study, 40 µg Niccine® was given to smokers on days 0, 28, 56, 90, 150, and 210, and smokers were also treated with varenicline between days 56–98 to aid smoking cessation. At 12 months, non-relapse rate was 43.3% in Niccine® group, while placebo group had a non-relapse rate of 51.1%, suggesting that Niccine® was not beneficial. No severe adverse side effects were observed in vaccine treated smokers. Although the nicotine-specific antibodies were increased after repeated vaccine injections, it is highly possible the antibody levels were not sufficient enough for relapse prevention. Due to the failure of the Phase II clinical trial, the producer has withdrawn this vaccine from future development. [96]

**SEL-068®**

SEL-068®, developed by Selecta Biosciences, is considered a next generation nicotine vaccine. [97] According to limited reports on this vaccine, SEL-068® is a synthetic nanoparticle based nicotine

vaccine composed of four major components, including a biodegradable and biocompatible polymer matrix, a synthetic Toll like receptor (TLR) agonist, a novel universal T-cell helper peptide and nicotine covalently conjugated to the nanoparticle surface. [98, 99] As introduced by the developer, SEL-068® has the following attractive characteristics: [99] first, the nanoparticles are designed to flow freely to the lymph nodes, enabling direct and concomitant delivery of all required components to the responsive cells of the immune system; second, encapsulation and controlled release of the TLR agonist in the nanoparticle minimizes the generation of systemic inflammatory cytokines, improving the overall safety profile and enabling the use of novel adjuvants; third, the novel universal T cell helper peptide used in SEL-068® elicited T cell recall responses in peripheral blood mononuclear cell (PBMC) from a broad panel of human donors. In preclinical trials, this vaccine showed excellent safety. The efficacy of SEL-068® was found to be dose dependent, and robust immune responses generating high-titer and high-affinity antibodies have been reported in mice and nonhuman primates. [99] In November 2011, SEL-068® launched Phase I studies in 80 healthy volunteers to test the safety and dose-dependence of immunogenicity. However, to date, no results from the Phase I study have been reported. In 2014, Selecta Bioscience received 8.1 million dollars from NIH to continue mid-stage clinical studies of SEL-068®.

**Conclusion**

Tobacco use is the biggest single preventable cause of many life threatening diseases, which currently are causing over 6 million deaths worldwide and countless economic losses each year. Pharmacological interventions, such as NRTs, bupropion, and varenicline are available to smokers for aiding smoking cessation. Generally, these medications target different withdrawal symptoms during smoking cessation. For example, NRTs can reduce craving for nicotine, bupropion alleviates depression, and varenicline is able to reduce rewarding effect of nicotine as well as provide minimal stimulation to

the central nervous system. Traditional pharmacological medications have proven helpful for smoking cessation, but the overall success rate is moderate (less than 30%) and the adverse side effects cause increasing concerns for their safety. Nicotine vaccines, which can produce nicotine specific antibodies and block the entrance of nicotine to brain, have being tested as a new option for helping people quit smoking. Extensive preclinical trials on animals have been carried out to test the efficacy and safety of nicotine vaccines, and the results are promising. Several nicotine vaccine candidates have even been advanced into human clinical trials, including NicVAX®, TA-NIC®, NIC002®, Niccine®, and SEL-068®. However, the first three traditional nicotine vaccines, which use hapten-protein conjugate as immunogen, were not effective in helping smoking cessation. In contrast, SEL-068®, which uses synthetic nanoparticle as delivery systems has shown many unique advantages over traditional carrier protein and virus-like particle based vaccines. The application of nanoparticle as nicotine vaccine carrier may enhance immunogenicity, improve specificity, and lengthen persistence of immune response; moreover, synthetic nanoparticles are biodegradable and biocompatible, minimizing possible adverse side effects.

## References

[1] Samet JM. Tobacco smoking: the leading cause of preventable disease worldwide. Thoracic Surgery Clinics. 2013;23:103-12.

[2] Chaloupka FJ, Cummings KM, Morley C, Horan J. Tax, price and cigarette smoking: evidence from the tobacco documents and implications for tobacco company marketing strategies. Tobacco Control. 2002;11:62-72.

[3] Giovino GA, Mirza SA, Samet JM, Gupta PC, Jarvis MJ, Bhala N, et al. Tobacco use in 3 billion individuals from 16 countries: an analysis of nationally representative cross-sectional household surveys. The Lancet. 2012;380:668-79.

[4] Agaku IT, King BA, Dube SR. Current cigarette smoking among adults-United States, 2005–2012. Morbidity and Mortality Weekly Report. 2014;63:29-34.

[5] Li Q, Hsia J, Yang G. Prevalence of smoking in China in 2010. New England Journal of Medicine. 2011;364:2469-70.

[6] Brandt AM. The cigarette century: the rise, fall, and deadly persistence of the product that defined America. Basic Books. 2007.

[7] Ochsner A, Debakey M. Primary pulmonary malignancy: treatment by total pneumonectomy; analysis of 79 collected cases and presentation of 7 personal cases. The Ochsner Journal. 1999;1:109-25.

[8] Pearl R. Tobacco smoking and longevity. Science. 1938;87:216-7.

[9] Centers for Disease Control and Prevention. How tobacco smoke causes disease: the biology and behavioral basis for smoking-attributable disease: a report of the surgeon general. Centers for Disease Control and Prevention (US). 2010.

[10] US Department of Health and Human Services. The health consequences of smoking—50 years of progress: a report of the surgeon general. Atlanta, GA: US Department of Health and Human Services, Centers for Disease Control and Prevention, National Center for Chronic Disease Prevention and Health Promotion, Office on Smoking and Health. 2014;17.

[11] Centers for Disease Control and Prevention. Reducing the health consequences of smoking: 25 years of progress. A report of the Surgeon General Washington DC, US Department of Health and Human Services. 1989.

[12] Lasser K, Boyd JW, Woolhandler S, Himmelstein DU, McCormick D, Bor DH. Smoking and mental illness: a population-based prevalence study. Journal of the American Medical Association. 2000;284:2606-10.

[13] Cancer Statistics Working Group. United States cancer statistics: 1999–2011 incidence and mortality web-based report. Atlanta (GA): Department of Health and Human Services, Centers for Disease Control and Prevention, and National Cancer Institute. 2014.

[14] Centers for Disease Control and Prevention. Secondhand smoke (SHS) facts. 2014. http://www.cdc.gov/tobacco/data_statistics/fact_sheets/secondhand_smoke/general_facts/

[15] Weiderpass E. Lifestyle and cancer risk. Journal of Preventive Medicine and Public Health. 2010;43:459-71.

[16] Lee Y, Hashibe M. Tobacco, alcohol, and cancer in low and high income countries. Annals of Global Health. 2013;80:378-83.

[17] The Practice Committee of the American Society for Reproductive Medicine. Smoking and infertility. Fertility and Sterility. 2008;90:S254.

[18] Ino T. Maternal smoking during pregnancy and offspring obesity: meta-analysis. Pediatrics International. 2010;52:94-9.

[19] Mund M, Louwen F, Klingelhoefer D, Gerber A. Smoking and pregnancy—a review on the first major environmental risk factor of the unborn. International Journal of Environmental Research and Public Health. 2013;10:6485-99.

[20] Dome P, Lazary J, Kalapos MP, Rihmer Z. Smoking, nicotine and neuropsychiatric disorders. Neuroscience & Biobehavioral Reviews. 2010;34:295-342.

[21] Almeida OP, Garrido GJ, Lautenschlager NT, Hulse GK, Jamrozik K, Flicker L. Smoking is associated with reduced cortical regional gray matter density in brain regions associated with incipient Alzheimer disease. The American Journal of Geriatric Psychiatry. 2008;16:92-8.

[22] Gazdzinski S, Durazzo TC, Studholme C, Song E, Banys P, Meyerhoff DJ. Quantitative brain MRI in alcohol dependence: preliminary evidence for effects of concurrent chronic cigarette smoking on regional brain volumes. Alcoholism: Clinical and Experimental Research. 2005;29:1484-95.

[23] Agrawal A, Lynskey MT, Pergadia ML, Bucholz KK, Heath AC, Martin NG, et al. Early cannabis use and DSM-IV nicotine dependence: a twin study. Addiction. 2008;103:1896-904.

[24] Wilens TE, Adamson J, Monuteaux MC, Faraone SV, Schillinger M, Westerberg D, et al. Effect of prior stimulant treatment for attention-deficit/hyperactivity disorder on subsequent risk for cigarette smoking and alcohol and drug use disorders in adolescents. Archives of Pediatrics & Adolescent Medicine. 2008;162:916-21.

[25] Littleton J, Barron S, Prendergast M, Nixon SJ. Smoking kills (alcoholics)! shouldn't we do something about it? Alcohol and Alcoholism. 2007;42:167-73.

[26] Centers for Disease Control and Prevention. Current cigarette smoking among adults-United States, 2011. MMWR Morbidity and Mortality Weekly Report. 2012;61:889.

[27] Trosclair A, Dube SR. Smoking among adults reporting lifetime depression, anxiety, anxiety with depression, and major depressive episode, United States, 2005–2006. Addictive Behaviors. 2010;35:438-43.

[28] Centers for Disease Control and Prevention. Quitting smoking among adults--United States, 2001-2010. MMWR Morbidity and Mortality Weekly Report. 2011;60:1513.

[29] World Health Organization. WHO Report on the global tobacco epidemic, 2011: warning about the dangers of tobacco. Geneva, Switzerland. 2011.

[30] Dani JA, De Biasi M. Cellular mechanisms of nicotine addiction. Pharmacology Biochemistry and Behavior. 2001;70:439-46.

[31] Balfour DJ, Wright AE, Benwell ME, Birrell CE. The putative role of extra-synaptic mesolimbic dopamine in the neurobiology of nicotine dependence. Behavioural Brain Research. 2000;113:73-83.

[32] Cadoni C, Di Chiara G. Differential changes in accumbens shell and core dopamine in behavioral sensitization to nicotine. European Journal of Pharmacology. 2000;387:R23-R5.

[33] Hukkanen J, Jacob P, Benowitz NL. Metabolism and disposition kinetics of nicotine. Pharmacological Reviews. 2005;57:79-115.

[34] Benowitz NL, Herrera B, Jacob P. Mentholated cigarette smoking inhibits nicotine metabolism. Journal of Pharmacology and Experimental Therapeutics. 2004;310:1208-15.

[35] Paterson D, Nordberg A. Neuronal nicotinic receptors in the human brain. Progress in Neurobiology. 2000;61:75-111.

[36] Benowitz NL. Nicotine addiction. The New England Journal of Medicine. 2010;362:2295.

[37] Dajas-Bailador F, Wonnacott S. Nicotinic acetylcholine receptors and the regulation of neuronal signalling. Trends in Pharmacological Sciences. 2004;25:317-24.

[38] Nestler EJ. Is there a common molecular pathway for addiction? Nature Neuroscience. 2005;8:1445-9.

[39] Hollander JA, Lu Q, Cameron MD, Kamenecka TM, Kenny PJ. Insular hypocretin transmission regulates nicotine reward. Proceedings of the National Academy of Sciences. 2008;105:19480-5.

[40] Balfour DJ. The neurobiology of tobacco dependence: a preclinical perspective on the role of the dopamine projections to the nucleus. Nicotine & Tobacco Research. 2004;6:899-912.

[41] Le Moal M, Koob GF. Drug addiction: pathways to the disease and pathophysiological perspectives. European Neuropsychopharmacology. 2007;17:377-93.

[42] Warren GW, Sobus S, Gritz ER. The biological and clinical effects of smoking by patients with cancer and strategies to implement evidence-based tobacco cessation support. The Lancet Oncology. 2014;15:e568-e80.

[43] Cooley ME, Emmons KM, Haddad R, Wang Q, Posner M, Bueno R, et al. Patient-reported receipt of and interest in smoking-cessation interventions after a diagnosis of cancer. Cancer. 2011;117:2961-9.

[44] Peto R, Darby S, Deo H, Silcocks P, Whitley E, Doll R. Smoking, smoking cessation, and lung cancer in the UK since 1950: combination of national statistics with two case-control studies. The BMJ. 2000;321:323-9.

[45] Anthonisen NR, Skeans MA, Wise RA, Manfreda J, Kanner RE, Connett JE. The effects of a smoking cessation intervention on 14.5-Year mortality: a randomized clinical trial. Annals of Internal Medicine. 2005;142:233-9.

[46] Siu EC, Tyndale RF. Non-nicotinic therapies for smoking cessation. Annual Review of Pharmacology and Toxicology. 2007;47:541-64.

[47] Murta-Nascimento C. The effect of smoking on prostate cancer survival: a cohort analysis in Barcelona. The 20th IEA World Congress of Epidemiology (17-21 August 2014, Anchorage, AK). 2014.

[48] Andreas S, Rittmeyer A, Hinterthaner M, Huber RM. Smoking cessation in lung cancer—achievable and effective. Deutsches Ärzteblatt International. 2013;110:719.

[49] Centers for Disease Control and Prevention. Cigarette smoking among adults and trends in smoking cessation-United States, 2008. MMWR Morbidity and Mortality Weekly Report. 2009;58:1227.

[50] Hughes JR, Keely J, Naud S. Shape of the relapse curve and long-term abstinence among untreated smokers. Addiction. 2004;99:29-38.

[51] Mendelsohn C. Optimising nicotine replacement therapy in clinical practice. Australian Family Physician. 2013;42:305.

[52] Haustein K. Pharmacotherapy of nicotine dependence. International Journal of Clinical Pharmacology and Therapeutics. 2000;38:273-90.

[53] Jain R, Majumder P, Gupta T. Pharmacological intervention of nicotine dependence. BioMed Research International. 2013.

[54] Stead LF, Perera R, Bullen C, Mant D, Hartmann-Boyce J, Cahill K, et al. Nicotine replacement therapy for smoking cessation. The Cochrane Library. 2012;11.

[55] Use T, Panel DG. Treating tobacco use and dependence: 2008 update. 2008.

[56] Schneider NG, Lunell E, Olmstead RE, Fagerström K-O. Clinical pharmacokinetics of nasal nicotine delivery. Clinical Pharmacokinetics. 1996;31:65-80.

[57] Hjalmarson A, Nilsson F, Sjöström L, Wiklund O. The nicotine inhaler in smoking cessation. Archives of Internal Medicine. 1997;157:1721-8.

[58] Stead LF, Perera R, Bullen C, Mant D, Lancaster T. Nicotine replacement therapy for smoking cessation. The Cochrane Library. 2008;1.

[59] Etter J-F, Stapleton JA. Nicotine replacement therapy for long-term smoking cessation: a meta-analysis. Tobacco Control. 2006;15:280-5.

[60] Silagy C, Lancaster T, Stead L, Mant D, Fowler G. Nicotine replacement therapy for smoking cessation. The Cochrane Library. 2004.

[61] Ebbert JO, Hatsukami DK, Croghan IT, Schroeder DR, Allen SS, Hays JT, et al. Combination varenicline and bupropion SR for tobacco-dependence treatment in cigarette smokers: a randomized trial. The Journal of the American Medical Association. 2014;311:155-63.

[62] Mihalak KB, Carroll FI, Luetje CW. Varenicline is a partial agonist at α4β2 and a full agonist at α7 neuronal nicotinic receptors. Molecular Pharmacology. 2006;70:801-5.

[63] Zatonski W, Cedzynska M, Tutka P, West R. An uncontrolled trial of cytisine (Tabex) for smoking cessation. Tobacco Control. 2006;15:481-4.

[64] Maity N, Chand P, Murthy P. Role of nicotine receptor partial agonists in tobacco cessation. Indian Journal of Psychiatry. 2014;56:17.

[65] Gonzales D, Rennard SI, Nides M, Oncken C, Azoulay S, Billing CB, et al. Varenicline, an α4β2 nicotinic acetylcholine receptor partial agonist, vs sustained-release bupropion and placebo for smoking cessation: a randomized controlled trial. The Journal of the American Medical Association. 2006;296:47-55.

[66] Aubin H-J, Bobak A, Britton JR, Oncken C, Billing CB, Gong J, et al. Varenicline versus transdermal nicotine patch for smoking cessation: results from a randomised open-label trial. Thorax. 2008;63:717-24.

[67] Oncken C, Watsky E, Reeves K, Anziano R. Varenicline is efficacious and well tolerated in promoting smoking cessation: results from a 7-week, randomized, placebo-and bupropion-controlled trial. Proceedings of the 11 Annual Meeting of the Society for Research on Nicotine and Tobacco. Prague. Czeck Republic. 2005.

[68] Niaura R, Hays JT, Jorenby DE, Leone FT, Pappas JE, Reeves KR, et al. The efficacy and safety of varenicline for smoking cessation using a flexible dosing strategy in adult smokers: a randomized controlled trial. Current Medical Research and Opinion. 2008;24:1931-41.

[69] Garrison GD, Dugan SE. Varenicline: a first-line treatment option for smoking cessation. Clinical Therapeutics. 2009;31:463-91.

[70] Tonstad S, Davies S, Flammer M, Russ C, Hughes J. Psychiatric adverse events in randomized, double-blind, placebo-controlled clinical trials of varenicline. Drug Safety. 2010;33:289-301.

[71] Gibbons RD, Mann JJ. Varenicline, smoking cessation, and neuropsychiatric adverse events. American Journal of Psychiatry. 2013;170:1460-7.

[72] Ahmed AI, Ali AN, Kramers C, Härmark LV, Burger DM, Verhoeven WM. Neuropsychiatric adverse events of varenicline: a systematic review of published reports. Journal of Clinical Psychopharmacology. 2013;33:55-62.

[73] US Food and Drug Administration. The smoking cessation aids varenicline (marketed as Chantix) and bupropion (marketed as Zyban and generics): suicidal ideation and behavior. FDA Drug Safety Newsletter. 2009;2:1-4.

[74] US Food and Drug Administration. FDA drug safety communication: safety review update of Chantix (varenicline) and risk of cardiovascular adverse events. Rockville, MD: US Food and Drug Administration. 2012.

[75] Crooks P, Bardo M, Dwoskin L. Nicotinic receptor antagonists as treatments for nicotine abuse. Advances in Pharmacology. 2013;69:513-51.

[76] Robyn R, Zwar N. Review of bupropion for smoking cessation. Drug and Alcohol Review. 2003;22,203-20.

[77] Hughes JR, Stead LF, Hartmann-Boyce J, Cahill K, Lancaster, T. Antidepressants for smoking cessation. The Cochrane Library. 2014.

[78] Hays JT, Ebbert JO. Bupropion sustained release for treatment of tobacco dependence. Mayo Clinic Proceedings. 2003;78:1020-4.

[79] Johnston JA, Geiss JD, Fiedler-Kelly J, Grasela TH, Glover ED, Sachs DP. Relationship between drug exposure and the efficacy and safety of bupropion sustained release for smoking cessation. Nicotine & Tobacco Research. 2001;3:131-40.

[80] Jorenby DE, Leischow SJ, Nides MA, Rennard SI, Johnston JA, Hughes AR, et al. A controlled trial of sustained-release bupropion, a nicotine patch, or both for smoking cessation. New England Journal of Medicine. 1999;340:685-91.

[81] Frishman WH. Smoking cessation pharmacotherapy—nicotine and non-nicotine preparations. Preventive Cardiology. 2007;10:10-22.

[82] Moore TJ, Singh S, Furberg CD. The FDA and new safety warnings. Archives of Internal Medicine. 2012;172:78-80.

[83] Pollock M, Mosholder A, Governale L. Suicidality: varenicline; bupropion; nicotine transdermal patch. Silver Spring, MD: US Food and Drug Administration Center for Drug Evaluation and Research. 2008.

[84] Fiore M. Treating tobacco use and dependence: 2008 update. Clinical Practice Guideline. 2008.

[85] Fahim RE, Kessler PD, Fuller SA, Kalnik MW. Nicotine vaccines. CNS & Neurological Disorders Drug Targets. 2011;10:905-15.

[86] Goniewicz ML, Delijewski M. Nicotine vaccines to treat tobacco dependence. Human Vaccines & Immunotherapeutics. 2013;9:13-25.

[87] Ottney AR. Nicotine conjugate vaccine as a novel approach to smoking cessation. Pharmacotherapy: The Journal of Human Pharmacology and Drug Therapy. 2011;31:703-13.

[88] Goniewicz ML, Delijewski M. Nicotine vaccines to treat tobacco dependence. Human Vaccines & Immunotherapeutics. 2013;9:13-25.

[89] Hatsukami D, Jorenby D, Gonzales D, Rigotti N, Glover E, Oncken C, et al. Immunogenicity and smoking-cessation outcomes for a novel nicotine immunotherapeutic. Clinical Pharmacology & Therapeutics. 2011;89:392-9.

[90] Syed BA, Chaudhari K. Smoking cessation drugs market. Nature Reviews Drug Discovery. 2013;12:97-8.

[91] EF Fahim R, D Kessler P, A Fuller S, W Kalnik M. Nicotine vaccines. CNS & Neurological Disorders-Drug Targets. 2011;10:905-15.

[92] Lockner JW, Janda K. Immunopharmacotherapy for nicotine addiction. Biotherapeutics: Recent Developments Using Chemical and Molecular. 2013:36-65.

[93] Maurer P, Jennings GT, Willers J, Rohner F, Lindman Y, Roubicek K, et al. A therapeutic vaccine for nicotine dependence: preclinical efficacy, and Phase I safety and immunogenicity. European Journal of Immunology. 2005;35:2031-40.

[94] Cornuz J, Zwahlen S, Jungi WF, Osterwalder J, Klingler K, Van Melle G, et al. A vaccine against nicotine for smoking cessation: a randomized controlled trial. PLoS One. 2008;3:e2547.

[95] de Villiers SH, Lindblom N, Kalayanov G, Gordon S, Baraznenok I, Malmerfelt A, et al. Nicotine hapten structure, antibody selectivity and effect relationships: results from a nicotine vaccine screening procedure. Vaccine. 2010;28:2161-8.

[96] Tonstad S, Heggen E, Giljam H, Lagerbäck P-Å, Tønnesen P, Wikingsson LD, et al. Niccine®, a nicotine vaccine, for relapse prevention: a phase II, randomized, placebo-controlled, multicenter clinical trial. Nicotine & Tobacco Research. 2013;15:1492-501.

[97] Pentel PR, LeSage MG. New directions in nicotine vaccine design and use. Advances in Pharmacology. 2014;69:553-80.

[98] Fahim RE, Kessler PD, Kalnik MW. Therapeutic vaccines against tobacco addiction. Expert Review of Vaccines. 2013;12:333-42.

[99] Pittet L, Altreuter D, Ilyinskii P, Fraser C, Gao Y, Baldwin S, et al. Development and preclinical evaluation of SEL-068®, a novel targeted Synthetic Vaccine Particle (tSVP™) for smoking cessation and relapse prevention that generates high titers of antibodies against nicotine. The Journal of Immunology. 2012;188:75.

## Chapter III (results): A novel and efficient nicotine vaccine using nano-lipoplex as a delivery vehicle

Yun Hu*, Hong Zheng*, Wei Huang, Chenming Zhang†

Department of Biological Systems Engineering, Virginia Tech, Blacksburg, VA 24061, U.S.A.

† To whom correspondence should be addressed. Office phone number: (540) 231-7601; E-mail address: chzhang2@vt.edu.

*These authors contributed equally to this work.

This paper was published in Human Vaccines & Immunotherapeutics 2014, 10:1-9. Reprinted with permission of the publisher.

**Key words:** Nicotine vaccine, Antigen delivery, Lipoplex nanoparticle, Active immunization; Nanovaccine, Nicotine

**Abbreviations:** APC, antigen presenting cells; BSA, bovine serum albumin; DC, dendritic cell; DLS, dynamic light scattering; DOTAP, 1,2-dioleoyl-3-trimethylammonium-propane (chloride salt); DSPE-PEG(2000)-maleimide, 1,2-distearoyl-sn-glycero-3-phosphoethanolamine-N-[maleimide(polyethylene glycol)-2000] (ammonium salt); ELISA, enzyme-linked immunosorbent assay; FITC, fluorescein isothiocyanate–dextran; rEPA, recombinant exotoxin A; NBL, Nic-BSA-Liposome; Nic, rac-trans 3'-hydroxymethylnicotine hemisuccinate; NicAb, anti-Nic antibodies; Nic-BSA, nicotine-BSA conjugate; RES, reticulo-endothelial system; Rhod B, Rhodamine B isothiocyanate; TEM, transmission electron microscope; TT, tetanus toxoid.

**Abstract*:***

A number of vaccines conjugating nicotine haptens with carrier proteins have been developed to combat nicotine caused tobacco dependence. Some vaccines, such as NicVAX®, NicQb®, advanced into clinical trials, but none of them were successful. Most of those vaccines have some innate disadvantages such as low nicotine loading capacity, easy degradation, and vulnerability to clearance by the reticulo-endothelial system (RES). Thus, there is undoubtedly an urgent need for developing novel vaccines against nicotine addiction. In this study, we assembled a liposome-protein based nanoparticle as a nicotine hapten delivery system. The nanoparticle (**Scheme 1**) was constructed by conjugating a model hapten carrier protein, bovine serum albumin (BSA), to cationic liposomes. This nano-sized complex, lipoplex, was characterized using zetasizer, transmission electron microscope (TEM), and flow cytometry. The efficacy of the lipoplex vaccine was evaluated in mice and compared with that of Nicotine-BSA conjugate (Nic-BSA). The lipoplex vaccine with Alum was able to elicit the highest NicAb titer of 11169±2112, which was significantly higher than that induced by either the vaccine without Alum or Nic-BSA with Alum. The significant immunostimulatory effect of this nano-lipoplex may provide a novel strategy to improve the immunogenic ability of current nicotine vaccine or other vaccines using small molecules as haptens.

## 1. Introduction

Tobacco smoking is one of the most devastating habits that people have ever indulged. Just in 2011, tobacco use killed 6 million people and caused hundreds of billions of dollars of economic damage worldwide. [1] Unfortunately, very few of the smokers are able to quit smoking completely even with pharmaceutical aid, [2] meanwhile, more and more people start their addiction to cigarettes. If such trends continue, more than one billion people will die from smoking related diseases in the 21st century. It is known that tobacco dependence is largely attributed to nicotine, which can stimulate brain

mesolimbic dopamine neurons and induce rewarding behavior. [3] Therefore, how to reduce the amount of nicotine that could be delivered to brain during smoking is the key question for smoking cessation. Currently, some pharmacological aids including nicotine replacement therapy, bupropion, varenicline are available for smoking cessation, but these approaches only impose short-term effects and majority of the quitters will relapse. [3] Inspired by the fact that human immune system is able to produce antibodies to clear foreign substances, such as virus, bacteria, and proteins, researchers have developed some innovative anti-nicotine vaccines to generate antibodies that are capable of specifically binding to nicotine molecules in peripheral circulation, and thus reducing their access to brain. [4] These vaccines share a common trait, in which nicotine haptens are conjugated to a variety of carrier proteins and injected with appropriate adjuvants during vaccination. Many of them are reported to elicit high titers of anti-nicotine antibodies during animal studies; some of them even advanced to human clinical phase trials. [5] However, most of the delivery systems used in previous nicotine vaccines contain solely carrier proteins, which are too small to effectively present the nicotine haptens to the antigen presenting cells (APC) to elicit strong immune response. [6] In addition, those carrier proteins themselves could be easily cleared by RES before presenting nicotine haptens to immune cells. [7] Moreover, the number of available ligands on carrier proteins for hapten conjugation is limited.

Therefore, it is necessary to develop new delivery systems that can both increase the antigen presenting efficiency and hapten loading capacity. Recently, cationic liposomes have been recognized as a novel adjuvant and vaccine delivery system due to some of their unique advantages over traditional carrier proteins on immunogenic stimulation: [8] first, a non-immunogenic substance may be converted to an immunogenic one; [9] second, sizes, charges, components of liposomes could be easily adjusted to cope with the need of different antigens; [10] third, toxicity of antigens may be reduced or eliminated by encapsulating antigens inside liposomes; [9] fourth, liposomes increase the antigen presentation to APCs. [11] In our previous work, lipoplex coupling cationic liposome with human liver

fatty acid binding protein 1 was assembled and well characterized as a potential vaccine delivery platform. [12] It is possible cationic liposomes combined with carrier proteins could be utilized to construct a delivery vehicle for haptens, such as small addictive compounds, to achieve high titers of effective antibodies.

Therefore, the aim of the present study was to explore the possibility of building up an efficient delivery system based on lipoplex for nicotine vaccine. Here, we present a method of preparing such a new nano-lipoplex assembled by incorporating BSA to the surface of cationic liposomes composed by 1,2-dioleoyl-3-trimethylammonium-propane (chloride salt) (DOTAP) and 1,2-distearoyl-sn-glycero-3-phosphoethanolamine-N-[maleimide(polyethylene glycol)-2000] (ammonium salt) (DSPE-PEG(2000)-maleimide), and demonstrate its significant value as a model delivery system for nicotine haptens to elicit high titers of anti-nicotine antibodies in mice study.

## *2.* Results

### 2.1 Analysis of Nic-BSA conjugates

Conjugates with various number of rac-trans 3'-hydroxymethylnicotine hemisuccinate (Nic) linked to BSA (0, 0, 15.1, 17.54, and 17.81) were constructed by coupling Nic to BSA at different initial molar ratio 1:10, 1:20, 1:50, 1:100, and 1:200 (Table 1). No Nic was detected on BSA with initial molar ratio of 1:10 and 1:20. The amount of coupled Nic could not be further increased by increasing the ratio to 1:200 compared to that at ratio of 1:100. The Nic-BSA conjugates with 15 Nic haptens were subsequently thiolated using 200 and 500 fold molar equivalents of Traut's reagent (Table 2). The thiolated Nic-BSA bearing 6 sulfhydryl groups was prepared for loading to cationic liposomes.

### 2.2 Analysis of physicochemical properties of Nic-BSA-Liposomes (NBLs)

The size, charge, and polydisperisty of NBLs constituted by various molar ratio of DSPE-PEG(2000)- maleimide/DOTAP (0.5%, 1%, 2%, and 4%) and Nic-BSA were measured using Malvern Nano-

ZS zetasizer (Table 3). For all formulations, lipids composition affects the size of liposomes. Decreasing sizes (276.97±6.66 nm, 271.33±4.33 nm, 254.67±2.21 nm, 178.67±4.16 nm) were detected using dynamic light scattering (DLS) with the increasing DSPE-PEG(2000)-maleimide ratio (0.5%, 1%, 2%, and 4%).

TEM investigation showed that DOTAP with addition of 4% DSPE-PEG (2000)-maleimide formed unilamellar vesicles with non-uniform diameters ranging from 100 to 300 nm (Figure 1), and this result was consistent with the size distribution obtained by DLS (Table 3). Zeta potentials were reduced from 29.53±1.29 mV to 8.88±0.85 mV as the amount of neutral DSPE and charge shielding agent PEG increased.

To confirm that BSA with sulfhydryl groups could be incorporated to liposomes with exposed maleimides, BSA and liposome were labeled with Rhodamine B isothiocyanate (Rhod B) and fluorescein isothiocyanate–dextran (FITC), respectively, and measured using flow cytometer. Figure 2 A showed that fluorescent signal for neither Rhod B nor FITC was detected in blank BSA-liposome nanoparticles; In FITC labeled liposome, only FITC signal was detected (Figure 2 B); Only Rhod B signal was detected in BSA-liposome nanoparticles with BSA labeled with Rhod B (Figure 2 C). The above results showed that without labeling, BSA-liposome nanoparticles did not emit either Rhod B signal or FITC signal, and BSA and liposome could be labeled with Rhod B and FITC, respectively. Figure 2 D demonstrated that the nanoparticle emitted both Rhod B and FITC signal, indicating BSA was incorporated with liposome. As shown in Figure 3, the association efficiency of Nic-BSA to cationic liposomes increased (13.67%, 27.41%, 57.47%, 75.02%, and 87.45%) with the increasing molar ratio of maleimide/Nic-BSA (0, 1:1, 2:1, 4:1, and 8:1). Since Nic-BSA was negatively charged, the increased association efficiency led to reduction in charge of NBL (Figure 4), which was indicated by the decreasing zeta potential of NBLs (41.56±1.00 mV, 29.53±1.29 mV, 22.20±0.98 mV, 11.80±0.75 mV, and 8.88±0.85 mV). Interestingly, the increasing

association rate displayed a highly linear relationship with the decreasing zeta potential of NBL (Figure 4), affirming that it was the association of Nic-BSA to liposome that led to the decrease in net charge on NBL. Furthermore, since high association efficiency would reduce the loss of Nic-BSA during NBL assembly and high concentration of haptens on the vaccine complex is more likely to induced immune response, NBL produced at 8:1 molar ratio of maleimide/Nic-BSA was chosen for animal studies.

### 2.3 Animal tests of assembled Nic vaccines

Mice were immunized on day 0, and boosted on days 14, 28 with NBL, Nic-BSA with Alum and NBL without Alum to study the immunogenicity of respective vaccines containing 50 μg Nic-BSA. Sera were collected on days 0, 13, 27, 33, 40, and anti-Nic antibodies (NicAb) were assayed on enzyme-linked immunosorbent assay (ELISA) plates coated with Nic- keyhole limpet hemocyanin (Nic-KLH). As shown in Figure 5, no NicAb was detected in sera collected on day 0, suggesting that there was no NicAb in the mice used in this study prior to Nic vaccine treatment. After the first immunization, NicAb titers of 320±208, 349±210, 131±27 were detected in samples injected respectively with NBL+Alum, NBL without Alum, and Nic-BSA+Alum. The NicAb titers achieved by NBL+Alum, NBL without Alum were significantly higher than that immunized with Nic-BSA+Alum. Titers for respective vaccines were further increased after first and second boost injection, and, in particular, the first boost drastically increased titers of NBL+Alum, NBL without Alum, and Nic-BSA+Alum to 7932±1047, 5720±3952, 3953±826, respectively. The maximal titers of 11169±2112, 9876 ±1932, and 7182±314 for the three vaccines were achieved on day 40.

## 3. Discussion

Much effort has been devoted to developing vaccines against nicotine, but so far there is no commercialized nicotine vaccine. Nicotine is non-immunogenic by itself; it has to be conjugated to

carrier proteins in order to elicit immune response. [13] The nicotine hapten used in this study is rac-trans 3'-hydroxymethylnicotine hemisuccinate, which possesses a carboxyl sidearm functional group enabling covalent link with amino group on carrier proteins. In previous studies, rac-trans 3'-hydroxymethylnicotine hemisuccinate coupled to human serum albumin and KLH was found to generate highly effective antibodies in rabbits. [14] Currently, most of the macromolecule carriers employed in nicotine vaccine are KLH, [3] recombinant exotoxin A (rEPA), [15] tetanus toxoid (TT), [16] and some virus like particles. [17] However, none of them has yielded a clinically approved nicotine vaccine to date. The limited success might be attributed to the fast degradation of carrier proteins by enzymes and its rapid nonspecific clearance by human body. In this study, we attempt to demonstrate the feasibility of using nano-lipoplex particle as a delivery system for nicotine vaccine development. BSA was used as a model carrier protein, and it recently has been shown to be effective as a carrier protein in vaccines development. The anti-cancer vaccine, in which BSA was conjugated with 3'-fluoro-TF antigen-MUC1, was able to generate high titers of antibodies which could specifically bind to the tumor-associated glycopeptide antigen analog. [18] In another vaccine against malaria, Asn-Ala-Asn-Pro (NANP) repeats were bound to BSA, and the resulting immunogens were able to elicit satisfying titers of antibodies against circumsporozoite protein. [19]

In this study, DOTAP was chosen as the major constituent of liposome, largely due to the fact that cationic liposomes promote a "depot effect" that facilitates antigen uptake. [20] Cationic liposomes have long been established to have immunostimulatory effect due to their active interaction with cells which usually possess negative charges, and such an interaction induces adsorptive endocytosis.[21] In addition, it was proven that cationic liposomes consisting of DOTAP and DOTMA could significantly enhance dendritic cell (DC) maturation by up regulating the expression of CD80 and CD86. [22] Furthermore, liposomes with diameters less than 500 nm were shown to efficiently enhance immunogenic performance of liposome vaccines over large liposomes (>500 nm). [23] Therefore, the

size of liposomes produced in this study was designed to be around 200 nm. Polyethylene glycol (PEG), a biocompatible and hydrophilic polymer, was utilized to provide a hydrophilic protective layer outside drugs that can prevent nonspecific absorption of serum protein and avoid clearance by RES, thereby prolonging the blood circulation time of drugs. [8] PEG(2000) incorporated into cationic liposomes has two important roles: first, PEG moiety is able to prevent particle aggregation, stretch the circulation time of liposomes by lowering adsorption of plasma proteins, reducing RES uptake, and thus improve the immunogenicity of cationic liposomes; second, it would be easier for maleimide, which is linked to the long chain of PEG(2000), to react with sulfhydryl-bearing BSA. Though some amine groups on BSA have been consumed during Nic-BSA conjugation, considerable amount of Nic-BSA was still conjugated to liposomes when the ratio between maleimide and Nic-BSA was increased, showing the high conjugation efficiency between maleimide and -SH groups on the protein.

In mice immunization, NBL with Alum achieved higher NicAb titer compared with either NBL without Alum or Nic-BSA+Alum. NicAb titers are essential to the efficacy of Nic vaccine, because higher titers of antibody are expected to bind more nicotine molecules in the periphery, and thus reduce the amount of nicotine entering brain. [24] Aluminum has been commonly used as an adjuvant in many vaccines licensed by the US Food and Drug Administration. [25] Adding Alum adjuvant to NBL significantly enhanced the immunogenicity of the vaccine, which was shown by the higher titers of NBL+Alum compared to NBL without Alum after the first boost injection. The significant difference in titers of NicAb induced by NBL alone and Nic-BSA+Alum suggested the remarkable immune-stimulating effect of nano-lipoplex.

Though the results of this current work proved the impressive ability of nano-lipoplex to enhance the immunogenicity of small and simple molecules such as nicotine hapten, numerous questions still need to be answered in order to improve this hapten delivery system. First, the carrier

protein used here is a model protein, BSA, which is not clinically approved. Therefore, it is necessary to search for substituting carrier proteins which are both medically acceptable and immunologically effective. Second, nicotine epitope density for NBL nanoparticles was not sufficiently optimized. Theoretically, the more nicotine epitope each NBL nanoparticle contains, the higher probability that the vaccine can be recognized by B cell receptors, and the higher chance that nicotine specific naïve B cell will be activated. In this study, epitope density was dictated by the number of Nic that was conjugated to BSA and the incorporation efficiency of BSA to liposome. Therefore, further work will be needed to optimized the experimental conditions in the above two sides to increase nicotine epitope density. Third, only titers of antibody were evaluated in this study. Further work needs to test the affinity of NicAb to nicotine and the specificity of those antibodies to nicotine. Fourth, this lipoplex could be further modified to enhance antibody response, for example targeting molecule can be associated with nano-lipoplex to specifically target the delivery system to immune cells.

To summarize, in this study, a novel nicotine vaccine using lipoplex nanoparticle as a delivery system was developed. The formation of this vaccine was realized through two major steps: first, nicotine haptens were covalently linked to BSA using EDC; second, the Nic-BSA was conjugated to cationic liposome via reaction between maleimide group in liposome and sulfhydryl group in BSA. By adjusting the molar ratio between Nic and BSA or between Nic-BSA and maleimide, we could flexibly control the amount of Nic loaded onto this vaccine nanoparticle. The physiochemical properties of this vaccine were characterized using TEM, zetasizer, and flow cytometer. As a proof of concept study, the results from animal test showed that nicotine vaccine using lipoplex as the delivery vehicle achieved significantly higher titer of anti-nicotine antibody than vaccine delivered by carrier protein alone. In future work, BSA will be replaced with some clinically approved carrier proteins such as rEPA, TT, and the specificity and affinity of generated antibodies to nicotine molecule will be evaluated.

## *4.* Materials and methods

### 4.1 Materials

DOTAP (CAT#: 890890C) in chloroform and DSPE-PEG(2000)-maleimide (CAT#: 880126) in chloroform were purchased from Avanti Polar Lipids, Inc. (Alabaster, AL). 2,4,6-trinitrobenzene-1-sulfonic acid (TNBS) (CAT#: P2297), N-(3-dimethylaminopropyl)-N'-ethylcarbodiimide hydrochloride (EDC) (CAT#: E6383), BSA (CAT#: A2153), and 2-iminothiolane hydrochloride (Traut's reagent) (CAT#: I6256), Rhodamine B isothiocyanate (CAT#: 83689), and fluorescein isothiocyanate–dextran (CAT#: F7250) were obtained from Sigma-Aldrich (St. Louis, MO). Rac-trans3'-hydroxymethylnicotine hemisuccinate (CAT#:H948190) was purchased from Toronto Research Chemicals (Toronto, Canada). The micro BCA assay kit (CAT#: 23235) was purchased from Thermo Scientific (Waltham, MA). All other chemicals and reagents were purchased from Fisher Scientific (Pittsburg, PA) and are of analytical grade.

### 4.2 Preparation of cationic liposome

Cationic liposomes were prepared according to the method described by Huang and Zhang. [26] In brief, lipid film consisting of 1.96 mg DOTAP and DSPE-PEG(2000)-maleimide ranging from 0.04 mg to 0.32 mg was hydrated with buffer containing 0.9% NaCl, 5% dextrose, and 10% sucrose in Tris-HCl buffer (0.05 M Tris Base, pH 7.4). The resulting suspension was incubated at 65 °C for one hour and extruded through polycarbonate membrane with pore sizes of 100 nm for 14 times. For FITC labeled liposomes, FITC and lipids at molar ratio of 1:10 was extruded according to the above method.

### 4.3 Synthesis of nicotine-BSA conjugates (Scheme 2 Step Ⅰ)

Ten milligrams of EDC dissolved in 700 µL DI water was mixed with appropriate volume of 100 mg/mL Nic also dissolved in DI water. After incubation at 0 °C for 10 minutes, the mixture was added with 10 mg BSA (40 mg/mL) and appropriate volume of DI water to a total volume of 1 mL, and stirred at room temperature for 12 hours. The pH of the DI water used in this step was adjusted to 6.76 with 0.01

M sodium hydroxide. The resulting Nic-BSA was purified by size exclusion chromatography with a Sephadex G-25 column using an AKTA FPLC system (Amersham Biosciences, Piscataway, NJ). Briefly, 0.5 mL sample was loaded onto the column, followed by elution using phosphate buffered saline (PBS) (0.1 M, pH 7.4) as the mobile phase at 1 mL/min. Nic-BSA was collected and concentrated to 1 mg/mL using Microcon centrifugal filter units (50,000 MWCO) from EMD Millipore (Billerica, MA,). The Rhod B labeled BSA was synthesized using the same method as Nic-BSA conjugation, except the molecular ratio between BSA and Rhod B was 50:1.

### 4.4 Quantifying the number of Nic hapten on Nic-BSA

The number of Nic haptens on Nic-BSA was determined by measuring difference in the number of unreacted lysine groups on surface of BSA before and after conjugation using TNBS. In brief, 200 µL of Nic-BSA mixed with 200 µL of 4% $NaHCO_3$ solution was added with 200 µL of 0.1% TNBS solution, and the resulting mixture was incubated for 1 h at 37 °C. The color of the solution was read at 335 nm. The quantity of $-NH_2$ groups consumed during conjugation of Nic to BSA was calculated from the difference between the O.D. of the control and the conjugate. [27]

### 4.5 Loading Nic-BSA onto liposomes

Thiol groups were introduced to Nic-BSA by incubating Nic-BSA obtained in the previous step with 1 mg/mL of Traut's reagent for one hour in darkness under continuous stirring (**Scheme 2 StepII**). The thiolated Nic-BSA was purified using FPLC as described for Nic-BSA purification and concentrated to 2 mg/mL in PBS (0.1 M, pH 7.4) by Microcon centrifugal filter units (50,000 MWCO). The amount of thiol groups on BSA was quantified through a colorimetric sulfhydryl assay using Ellman's reagent (5,5'-dithiobis(2-nitrobenzoic acid). [28] Briefly, 80 µL of 4 mg/mL Ellman's reagent was added to 800 µL of thiolated Nic-BSA, and the mixture was incubated at room temperature for 15 minutes. Free sulfhydryl levels were determined from the absorbance at 412 nm using the following formula generated from a

set of cysteine standards: $SH=1.1A_{412}/ 14398C_{Nic\text{-}BSA}$,where $A_{412}$ is the absorbance at 412nm, $C_{Nic\text{-}BSA}$ is the protein concentration and SH is the number of thiol equivalents. 125 µL Mal-PEG-liposome, 450 µL thiolated Nic-BSA conjugates, and 425 µL 0.15M NaCl-0.2mM EDTA (pH 7.4) were mixed to form Nic-BSA-Liposome (**Scheme 2 Step Ⅲ**). The resulting Nic-BSA-Liposome was purified by dialysis using dialysis membrane (MWCO 1000 kD) from Spectrum Laboratories (Rancho Dominguez, CA) in 10 mM NaCl.

### 4.6 Measuring the amount of Nic-BSA loaded to liposomes

Nic-BSA associated with liposomes was assayed using a modified protocol described by Steven M. Ansell.[29] In detail, 20 µL of prepared liposomes (before/after purification) were withdrawn and diluted with 1 ml 0.15M pH 7.4 NaCl solution (working-dispersion). To assess the total and conjugated protein concentration, 500 µL of working-dispersion was mixed with 100 µL of 5% (v/v) Triton X-100 and this dispersion was maintained at 65°C for 5 min to disrupt all the vesicles. Both total and conjugated Nic-BSA concentrations were assessed using micro BCA protein assay kit from Pierce. The association efficiency of Nic-BSA to liposomes was calculated according to the following equation: Association efficiency (%) = $BSA_{conjugated}/BSA_{Total}\times100$.

### 4.7 DLS analysis

The sizes of NBL nanoparticles were evaluated using DLS. DLS measurements were performed using a Malvern Nano-ZS zetasizer (Malvern Instruments Ltd, Worcestershire, United Kingdom). Newly prepared samples were diluted by 10 fold with 0.9% sodium chloride saline (pH 7.4) and each measurement was done in triplicate.

### 4.8 Zeta potential measurements

Freshly made NBLs were diluted by 10 fold with deionized water (pH 7.0) and zeta potential of these samples was measured with the Malvern Nano ZS using the technique of Laser Doppler Velocimetry (LDV). Zeta potential was measured six times for each sample. [30]

### 4.9 TEM analysis of liposome

Sample grids (carbon coated copper) were put into one drop of liposome for 30 s, then in distilled water drop for washing (10 s) and finally in a phosphotungstic acid drop for staining (10 s).[30] The excessive stain on the grids was removed using filter paper. The prepared grids were analyzed by Morgagni™ Transmission Electron Microscope.

### 4.10 Active immunization of mice with nicotine vaccines

All animal studies were carried out following the National Institutes of Health guidelines for animal care and use. Animal protocols were approved by the Institutional Animal Care and Use Committee at Virginia Polytechnic Institute and State University. Groups of 8 female BALB/c mice (6−7 weeks, 16−20 g) were immunized by subcutaneous (s.c.) injection on days 0, 14, and 28 with Nic-BSA conjugates, Nic-BSA-liposome conjugates (50 μg for Nic-BSA) in 0.9% sodium chloride saline with Imject Alum Adjuvant (Pierce Biotechnology Inc., Rockford, IL) or Nic-BSA-liposome conjugates (50 μg for Nic-BSA) without Alum adjuvant (total volume was 100 μl). Following vaccine administration, blood samples (～200 μl) were collected on days 0, 13, 27, 33, 40 via retroorbital puncture from each mouse. Sera (100μl for each sample) centrifuged from blood were stored at −80 °C.

### 4.11 ELISA measurement

Mice sera were analyzed according to the ELISA procedure described by de Villiers et al. (2010) with appropriate modification. [3] Nic was conjugated to KLH using the same method for Nic-BSA conjugate. Nic-KLH was used as coating material to prevent nonspecific binding of BSA and liposome derived antibodies. ELISA-plates were coated with 100 μL of 10 μg/mL Nic-KLH conjugate at 25 °C for 5 h. The plates were washed with washing buffer for 4 times and DI water for 2 times, and were blocked with 300 μL non-protein blocking buffer from Pierce for 12 h. After washing, 100 μL of each dilution (1:25, 1:125, 1:625, 1:3125, 1:15625, and 1:78125) of serum from each mouse was incubated in plates at

25 °C for 2 h. The plates were washed again, and incubated with 100 µL anti-mouse IgG HRP (1:10000) from Sigma-Aldrich for 1 h. After washing as before, 100 µL of TMB One Component Microwell Substrate was added into each well and incubated for 10 min, and the reaction was stopped by adding 100 µL of 0.5% (v/v) $H_2SO_4$. The absorbance for each well at 450 nm was recorded. Titer was defined as the dilution factor at which $OD_{450}$ fell to half of the maximal.

### 4.12 Data analysis

Serum NicAb concentrations were compared among groups using one way ANOVA and comparisons among paired groups were analyzed with Tukey's HSD. The difference is considered as significant when P-value is less than 0.05. Each measurement was carried out at least three times, and the results were expressed as mean ± standard deviation.

**Acknowledgement**

Thank Dr. Debbie Kelly and her group members from VTCRI for taking TEM images of liposomes for this paper. We also thank Dr. Paul Pentel for providing us with Nic-KLH used in the ELISA analyses. This work was financially supported by National Institute on Drug Abuse (R21 DA030083).

## References

[1] Mackay J. The global epidemiology of tobacco and related chronic diseases. Public Health. 2012;126:199-201.

[2] Messer K, Trinidad DR, Al-Delaimy WK, Pierce JP. Smoking cessation rates in the United States: a comparison of young adult and older smokers. American Journal of Public Health. 2008;98:317-22.

[3] de Villiers SH, Lindblom N, Kalayanov G, Gordon S, Baraznenok I, Malmerfelt A, et al. Nicotine hapten structure, antibody selectivity and effect relationships: results from a nicotine vaccine screening procedure. Vaccine. 2010;28:2161-8.

[4] Sanderson SD, Cheruku SR, Padmanilayam MP, Vennerstrom JL, Thiele GM, Palmatier MI, et al. Immunization to nicotine with a peptide-based vaccine composed of a conformationally biased agonist of C5a as a molecular adjuvant. International Immunopharmacology. 2003;3:137-46.

[5] Raupach T, Hoogsteder PH, Onno van Schayck CP. Nicotine vaccines to assist with smoking cessation: current status of research. Drugs. 2012;72:e1-16.

[6] Manolova V, Flace A, Bauer M, Schwarz K, Saudan P, Bachmann MF. Nanoparticles target distinct dendritic cell populations according to their size. European Journal of Immunology. 2008;38:1404-13.

[7] Petrovsky N, Aguilar JC. Vaccine adjuvants: current state and future trends. Immunology and Cell Biology. 2004;82:488-96.

[8] Zhuang Y, Ma Y, Wang C, Hai L, Yan C, Zhang Y, et al. PEGylated cationic liposomes robustly augment vaccine-induced immune responses: role of lymphatic trafficking and biodistribution. Journal of Controlled Release. 2012;159:135-42.

[9] Alving CR. Liposomes as carriers of antigens and adjuvants. Journal of Immunological Methods. 1991;140:1-13.

[10] Wieber A, Selzer T, Kreuter J. Physico-chemical characterisation of cationic DOTAP liposomes as drug delivery system for a hydrophilic decapeptide before and after freeze-drying. European Journal of Pharmaceutics and Biopharmaceutics. 2012;80:358-67.

[11] Henriksen-Lacey M, Christensen D, Bramwell VW, Lindenstrom T, Agger EM, Andersen P, et al. Liposomal cationic charge and antigen adsorption are important properties for the efficient deposition of antigen at the injection site and ability of the vaccine to induce a CMI response. Journal of Controlled Release. 2010;145:102-8.

[12] Huang W, Zhang C. Assembly and characterization of lipid-lipid binding protein particles. Journal of Biotechnology. 2011;154:60-7.

[13] Pravetoni M, Keyler DE, Pidaparthi RR, Carroll FI, Runyon SP, Murtaugh MP, et al. Structurally distinct nicotine immunogens elicit antibodies with non-overlapping specificities. Biochemical Pharmacology. 2012;83:543-50.

[14] Langone JJ, Gjika HB, Van Vunakis H. Nicotine and its metabolites. Radioimmunoassays for nicotine and cotinine. Biochemistry. 1973;12:5025-30.

[15] Kamaly N, Xiao Z, Valencia PM, Radovic-Moreno AF, Farokhzad OC. Targeted polymeric therapeutic nanoparticles: design, development and clinical translation. Chemical Society Reviews. 2012;41:2971-3010.

[16] Moreno AY, Azar MR, Warren NA, Dickerson TJ, Koob GF, Janda KD. A critical evaluation of a nicotine vaccine within a self-administration behavioral model. Molecular Pharmaceutics. 2010;7:431-41.

[17] Polosa R, Benowitz NL. Treatment of nicotine addiction: present therapeutic options and pipeline developments. Trends in Pharmacological Sciences. 2011;32:281-9.

[18] Hoffmann-Roder A, Johannes M. Synthesis of a MUC1-glycopeptide-BSA conjugate vaccine bearing the 3'-deoxy-3'-fluoro-Thomsen-Friedenreich antigen. Chemical Communications. 2011;47:9903-5.

[19] Kubler-Kielb J, Majadly F, Biesova Z, Mocca CP, Guo C, Nussenzweig R, et al. A bicomponent Plasmodium falciparum investigational vaccine composed of protein-peptide conjugates. Proceedings of the National Academy of Sciences of the United States of America. 2010;107:1172-7.

[20] Kaur R, Bramwell VW, Kirby DJ, Perrie Y. Pegylation of DDA:TDB liposomal adjuvants reduces the vaccine depot effect and alters the Th1/Th2 immune responses. Journal of Controlled Release. 2012;158:72-7.

[21] Ma Y, Zhuang Y, Xie X, Wang C, Wang F, Zhou D, et al. The role of surface charge density in cationic liposome-promoted dendritic cell maturation and vaccine-induced immune responses. Nanoscale. 2011;3:2307-14.

[22] Vangasseri DP, Cui Z, Chen W, Hokey DA, Falo LD, Jr., Huang L. Immunostimulation of dendritic cells by cationic liposomes. Molecular Membrane Biology. 2006;23:385-95.

[23] Carstens MG, Camps MG, Henriksen-Lacey M, Franken K, Ottenhoff TH, Perrie Y, et al. Effect of vesicle size on tissue localization and immunogenicity of liposomal DNA vaccines. Vaccine. 2011;29:4761-70.

[24] Itano AA, Jenkins MK. Antigen presentation to naive CD4 T cells in the lymph node. Nature Immunology. 2003;4:733-9.

[25] Baylor NW, Egan W, Richman P. Aluminum salts in vaccines--US perspective. Vaccine. 2002;20 Suppl 3:S18-23.

[26] Huang W, Zhang J, Dorn HC, Geohegan D, Zhang C. Assembly of single-walled carbon nanohorn supported liposome particles. Bioconjugate Chemistry. 2011;22:1012-6.

[27] Singh KV, Kaur J, Varshney GC, Raje M, Suri CR. Synthesis and characterization of hapten-protein conjugates for antibody production against small molecules. Bioconjugate Chemistry. 2004;15:168-73.

[28] Ansell SM, Tardi PG, Buchkowsky SS. 3-(2-pyridyldithio)propionic acid hydrazide as a cross-linker in the formation of liposome-antibody conjugates. Bioconjugate Chemistry. 1996;7:490-6.

[29] Ansell SM, Harasym TO, Tardi PG, Buchkowsky SS, Bally MB, Cullis PR. Antibody conjugation methods for active targeting of liposomes. Methods in Molecular Medicine. 2000;25:51-68.

[30] Kaszuba M, Corbett J, Watson FM, Jones A. High-concentration zeta potential measurements using light-scattering techniques. Philosophical transactions Series A, Mathematical, Physical, and Engineering Sciences. 2010;368:4439-51.

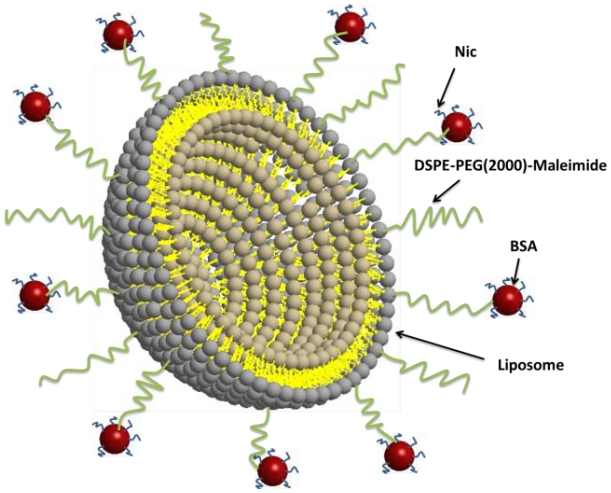


**Scheme 1.** Illustration of lipoplex based nicotine vaccine.

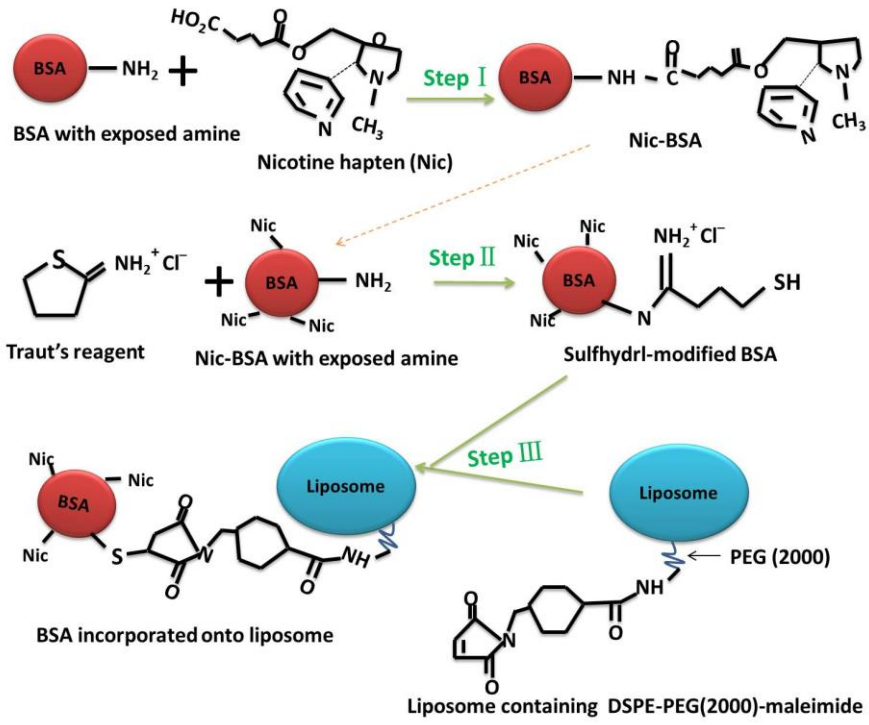


**Scheme 2.** Illustration of NBL vaccine synthesis.

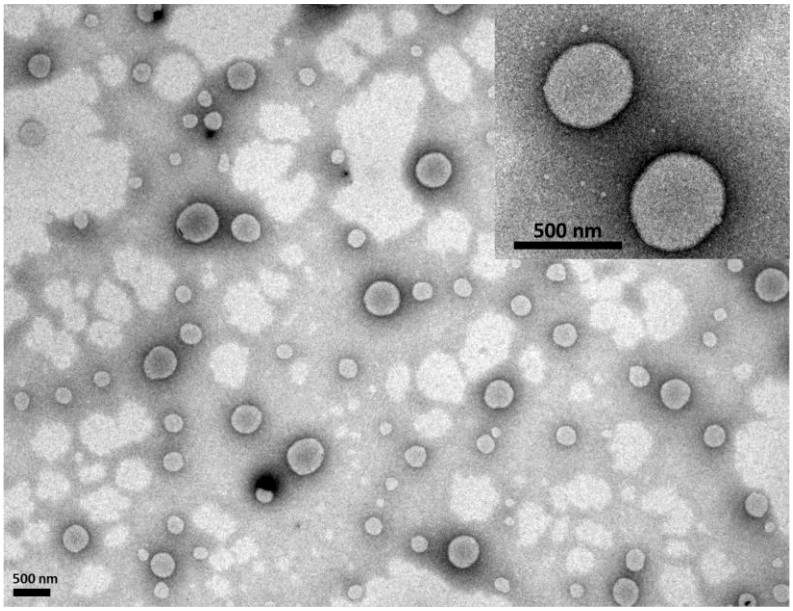


**Figure 1.** TEM image of liposome.

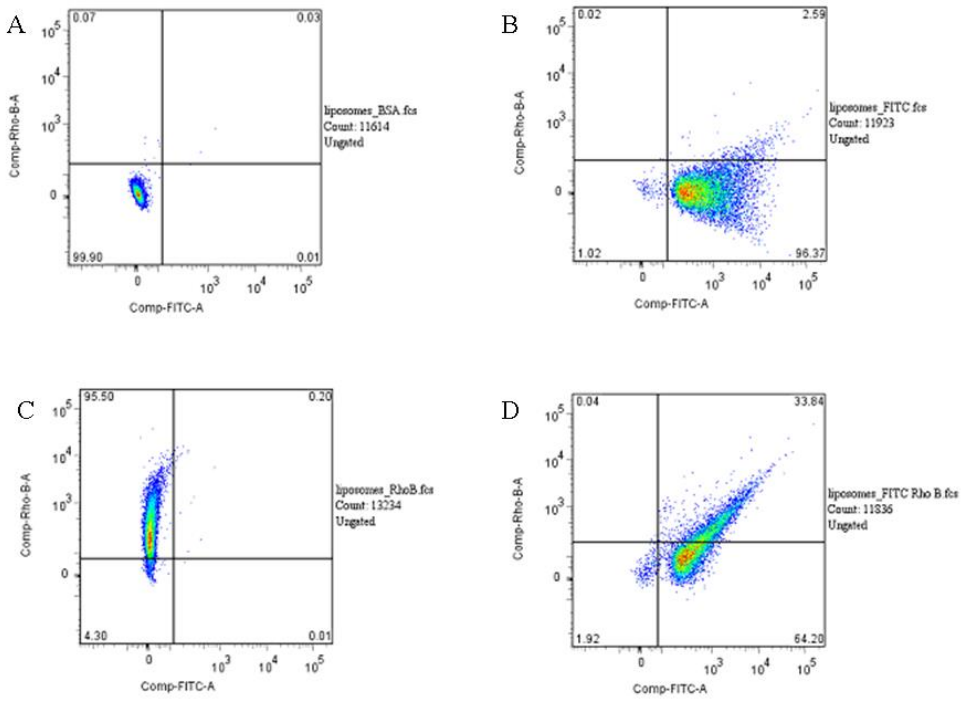


**Figure 2.** Flow cytometric analysis of BSA-liposome complex. (A) BSA-Liposome without labeling; (B) FITC labeled liposome; (C) Rhod B-BSA-Liposome; (D) Rhod B-BSA-FITC-liposome.

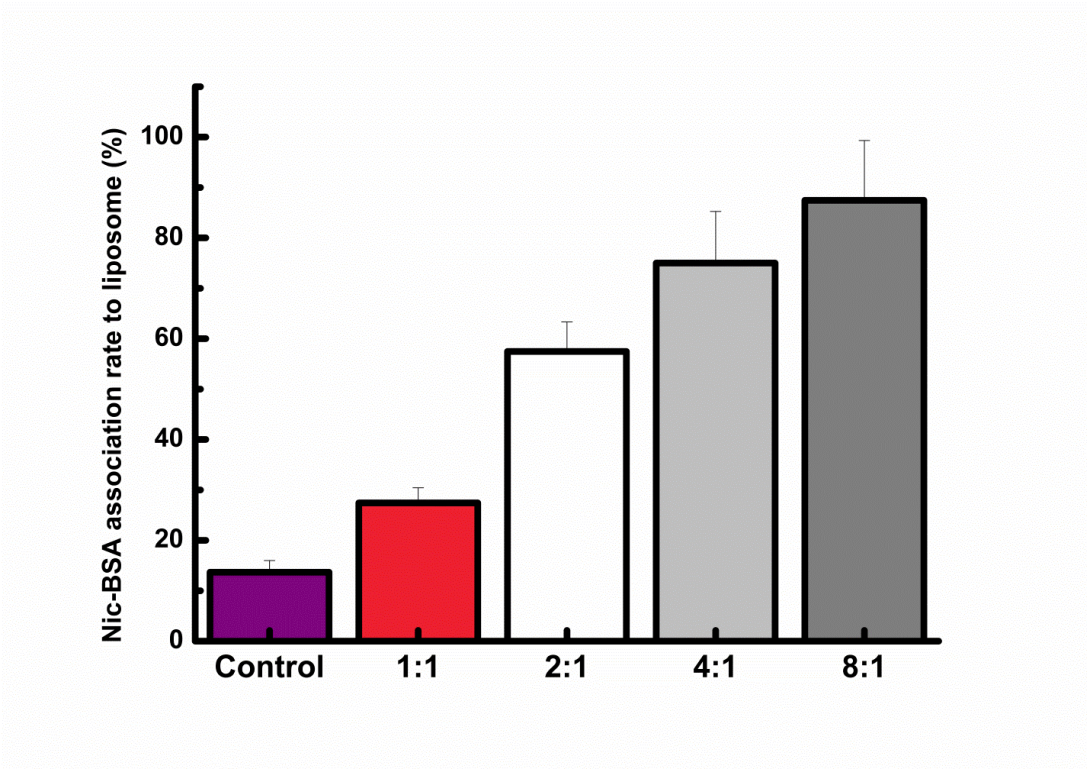


**Figure 3.** Association efficiency of Nic-BSA to liposome at maleimide/ Nic-BSA molar ratio of 0, 1:1, 2:1, 4:1, 8:1, respectively.

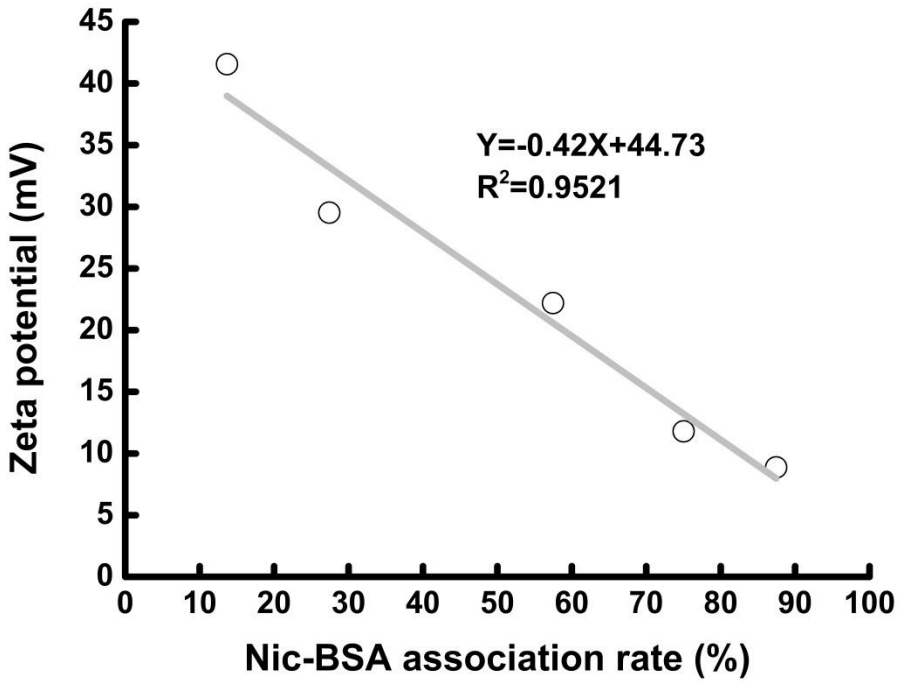


**Figure 4.** The relationship between association efficiency of Nic-BSA to liposome and charge of Nic-BSA-liposome complex.

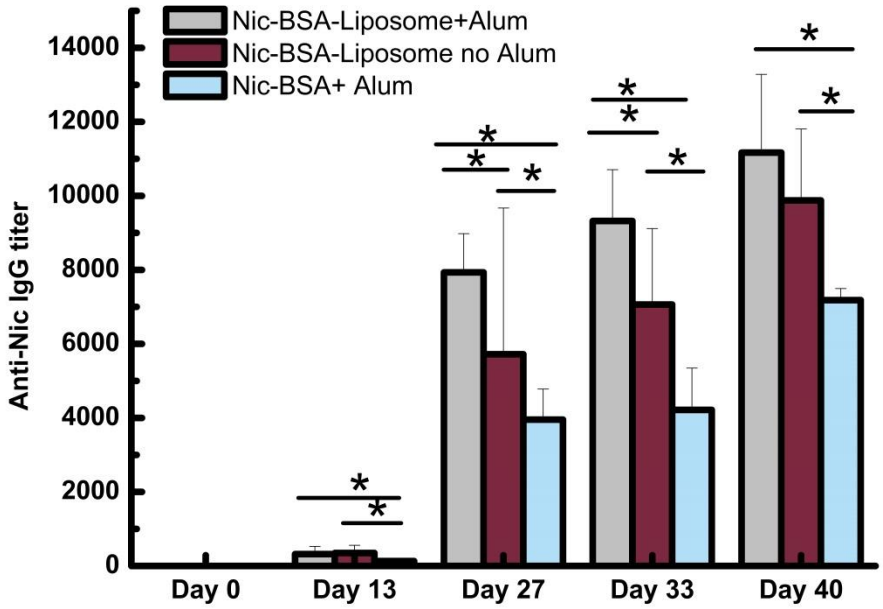


**Figure 5.** Time course of nicotine specific antibodies elicited by Nic-BSA-liposome+Alum, Nic-BSA-liposome without Alum, and Nic-BSA+Alum (* means P-value < 0.05).

**Table 1.** The coupling efficiency of Nic to BSA at various molar ratios.

| Molar ratio of BSA/Nic | Amino groups on BSA consumed (%) | Number of Nic conjugatedto BSA |
|---|---|---|
| **1:10** | 0.0 | 0.0 |
| **1:20** | 0.0 | 0.0 |
| **1:50** | 26.0 | 15 |
| **1:100** | 30.0 | 18 |
| **1:200** | 30.0 | 18 |

**Table 2.** The degree of Nic-BSA thiolation at different molar ratio of Nic-BSA/Traut's reagent.

| BSA : Nic (Molar ratio) | Nic-BSA : Traut's reagent (Molar ratio ) | Thiol equivalents coupled to BSA |
|---|---|---|
| **1:50** | 1:200 | 6 |
| **1:50** | 1:500 | 8 |

**Table 3.** Comparison of size and surface-charge of Nic-BSA-liposmes with different ratios of DSPE-PEG(2000)-Maleimide and DOTAP (mean ± S.D.; n=3).

| DSPE-PEG(2000)-Maleimide : DOTAP(% ) | Zeta potential(mV) | Size(nm) | Polydispersity |
|---|---|---|---|
| **0.5** | 29.53±1.29 | 276.97±6.66 | 0.20± 0.02 |
| **1** | 22.20±0.98 | 271.33±4.33 | 0.23± 0.02 |
| **2** | 11.80±0.75 | 254.67±2.21 | 0.19± 0.02 |
| **4** | 8.88±0.85 | 178.67±4.16 | 0.14± 0.03 |

## Chapter IV (results): Negatively charged carbon nanohorn supported cationic liposome nanoparticles: a novel delivery vehicle for anti-nicotine vaccine

Hong Zheng,[1]* Yun Hu,[1]* Wei Huang,[1] Sabina de Villiers,[2,3] Paul Pentel,[2] Jianfei Zhang,[4] Harry Dorn,[4] Marion Ehrich,[5] Chenming Zhang[1]†

1. Department of Biological Systems Engineering, Virginia Tech, Blacksburg, VA 24061

2. Minneapolis Medical Research Foundation, Minneapolis, MN 55404

3. Department of Physiology and Pharmacology, Karolinska Institute, Stockholm, Sweden

4. Department of Chemistry, Virginia Tech, Blacksburg, VA 24061

5. Department of Biomedical Sciences & Pathobiology, Virginia Tech, Blacksburg, VA 24061

†Correspondence to:

Chenming (Mike) Zhang

210 Seitz Hall

Dept. of Biological Systems Engineering

Virginia Tech

Blacksburg, VA 24061

(540) 231-7601

Chzhang2@vt.edu

*These authors contributed equally to this work.

This paper has been accepted for publication in Journal of Biomedical Nanotechnology 2015, 11:1-14.



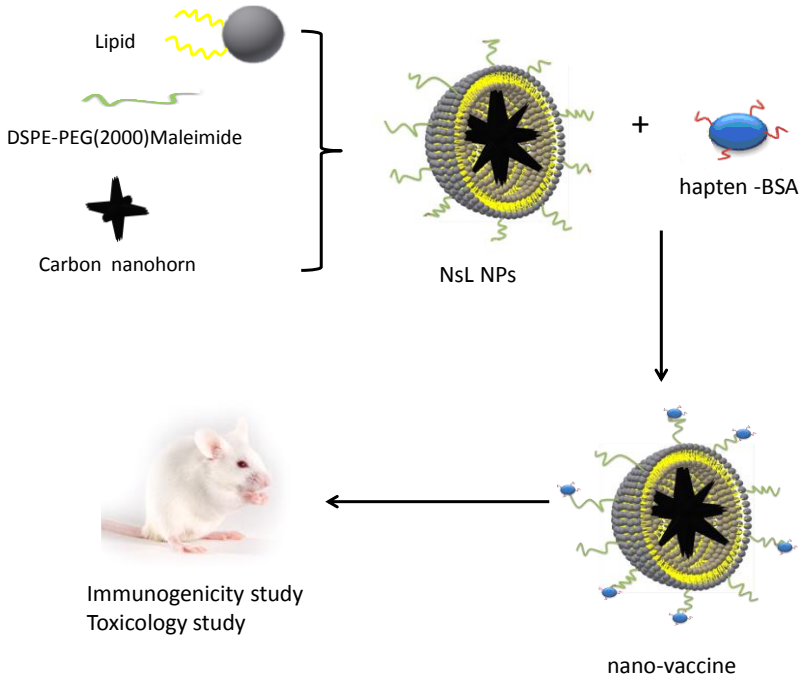


**Abstract**

Tobacco addiction is the second-leading cause of death in the world. Due to the nature of nicotine (a small molecule), finding ways to combat nicotine's deleterious effects has been a constant challenge to the society and the medical field. In the present work, a novel anti-nicotine vaccine based on nanohorn supported liposome nanoparticles (NsL NPs) was developed. The nano-vaccine was constructed by using negatively charged carbon nanohorns as a scaffold for the assembly of cationic liposomes, which allow the conjugation of hapten conjugated carrier proteins. The assembled bio-nanoparticles are stable. Mice were immunized subcutaneously with the nano-vaccine, which induced high titer and high affinity of nicotine specific antibodies in mice. Furthermore, no evidence of clinical

signs or systemic toxicity followed multiple administrations of NsL-based anti-nicotine vaccine. These results suggest that NsL-based anti-nicotine vaccine is a promising candidate in treating nicotine dependence and could have potential to significantly contribute to smoking cessation.

**Keywords**

Nicotine; nicotine vaccine; anti-nicotine; bionanoparticle; carbon nanohorn; nano-vaccine.

## 1. Introduction

Tobacco addiction is the second-leading cause of death in the world. [1, 2] How to help smokers to quit smoking has been a constant challenge to medical scientists. To date, three medications are FDA-approved for smoking cessation: nicotine replacement therapy, sustained-release bupropion, and varenicline. [3, 4] Despite the relative efficacy of these first-line medications, long-term abstinence rates remain disappointingly low. [5] Clearly, more effective treatment options are needed. Immunopharmacotherapy, or vaccination, has shown tremendous promise in fighting against nicotine addiction. [6] Nicotine vaccines have the following advantages: 1) vaccines can have a prolonged effect on the immune system (6-12 months), and could thus reduce the relapse rates, 2) daily administration is not required; only occasional booster shots are needed to maintain an adequate antibody titer, 3) vaccines have minimal to no side effects, and 4) vaccines are potentially compatible with other smoking cessation methods. However, all current nicotine vaccines, particularly the ones that have undergone human clinical trials, demonstrated limited efficacy. [6-8] The recently released clinical trial results of NicVAX® by Nabi Biopharmaceuticals were particularly disappointing. [9] On the other hand, a recent report described a successful trial in mice treated with adeno-associated virus (AAV) vector expressing a gene encoding a full-length anti-nicotine antibody. [10] However, it is still unclear how this success can be translated to humans, and the long-term safety of the system is still a significant obstacle. Because

the success of drug vaccines appears to be directly correlated with the antibody titer in vaccinated subjects, there is a need for improved vaccines that can elicit a strong immune response. [6-10]

Over the past decade, particulate carriers have emerged as an attractive means for enhancing the delivery efficacy and potency of vaccines and associated immunomodulatory molecules. Specifically, polymer-based micro and nanoparticles are being extensively studied for this purpose. Polymeric micro and nanoparticles can carry cargo, whether antigens, adjuvants or both, either encapsulated within the particle or on the surface of the particle. They provide an efficient means for delivering antigen to antigen presenting cells (APCs), either in a passive manner through non-specific phagocytosis or in a more active manner through receptor targeting and endocytosis. The latter can be achieved by modifying the particle surface with antibodies against surface receptors of specific APC subsets e.g., DEC205 attachment for targeting to epidermal Langerhans cells. [11]

In addition to the particulate nanoparticles, proteins and peptides have demonstrated potential for being effective vaccine carriers. Protein derived particulate systems are biocompatible and degraded into natural byproducts, and they can be easily modified due to the large repertoire of amino acids with a variety of physical-chemical properties. Peptide/protein-based particles made of amino acids, denatured collagen (gelatin), and albumin have been shown to be effective in eliciting immune responses. [12-14] Moreover, liposomes, particulate structures composed largely of natural or synthetic phospholipids, can encapsulate both antigenic and immunomodulatory agents, allowing targeted delivery to specific immune cells such as dendritic cells in vivo. [15-18] Depending on their lipid composition, liposomes also may exhibit potent adjuvant-like properties. [19, 20] However, one of the main limitations of liposomes is that they are intrinsically unstable and often have a tendency to flocculate. [21]

In this study, novel negatively charged (anionic) carbon single-walled nanohorns (SWNHs) were used as a scaffold, providing support to the soft body of cationic liposomes. This support prevented the liposomes from precipitation or flocculation. The SWNHs are nontoxic, nanoparticle aggregates of single graphene tubules and are spherical dahlia-like-shaped with a narrow diameter range reported as 80-100 nm. [22-24] For this study, nanohorns with a diameter of around 100 nm were encapsulated into liposomes through a simple freeze-thaw method as described in our previous work. [25] The nanohorn supported liposome nanoparticles (NsL NPs) were used as a vaccine delivery vehicle. The hapten derivative, O-succinyl-3'-hydroxmethyl-(±) nicotine (Nic), was used as the immunogen. [26] The immunogenicity and toxicity of the nano-vaccines were studied in mice.

## *2.* Materials and methods

### 2.1. Materials

All chemicals were obtained from Sigma-Aldrich (St. Louis, MO, USA) unless otherwise noted. 1,2-dioleoyl-3-trimethylammonium-propane (DOTAP) and 1,2-distearoyl-sn-glycero-3-phosphoethanolamine-N-[maleimide(polyethylene glycol)-2000] (ammonium salt) (DSPE-PEG(2000)-Maleimide) were purchased from Avanti Polar Lipids (Alabaster, AL, USA). EDC (1-ethyl-3-[3-dimethylaminopropyl] carbodiimide) was obtained from Pierce (Rockford, IL, USA). O-succinyl-3'-hydroxmethyl-(±) nicotine (nicotine hapten) was purchased from Toronto Research Chemicals (Toronto, ON, Canada).

### 2.2. Preparation of nanohorn supported liposome nanoparticles (NsL)

NsL NPs were prepared according to the method described by Huang et al. [25] Briefly, cationic liposomes were made by extruding 1.96 mg hydrated DOTAP and 0.32 mg DSPE-PEG(2000)-maleimide lipid film through polycarbonate membranes with pore sizes of 100 nm. The hydration buffer contained 0.9% NaCl, 5% dextrose, and 10% sucrose in Tris-HCl buffer with pH at 7.4. Single-walled nanohorns

(SWNH) were synthesized by Nd:YAG laser vaporization of graphite rods in an argon atmosphere at 1100 °C. [27, 28] Negatively charged (anionic) nanohorns with carboxyl groups were prepared by high-speed vibration milling. [29] Anionic nanohorns were briefly sonicated to break up aggregates and incubated with freshly made cationic liposomes at a volume ratio of 1:4. Three freeze-and-thaw cycles were applied using -80 °C and a warm water bath (30 °C). Samples were finally centrifuged under 10,000 × g for 10 min, and nanohorn supported liposomes were collected from the top layer of the solution.

**2.3. Synthesis and Quantification of Nic-BSA conjugates**

The synthesis of Nic-BSA conjugates was based on the procedure described elsewhere. [30] Briefly, a solution of 1-ethyl-3-(3-dimethylaminopropyl) carbodiimide (EDC, 10 molar equivalents compared to nicotine hapten) in distilled H2O was added to 10 mg nicotine hapten water solution (100 mg/mL) and kept at 0 °C for 10 min. The solution was then mixed with 10 mg bovine serum albumin (BSA) solution (40 mg/mL) and an appropriate amount of distilled water to prepare a total volume of 1 mL. The solution was stirred at 0 °C for 10 min, and stored at room temperature overnight. During this step, pH was checked and adjusted to 6.76 with 0.01 M sodium hydroxide if needed. Nic-BSA conjugates were purified by size exclusion chromatography with a Sephadex G-25 column using an AKTA FPLC system (GE Healthcare, Piscataway, NJ). Nic-BSA was then concentrated to 1 mg/mL using Microcon centrifugal filter units (EMD Millipore Corporation, Billerica, MA) with a 50,000 molecular weight cut-off (MWCO). The number of -NH2 groups used during conjugation of hapten to BSA molecules was determined from the difference between the optical density of the control and the conjugate by a method utilizing 2,4,6-trinitrobenzene-1-sulfonic acid (TNBS). [31]

**2.4. Thiolation of Nic-BSA conjugates**

Thiol groups were introduced to Nic-BSA by incubating Nic-BSA obtained in the previous step with 1 mg/mL of 2-iminothiolane (Traut's reagent) for one hour in darkness under continuous stirring.

[32] The thiolated Nic-BSA was purified using FPLC as described for Nic-BSA purification and concentrated to 2 mg/mL in phosphate buffered saline (PBS, pH 7.4) by Microcon centrifugal filter units (50,000 MWCO). The amount of thiol groups on BSA was quantified by a colorimetric sulfhydryl assay using Ellman's reagent (5,5'-dithiobis(2-nitrobenzoic acid). [33] Briefly, Ellman's reagent (80 µL of a 4 mg/mL solution in PBS) was added to 0.6 mL aliquots of a control and the samples and allowed to incubate at room temperature for 20 min. Sulfhydryl levels were determined from the absorbance at 412 nm (ε = 14398) using the equation,

SH=1.1A412/ 14398CNic-BSA

where A412 is the absorbance at 412 nm, CNic-BSA is the protein concentration, and SH is the number of thiol equivalents.

**2.5. Conjugation of thiolated Nic-BSA to NsL**

The thiolated Nic-BSA was mixed with the maleimide-PEG–containing nanohorn supported liposomes in 0.15 M NaCl, 0.2 mM EDTA (pH 7.4) at a molar ratio of 1:8 and allowed to react overnight. Unbound protein was separated from the liposomes by dialysis using dialysis membrane (MWCO 1000 kD) from Spectrum Laboratories in 0.15 M NaCl pH 7.4 solution. Nic-BSA associated with liposomes was assayed using a modified protocol described by Ansell. [34] Briefly, 20 µL of prepared liposomes (before and after purification) were diluted with 1 mL 0.15 M NaCl pH 7.4 solution (working dispersion). To assess the total and conjugated protein concentration, 500 µL of working dispersion were mixed with 100 µL of 5% (v/v) Triton X-100, and this mixture was maintained at 65 °C for 5 min to disrupt all lipid vesicles. Both total and conjugated Nic-BSA concentrations were measured using a micro BCA protein assay kit from Pierce (Rockford, IL). The association efficiency (AE) and the loading capacity (LC) of Nic-BSA to nanohorn supported liposomes were calculated according to the following equations: AE(%) = Nic-BSAconjugated/Nic-BSATotal×100%; LC(%) = Nic-BSAconjugated /NPs×100%.

### 2.6. Characterization of NPs

#### 2.6.1. Dynamic light scattering (DLS) and zeta-potential

Particle sizes and distribution of the nanohorn, liposomes, NsL and Nic-BSA-NsL were measured by photon correlation spectroscopy (PCS) using a Zetasizer Nano (Malvern Instruments, UK). Prior to the DLS measurement, each sample was diluted with 0.15 M NaCl pH 7.4 solution until a measurable concentration of particles was achieved. Similarly, the zeta potential of the samples was measured using the same equipment with Laser Doppler Velocimetry. [35] Both measurements were repeated three times for each sample.

#### 2.6.2. Transmission electron microscopy (TEM)

Sample grids (carbon coated copper) were put into one drop of liposomes for 30 s, then in a distilled water drop for washing (10 s) and finally in a phosphotungstic acid drop for staining (10 s). [36] The excessive stain on the grids was removed using filter paper. The prepared grids were analyzed using a Morgagni™ Transmission Electron Microscope (FEI Corporate, Hillsboro, OR).

#### 2.6.3. Stability of NsL NPs

Stability was monitored using imaging of fluorescent dyes encapsulated following a published method. [37] Briefly, lipid films containing 1.96 mg 1,2-dioleoyl-3-trimethylammonium-propane (DOTAP) and 0.2 mg fluorescein isothiocyanate (FITC) isomer I (molar ratio, 100:2) were hydrated with 250 µL of hydration buffer (section 2.2). The resulting emulsion was incubated at 65 °C for one hour and extruded 14 times through polycarbonate membranes with pore sizes of 100 nm. For nanohorn supported liposomes, the FITC labeled liposomes underwent 5 cycles of freeze-and-thaw at -80 °C and 35 °C when 62.5 µL of a nanohorn solution (1 mg/mL) were added. The resulting mixture was centrifuged at 16,000 × g for 30 min, and the nanohorn supported liposomes were collected from the top layer of the solution. Excessive FITC in both liposomes and nanohorn liposomes was removed by 24 h of dialysis using 100 kD

Biotech CE Dialysis Tubing (Spectrum Laboratories, Inc., Rancho Dominguez, CA, USA) in distilled water. Morphology was viewed on a LSM510 confocal laser scanning microscope (Carl Zeiss Inc, Thornwood, NY, USA).

### 2.7. Vaccination

#### 2.7.1. Immunization procedures

All animal studies were carried out following the National Institutes of Health (NIH) guidelines for animal care and use. Animal protocols were approved by the Institutional Animal Care and Use Committee at Virginia Polytechnic Institute and State University. Female Balb/c mice (6-7 weeks, 16-20 g, 8 per group) were randomized into vaccine and control groups. The immunization schedules and administration doses are shown in Table 1. Vaccine groups (Groups 1-5) were immunized subcutaneously (s.c.) with 100 µL of a saline suspension of Nic-BSA conjugates, or Nic-BSA-liposome conjugates or Nic-BSA-nanohorn-liposome conjugates mixed with or without Alum adjuvant (3 mg, Imject, Pierce Biotechnology Inc., Rockford, IL). Control groups (Groups 6 and 7) received liposomes or nanohorn-supported-liposomes formulated with Alum (3mg) in 100 µL saline. All mice were immunized with three injections, given on day 0 with booster immunizations on days 14 and 28. Antibody titers were monitored following vaccine administration using blood samples (～200 µL) taken on days 0, 13, 27, 33, 40 from the retroorbital plexus of mice under isofluorane anesthesia. The blood samples were kept at 37 °C for 30 min and then centrifuged at 4 °C at 2000 × g for 30 min, with the supernatant centrifuged a second time. Aliquots of sera were stored at −80 °C prior to analysis.

#### 2.7.2. Measurement of specific anti-nicotine IgG antibodies using ELISA

Mice sera were analyzed according to the ELISA procedure described by de Villiers et al. with appropriate modification. [38] Briefly, the nicotine hapten was conjugated to keyhole limpet hemocyanin (KLH) according to the same method used for the preparation of Nic-BSA conjugate.

MICROLON® 96 well plates (Greiner Bio-One, Longwood, FL) were coated with Nic-KLH conjugate (10 µg/mL in carbonate buffer, 0.05 M, pH 9.6, 100 µL/well) and incubated at 25 °C for 5 h. The plates were washed with PBS-Tween (0.1%) for 4 times and distilled water for 2 times, followed by blocking with 300 µL Pierce® protein-free T20 blocking buffer for 12 h. Sera from immunized mice were serially diluted at different dilution (1:25, 1:125, 1:625, 1:3125, 1:15625, and 1:78125) in PBS, and 100 µL of each dilution was added to the plate which was subsequently incubated at 25 °C for 2 h. The plates were washed again, and incubated with 100 µL Anti-Mouse IgG HRP (1:10000) from Alpha Diagnostic Intl (San Antonio, TX) for 1 h. After washing as before, plates were incubated with tetramethylbenzidine (TMB) peroxidase (100 µL/well) for 10 min in the dark. Sulphuric acid was added (0.5%, 100 µL/well) and absorbance was measured at 450 nm, using a Microplate Reader (Synergy HTS Multi-Mode, BioTek Instruments, Inc., Winooski, VT). The ELISA titer was defined as the dilution of the serum which gives a half-maximal optical density signal (OD 50%) in the ELISA.

**2.7.3. Determination of anti-nicotine specific IgG subclasses**

For the IgG subtype determination, duplicate ELISA were done for the four antibody isotypes in serum from mice of each group. Horseradish peroxidase conjugated sheep anti-mouse IgG1, IgG2a, IgG2b and IgG3 (Alpha Diagnostic Intl.) were used as the secondary antibodies.

**2.7.4. Th1/Th2 index calculation**

To determine whether the addition of nanohorn, liposomes and Alum adjuvant in the immunization protocol induced a Th1 (IgG2a and IgG3) or Th2 (IgG1) polarization, Th1:Th2 index was calculated as ([IgG2a+IgG3]/2)/(IgG1) for each immunization groups. According to such calculation, an index value < 1 stands for a Th2 polarization; an index value > 1 stands for a Th1 polarization. [39]

### 2.7.5. Antibody affinity for nicotine evaluation by equilibrium dialysis

In order to assess antibody affinity (Kd) and maximum nicotine binding capacity (Bmax), sera from immunized mice treated with NsL-based anti-nicotine vaccine in the presence and absence of Alum on day 40 were diluted with control sera (Balb/C mouse serum, Innovative Research Inc., Novi, MI), due to small sample sizes. These were then dialyzed against six different concentrations of nicotine using a 96-well Equil DIALYZER (MWCO 10 kD, the Nest Group, Inc. Southborough, MA). Unlabeled ((-)-nicotine hydrogen tartrate salt, Sigma-Aldrich, St. Louis, MO) and tritiated nicotine, (L-(-)-[N-methyl-3H]-nicotine, PerkinElmer, Boston, MA) were diluted in control sera to total nicotine concentrations ranging from 1 ng/mL to 1024 ng/mL (expressed as free base). The plate was placed vertically on a shaker and incubated for 72 h at room temperature, until equilibrium had been reached. Samples from both sides of the dialysis membrane were collected and counted using a 1450 MicroBeta TriLux Liquid scintillation counter (EG&G Wallac) with MicroBeta workstation software (version 2.7). Disintegrations per minute (DPM) were transformed to total nicotine concentrations based on the radioactivity of the original solutions. Bound versus free nicotine was plotted to create a saturation binding curve from which Kd, the concentration resulting in half of the binding sites being occupied, and Bmax (GraphPad Prism 5, GraphPad Software, Inc.) were determined. Values for Bmax were adjusted for the serum dilution.

## 2.8. Mouse toxicology studies

### 2.8.1. Animals and animal husbandry

This study was conducted in accordance with the U.S. Food and Drug Administration Good Laboratory Practice Regulations for Nonclinical Laboratory Studies, the Guide for the Care and Use of Laboratory Animals, and under a protocol approved by the Institutional Animal Care and Use Committee at Virginia Polytechnic Institute and State University. [40-42]

The experimental animals were female Balb/cByJ mice (The Jackson Laboratory, Inc., Bar Harbor, ME, USA), 5 weeks old upon arrival. The Balb/c mouse was chosen to conform to the requirements by the National Toxicology Program (NTP). [43,44] Animals were individually identified by ear notching during a 7-day quarantine. The study began after the quarantine when the mice were 6 weeks old. Mice were housed individually in solid-bottom, polycarbonate cages with stainless steel lids (Laboratory Products, Rochelle Park, NJ) and Certified Sani-Chip® hardwood cage litter (P. J. Murphy, Montville, NJ). Feed (Purina Certified Rodent Chow (#5002), PMI, St. Louis, MO) and tap water (Blacksburg, VA) were provided ad libitum throughout the study. The light cycle (12 h light, 12 h dark) and temperature and relative humidity in the animal rooms were controlled and monitored (Siebe/Barber-Coleman Network 8000® System with SIGNAL® Software [Version 4.1], Siebe Environmental Controls (SEC)/Barber-Colman Company, Loves Park, IL) throughout the study. Temperature and relative humidity were within their respective target ranges (69-75 °F and 35-65%).

**2.8.2. Evaluation of body weight, feed and water consumption, and clinical signs**

After the 7-day quarantine, the animals were randomly divided into seven groups containing eight animals per group. During the treatment period of seven weeks (see section on Immunization procedures, 2.7.1), body weight, feed consumption, and water consumption were measured by the method of McNair and Bryson and recorded twice per week. [45] In the studies, clinical signs of toxicity included body condition, lethargy, abnormal posture, and ruffled fur.

**2.8.3. Evaluation of organ/body weight ratios**

On day 45, after 7 weeks of observation described above, all animals were weighed and then euthanized under CO2. The hearts, lungs, livers, spleens and kidneys were excised and weighed accurately. Organ/body weight ratios were calculated as organ weight/body weight ×100 (%).[46]

### 2.8.4. Histopathological evaluation

Histopathological analysis of hearts, lungs, livers, spleens, kidneys and skin tissues from the vaccine sites of each experiment group was performed by the method of Iranloye and Bolarinwal. [47] Briefly, organs (hearts, lungs, livers, spleens, kidneys and skins) were fixed in a neutral 10% buffered formalin. Then tissue blocks were embedded in paraffin and routine sections stained as described by Lillie with hematoxylin and eosin. [48] After hematoxylin-eosin (HE) staining, sections were examined by light microscopy on a Nikon Eclipse E600 scope and images captured using a Nikon DS-Fi1 camera run by NIS Elements software (Nikon, Melville, NY).

### 2.9. Statistical analysis

Statistical analysis was performed using the Student's t-test for the difference between the experimental groups and the control group. Bonferroni correction was used where multiple comparisons were made. Differences between means were considered significant at $P<0.05$, very significant at $P<0.01$ and highly significant at $P<0.001$.

## 3. Results and discussion

### 3.1. Conjugating antigen to nanohorn-supported-liposomes

In this present study, nicotine derivative, O-succinyl-3’-hydroxmethyl-(±) nicotine26 was used as the target hapten. Antibodies induced by this hapten (coupled to virus-like particles derived from the coat protein of the bacteriophage Qb) have been shown to have a high affinity for nicotine (Kd = 35 nM) and no cross-reactivity with acetylcholine, the major nicotine metabolites cotinine and nicotine-N-oxide, and a variety of other neurotransmitters or drugs. Bovine serum albumin (BSA) acted as a model carrier protein to conjugate with the hapten in this study. BSA (67 kD) is a commonly used model carrier protein in vaccine development. For example, the anti-cancer vaccine, in which BSA was conjugated

with 3'-fluoro-TF antigen-MUC1, was able to generate high titers of antibodies that could specifically bind to a tumor-associated glycopeptide antigen analog. [49]

Covalent attachment of carboxylic acid hapten to the carrier protein (BSA) via available surface amino groups on BSA (26 surface lysines) was confirmed by reacting the prepared conjugates with TNBS reagent. The number of amino groups present in the carrier protein before and after conjugation was quantified with a UV/Vis spectrophotometer (Shimadzu 1601) set at 335 nm. The gradual decrease of the available surface lysines on the protein after reaction with different molar ratios of hapten confirmed the increase in conjugation density (number of hapten molecules per protein molecule) with the increasing hapten-protein molar ratio.

Conjugation of protein to the liposome surface was based on a chemical reaction between the maleimide of the PEGylated lipid with a derivatized sulfhydryl group at the primary amines of a protein by adding Traut's reagent, as previously described for conjugation of lactoferrin to the liposome surface. [50] The thiolation level was measured using 5,5'-dithiobis(2-nitrobenzoic acid) (Ellman's reagent) as described by Benzinger et al. [51] By optimizing the molar ratio of BSA:Nic:Traut's reagent:DSPE-Mal-PEG2000, higher association efficiency of Nic-BSA to NsL can be obtained (Table 2). Conjugates with 15 Nic haptens per BSA were produced by using a 50-fold excess of Nic-hapten. A 200-fold excess of 2-iminothiolane resulted in 5 thiol groups per Nic-BSA conjugate molecule. Moreover, a ratio of 1:4 or 1:8 of Nic-BSA:DSPE-Mal-PEG2000 was used for conjugation, and a strong antigen-NsL association efficiency of 50.4% or 65.8% and loading efficiency of 21.7% or 25.3% were achieved, respectively.

### 3.2. Physicochemical properties of NsL NPs

#### 3.2.1. Particle size, zeta potential analysis

The particle sizes and zeta potentials of nanohorns, liposomes, NsL and Nic-BSA-NsL are presented in Table 3. The results show that the mean diameter of nanohorns, liposomes, NsL and Nic-

BSA-NsL was 107.8± 3.3, 152.0± 6.0, 164.9± 2.5 and 175.3± 3.2 nm, respectively, suggesting there was no significant difference in size after the encapsulation of a nanohorn in a cationic liposome and the conjugation of antigens. In addition, the DLS analysis results of nanoparticle size agree well with the size obtained by TEM (Figure 1). The zeta potentials of liposomes were around 40 mV regardless of the presence of nanohorn, suggesting that negatively charged nanohorns embedded into the cationic liposomes did not significantly change the zeta potential of the liposome nanoparticles. It has been suggested that full electrostatic stabilization requires a zeta potential >30 mV (ideally >60 mV), potentials between 5 mV and 15 mV result in limited flocculation, and potentials between −5 mV and +3 mV yield maximum flocculation. [52,53] Therefore, the zeta potentials obtained in the present study were within the range of full electrostatic stabilization, and values near 40 mV indicate the presence of strong forces of repulsion among the nanoparticles and little tendency for aggregation. Furthermore, charged nanoparticles adsorbed to the liposome can provide additional steric stabilization of liposomes. [37] Thus the nanohorn-supported liposomes prepared in this study should, therefore, remain stable for a relatively long period of time.

**3.2.2. TEM analysis**

Figure 1 shows TEM images of nanohorns, empty liposomes, and nanohorn supported liposome nanoparticles. Evidently, carbon nanohorns are nearly spherical particles, approximately 100 nm in diameter, with a so-called ‘dahlia flower’ structure (Figure 1A). [24] The empty DOTAP liposomes and the nanohorn supported liposome nanoparticles (NsL) have nearly spherical shapes with sizes of 100-300 nm (Figure 1B, 1C). The size of the nanoparticles observed by TEM was consistent with the results of dynamic light scattering (Table 3). As shown in Figure 1C, a nanohorn supported liposome is a combination of the particles shown in Figure 1A and Figure 1B.

Liposomes with diameters of less than 500 nm were shown to efficiently enhance the immunogenic performance of liposome vaccines over large liposomes (>500 nm). [54] This is expected because the optimal particle diameter for uptake by APCs is below 500 nm. Particles of small size are also essential if non-liposome vectors are to induce a high immune response. For example poly(D, L-lactic-co-glycolic acid) (PLGA)particles of 300 nm loaded with DNA induced much higher antibody titers than particles with a diameter of 1 μm. [55] Moreover, for the present study, nicotine haptens were designed to bind to the surface of liposomes, and thus small nanohorn supported liposome nanoparticles will not only fit the size requirement of particles preferred for APC uptake but also provide the higher surface/volume ratio that increases capacity for hapten loading.

**3.2.3. Stability of nanohorn supported liposome nanoparticles**

The efficiency of liposomes as a delivery vehicle is usually compromised after administration into human body by liposomal instability during storage or circulation. [56] The instability can be caused by oxidation, degradation or fusion of liposomes with each other. [57, 58] In vaccine development, the desirable size of liposomes should be less than 300 nm due to uptake preference of the major antigen presenting cells (especially dendritic cells). However, the fusion of liposomes tends to result in particles with larger size. Many strategies can overcome this problem, and among them, including PEGylation of the liposomes. Despite the stabilizing effect on liposomes, PEGylation may lead to reduced uptake of liposomes by target cells due to reduced interaction between liposomes and cells. [56, 59] In this study, negatively charge nanohorns were the scaffold introduced into positively charged liposomes. Figure 2 shows that during liposome preparation, nanohorn supported liposomes exhibited better uniformity and smaller size than blank liposomes. Aggregates in Figure 2A indicate that even during preparation, liposome tended to fuse with each other to form larger particles. However, liposomes supported by nanohorns displayed smaller and more uniform morphology (Figure 2B). Significant fusion occurred with liposomes alone after storage for 5 days at 4 °C, as shown by the clusters in Figure 2C. In addition, the

presence of smaller particles in Figure 2C suggests that some degradation also occurred. Although increased size was detected in nanohorn supported liposomes, many still maintained their original size (Figure 2D). The comparison between liposome images with and without nanohorns suggests that nanohorns exerted a stabilizing effect on liposomes during both preparation and storage.

### 3.3. Immunogenicity study

#### 3.3.1. Time course for serum IgG antibody responses to Nic-BSA, Nic-BSA-LIP and Nic-BSA-NsL immunization by subcutaneous injection with or without Alum

The development of anti-nicotine immune response was determined by analyzing serum samples collected during animal study using ELISA. ELISA plates were coated with Nic-KLH conjugates. The results demonstrated that all subcutaneously-administered vaccines, each containing 50 μg Nic-BSA, resulted in gradual increase of serum anti-nicotine IgG antibody titers (Fig 3). This occurred both in the presence and absence of Alum. Maximum titers were obtained two weeks after the second booster of a vaccine. Nicotine-specific IgG antibody (NicAb) titers in the presence of Alum were higher than those in the absence of Alum in groups given Nic-BSA-LIP and Nic-BSA-NsL (Figure 3). No NicAb were detected in sera collected on day 0, showing that Nic vaccine treatment was necessary for the production of antibodies. After the primary immunization and two additional boosters, the titer of NicAb elicited in response to Nic-BSA-NsL with Alum was significantly greater than titers in other groups whether or not the vaccines were given with or without Alum. In addition, even in the absence of Alum, a significant level of nicotine-specific antibodies could be observed in the Nic-BSA-NsL group.

In this study an NsL-based anti-nicotine vaccine delivery system was developed. When administered subcutaneously, the vaccine elicited a strong immune response, inducing 5 and 7 fold increases in total IgG titers compared to the anti-nicotine vaccine (Nic-BSA) formulated with or without liposomes, respectively. It is worth noting that the total antibody titer for Nic-BSA-NsL, even with the

absence of Alum, is similar to the titer of the nicotine vaccine by Selecta Biosciences, SEL-068® ($5\times10^4$ for Nic-BSA-NsL, $1\times10^5$ for SEL-068®), which, based on the limited available information, has haptens conjugated to the surface of the nanoparticles and a universal antigen peptide encapsulated inside the nanoparticles. [60] It has also been reported that the anti-nicotine vaccine, which is based on virus-like particles (VLPs) of the RNA phage Qb to which nicotine haptens are covalently coupled via succinimate linkers (NicQb), induced potent and long-lived antibody responses in mice as well as humans. [61-64] Compared with the hapten delivered by the virus-like particles, NicQb by Cytos AG61, this nano-vaccine was larger in size (~100 nm compared to 25 nm) and contained lipids that induced a stronger immune response. [61, 65]

### 3.3.2. Detection of subclass distribution of nicotine-specific antibodies after vaccination

Human IgG consists of four subclasses contributing in different ways to humoral immunity against pathogens. Mice, similarly to humans, have four different classes of IgGs, namely IgG1, IgG2a, IgG2b and IgG3, which functionally correspond to the human IgG1, IgG2, IgG4 and IgG3, respectively. Despite some species differences in the IgG subclasses, the overall structure of the humoral IgG pattern in mice and humans are quite similar. In general, mouse IgG1 (as well as IgG4 in humans) is associated with a Th2 profile and the other subclasses are mainly associated with a Th1 profile. [66] In this study, the pattern of IgG subclasses induced by the different anti-nicotine vaccines was evaluated by using secondary goat anti-mouse antibodies specific for each IgG subclass. Sera from animals immunized with Nic-BSA+Alum showed low titers (3182, 16 and 9, respectively) of both Th2- associated IgG1 subclasses and Th1-associated IgG2a and IgG3 subclasses (Figure 4). Liposome-based anti-nicotine vaccines (Nic-BSA-LIP) in the presence and absence of Alum adjuvant did not significantly enhance IgG1 and IgG3 titers, but induced a 100-fold enhancement in anti-Nicotine IgG2a titers (1859 and 1492, respectively) compared to Nic-BSA+Alum (Figure 4). In contrast, NsL-based anti-nicotine vaccines (Nic-BSA-NsL) in the presence and absence of Alum adjuvant induced significantly higher titers of all four IgG subclasses

(Figure 4), with the highest titers observed for Th2-associated subclasses (IgG1>>Ig2a>Ig2b>Ig3). Evaluation of IgG subclasses demonstrated that NsL-based anti-nicotine vaccines are capable of inducing stronger humoral immune responses, indicated by the induction of significant antigen specific IgG1 and IgG2a titers.

**3.3.3. Th1:Th2 index calculation**

To assess whether NsL, LIP and Alum adjuvant formulation elicited a specific IgG subclass profile or induced an increase in all subclasses, a Th1: Th2 index was calculated for each vaccine (Table 4). Such index takes into consideration of both Th1-associated IgG2a and IgG3 subclasses and Th2-associated IgG1 subclass. The Th1:Th2 index shows that, in sera of animals immunized with Nic-BSA+Alum, the antibody response to nicotine was Th2 polarized and Th1: Th2 index was 0.004. However, both Th2-related IgG1 and Th1-related IgG2a and IgG3 antibody responses were all significantly elevated in the mice vaccinated with the Nic-BSA using NsL or LIP-based vaccine delivery ($p < 0.001$) (Figure 4 and Table 4). In addition, Th1/Th2 balance was improved after vaccination using NsL or LIP-based vaccine delivery even in the absence of Alum adjuvant (Th1: Th2 index 0.085 and 0.160, respectively) (Table 4).

Vaccine-induced immune responses can be generally divided into two different biased effects: Th1 vs. Th2 types. Many factors can contribute to the type of specific immune response of a vaccine, including the type and relative amounts of antigens and adjuvants. Aluminum salts as adjuvant generally are well known to induce a Th2-type immune response. [67-68] On the contrary, liposomes developed as potential adjuvants generally elicit a Th1-type immune response. [69] In addition, Balb/c and C57BL/6 are widely used mouse strains, showing polarized Th cell responses. Balb/c mice typically develop Th2-skewed immune responses, whereas C57BL/6 mice are prone to Th1-dominated immunity. [70] Our results demonstrated that NsL or LIP modulated immune responses from a predominantly Th2 type response to a mixed Th1/Th2 response. Results also demonstrated that NsL-based anti-nicotine vaccine

delivered by subcutaneous administration to Balb/c mice can not only significantly enhance both Th1 and Th2 immune responses but also improve Th1/Th2 balance. However, the immunological mechanism of this effect is not clear and requires further investigation.

### 3.3.4. Antibody affinity to nicotine

Individual serum samples were diluted with control mice serum and dialyzed against 5 different nicotine concentrations. From this saturation binding experiment, the affinity (Kd), and maximum number of binding sites (Bmax) were determined. The antibody concentration was calculated from the Bmax, assuming two binding sites per antibody molecule and a molecular weight of the antibody of 150 kD. Both values were obtained by calculating back to undiluted sera. The equilibrium dialysis method does not require any washing steps that might wash away low affinity antibodies, so total binding is measured. At the time the last blood sample was collected, the Kd for nicotine was $5.84\times10^{2}\pm1.86\times10^{2}$ nM and the Bmax was $2.85\times10^{3}\pm1.26\times10^{3}$ nM, corresponding to $2.14\times10^{2}\pm0.95\times10^{2}$ μg/mL of nicotine-specific IgG in the group of mice immunized with NsL-based anti-nicotine vaccine without Alum. For the group of mice given NsL-based anti-nicotine vaccine with Alum, Kd and Bmax were $1.27\times10^{3}\pm0.58\times10^{3}$ and $4.14\times10^{3}\pm1.04\times10^{3}$ nM, respectively, which were equivalent to $3.11\times10^{2}\pm0.61\times10^{2}$ μg/mL of nicotine-specific IgG. Our results demonstrated that NsL-based anti-nicotine vaccines prepared in the absence of Alum generated an anti-nicotine antibody with high affinity and a high concentration in the serum of vaccinated mice.

## 3.4. Preclinical animal toxicity studies

### 3.4.1. Body weights, feed, and water consumption

Mice continued to grow during their 7-week treatment with anti-nicotine vaccines. Behaviors such as feeding, drinking and activity were normal in all seven groups and there were no overt signs of toxicity. Mean body weights, weight gains, feed consumption and water consumption were all

equivalent (P>0.05) (Table 5). Although nicotine administration can induce weight loss and change eating behavior in both humans and rodents, there was no significant difference between the mice in the vaccinated groups and the mice in the control groups. [71-73] Our vaccines were formulated with low doses of nicotine hapten-BSA conjugates, which may have contributed to this benefit.

### 3.4.2. Gross pathology

Toxicities may also be indicated by changes in tissue or organ weight, size, color, and gross appearance. Table 6 shows body weight and organ/body weight ratios (%) of the liver, kidney, spleen, lung and heart of mice in the five vaccinated groups and two control groups. No significant differences were measured between the treated and the control groups ($P > 0.05$).

### 3.4.3. Histopathological assessment

Histopathological review indicated that there were no significant lesions in the heart, lung, liver, spleen and kidney of mice in the two control groups and the five vaccinated groups whether or not Alum was included in the vaccines (examples provided in Figure 5A-E). However, occasional background lesions were noted, especially in mice vaccinated with Alum. For example, all of these mice had subcutaneous necrosis with associated granulomatous inflammation (Figure 5F), some of which included focal epicardial calcification. [74] A pulmonary embolus was also seen in the group of mice vaccinated with LIP with Alum. This finding of subcutaneous lesions is in agreement with the report of Goto et al. suggesting that Alum injection was responsible for the induction of granulomas at the injection sites of guinea pigs. [75] Aluminum adjuvants have been commonly used both in veterinary and human vaccines for many years, but they occasionally produce subcutaneous nodules, granulomatous inflammation, and sterile abscesses as local side reactions. [69, 72, 78-82] Although seen in Alum-treated mice in this study, NsL-based anti-nicotine vaccines without Alum did not induce any histopathologic lesions at injection sites.

## 4. Conclusions

A novel anti-nicotine vaccine, based on NsL NPs, has been successfully developed. The carbon nanohorns are negatively charged (anionic) and act as a scaffold for the assembly of cationic liposomes. NsL NPs were stable after an extended period of storage. The nano-vaccine induced strong, anti-nicotine antibody responses in mice when administrated subcutaneously, leading to production of high titer and high affinity anti-nicotine antibodies for treatment of nicotine dependence. The total antibody titer for NsL -based anti-nicotine vaccine, even without the presence of Alum, reached ~$5\times10^4$. The Kd for nicotine was $5.84\times10^2\pm1.86\times10^2$ nM and Bmax was $2.85\times10^3\pm1.26\times10^3$ nM corresponding to $2.14\times10^2\pm0.95\times10^2$ μg/mL of nicotine-specific IgG for this nano-vaccine without Alum. In addition, evaluation of IgG subclasses demonstrated that NsL-based anti-nicotine vaccine was capable of inducing a more balanced Th1 and Th2 response. Furthermore, the safety evaluation of NsL NPs in mice revealed no apparent toxicity.

## Acknowledgements

This research was supported by National Institute on Drug Abuse (R21 DA030083, PI: C. Zhang). We are grateful to Dr. B. Jortner for his assistance in histopathological evaluations.

## References

[1] L. Esson, S.R. Leeder, The millennium development goals and tobacco control: an opportunity for global partnership. World Health Organization (WHO); Geneva (2004)

[2] World Health Organization Why is tobacco a public health priority? A Tobacco Free Initiative. (2005)

[3] H.J., Aubin, L. Karila, M. Reynaud, Pharmacotherapy for smoking cessation: present and future. Curr. Pharm. Des. 17, 1343–1350 (2011)

[4] J.T. Hays, J.O. Ebbert, Adverse effects and tolerability of medications for the treatment of tobacco use and dependence. Drugs. 24, 2357–2372 (2010)

[5] The Health Consequences of Smoking, Centers for Disease Control and Prevention USA. Surgeon's General Report (2004)

[6] A.Y. Moreno, K. Janda, Immunopharmacotherapy: vaccination strategies as a treatment for drug abuse and dependence. Pharmacol. Biochem. Behav. 92, 199-205(2009)

[7] J. Cornuz, S. Zwahlen, W.F. Jungi. J. Osterwalder, K. Klingler, G. van Melle, Y. Bangala, I. Guessous, P. Müller, J. Willers, P. Maurer, M.F. Bachmann, T. Cerny, A vaccine against nicotine for smoking cessation: a randomized controlled trial. PLoS One 3, e2547(2008)

[8] E.H. Cerny, T. Cerny, Vaccines against nicotine. Hum. Vaccin. 5, 200-205 (2009)

[9] News release, Nabi Biopharmaceuticals, Nov. 7, (http://phx.corporateir.net/phoenix.zhtml?c=100445&p=irol-news) (2011)

[10] M.J. Hicks, J.B. Rosenberg, B.P. De, O.E. Pagovich, C.N. Young, J. Qiu, S.M., Kaminsky N.R. Hackett, S. Worgall, K.D. Janda, R.L. Davisson, R.G. Crysal, AAV-directed persistent expression of a gene encoding anti-nicotine antibody for smoking cessation. Sci. Transl. Med. 4, 140ra87 (2012)

[11] Y.J. Kwon, E. James, N. Shastri, J.M. Fréchet, In vivo targeting of dendritic cells for activation of cellular immunity using vaccine carriers based on pH-responsive microparticles. Proc. Natl. Acad. Sci. U.S.A. 102, 18264-18268 (2005)

[12] T. Akagi, X. Wang, T. Uto, M. Baba, M. Akashi, Protein direct delivery to dendritic cells using nanoparticles based on amphiphilic poly(amino acid) derivatives. Biomaterials. 28, 3427-3436 (2007)

[13] C. Coester, P. Nayyar, J. Samuel, In vitro uptake of gelatin nanoparticles by murine dendritic cells and their intracellular localisation. Eur. J. Pharm. Biopharm. 62, 306-314 (2006)

[14] K.G. Yeboah, M.J. D'souza, Evaluation of albumin microspheres as oral delivery system for Mycobacterium tuberculosis vaccines. J. Microencapsul. 26, 166-179 (2009)

[15] G. Chikh, M.P. Schutze-Redelmeier, Liposomal delivery of CTL epitopes to dendritic cells. Biosci. Rep. 22, 339-353 (2002)

[16] M.J. Copland, M.A., Baird T. Rades, J.L. McKenzie, B. Becker, F., Reck P.C. Tyler, N.M. Davies, Liposomal delivery of antigen to human dendritic cells. Vaccine. 21, 883-890 (2003)

[17] E. Shahum, H.M. Thérien, Effect of liposomal antigens on the priming and activation of the immune system by dendritic cells. Int. Immunopharmacol. 2, 591-601(2002)

[18] K. Moribe, K. Maruyama, Pharmaceutical design of the liposomal antimicrobial agents for infectious disease. Curr. Pharm. Des. 8, 441-454 (2002)

[19] G.D. Sprott, C.J. Dicaire, K. Gurnani, L.A. Deschatelets, L. Krishnan, Liposome adjuvants prepared from the total polar lipids of Haloferax volcanii, Planococcus spp. and Bacillus firmus differ in ability to elicit and sustain immune responses. Vaccine. 22, 2154-2162 (2002)

[20] C.R. Alving, V. Koulchin, G.M. Glenn, M. Rao, Liposomes as carriers of peptide antigens: induction of antibodies and cytotoxic T lymphocytes to conjugated and unconjugated peptides. Immunol. Rev. 145, 5-31 (1995)

[21] R.G. Laughlin, Equilibrium vesicles: fact or fiction? Colloids Surf. A, 128, 27–38 (1997)

[22] Miyawaki, J., Yudasaka, M., Azami, T., Kubo, Y., and Iijima, S, Toxicity of single-walled carbon nanohorns. ACS Nano. 2, 213–26 (2008)

[23] R. M. Lynch, B. H. Voy, D. F. Glass, S. M. Mahurin, B. Zhao, H. Hu, A. M. Saxton, , R. L. Donnell, and M. D. Cheng, Assessing the pulmonary toxicity of single-walled carbon nanohorns. Nanotoxicology. 1, 157–66 (2007)

[24] S. Iijima, M. Yudasaka, R. Yamada, S. Bandow, K. Suenaga, F. Kokai, K. Takahashi, Nano-aggregates of single-walled graphitic carbon nanohorns. Chem. Phys. Lett. 309, 165-170 (1999)

[25] W. Huang, J. Zhang, H.C. Dorn, D. Geohegan, and C. Zhang, Assembly of single-walled carbon nanohorn supported liposome particles. Bioconjug. Chem. 22, 1012-1016 (2011)

[26] P. Maurer, G.T. Jennings, J. Willers, F. Rohner, Y. Lindman, K. Roubicek, W.A. Renner, P. Müller, M.F. Bachmann, A therapeutic vaccine for nicotine dependence: preclinical efficacy, and phase I safety and immunogenicity. Eur. J. Immunol. 35, 2031-2040 (2005)

[27] D. Kasuya, M. Yudasaka, K. Takahashi, F. Kokai, and S Iijima, Selective production of single-wall carbon nanohorn aggregates and their formation mechanism. J. Phys. Chem. B. 106, 4947–4951 (2002)

[28] J. Zhang, J. Ge, M. D. Shultz, E. Chung, G. Singh, C. Shu, P. P. Fatouros, S.C. Henderson, F.D. Corwin, D.B. Geohegan, A.A. Puretzky, C.M. Rouleau, K. More, C. Rylander, M.N. Rylander, H.W. Gibson, and H.C. Dorn, In vitro and in vivo studies of single-walled carbon nanohorns with encapsulated metallofullerenes and exohedrally functionalized quantum dots. Nano Lett. 10, 2843–2848 (2010)

[29] C. Shu, J. Zhang, J. Ge, J.H. Sim, B.G. Burke, K.A. Williams, N.M. Rylander, T. Campbell, A. Puretzky, C. Rouleau, D.B. Geohean, K. More, A.R. Esker, H.W. Gibson, and H.C. Dorn, A facile high-speed vibration milling method to water-disperse single-walled carbon nanohorns. Chem. Mater. 22, 347– 351 (2010)

[30] Y. Hu, H Zheng, W Huang, C.M. Zhang, A novel and efficient nicotine vaccine using nano-lipoplex as a delivery vehicle. Hum. Vaccin. Immunother. 10, 1-9 (2014)

[31] AFSA. Habeeb, Determination of free amino groups in proteins by trinitrobenzene-sulfonic acid. Anal. Biochem. 14, 328–336 (1966)

[32] R. Jue, J.M. Lambert, L.R. Pierce, R.R. Traut, Addition of sulfhydryl groups to Escherichia coli ribosomes by protein modification with 2-iminothiolane (methyl 4-mercaptobutyrimidate). Biochemistry. 17, 5399-5406 (1978)

[33] S.M. Ansell, P.G. Tardi, and S.S. Buchkowsky, 3-(2-pyridyldithio)propionic acid hydrazide as a cross-linker in the formation of liposome-antibody conjugates. Bioconjug. Chem. 7, 490-496 (1996)

[34] S.M. Ansell, T.O. Harasym, P.G. Tardi, S.S. Buchkowsky, M.B. Bally, and P.R. Cullis,Antibody conjugation methods for active targeting of liposomes. Methods Mol. Med. 25, 51-68 (2000)

[35] M. Kaszuba, J. Corbett, F.M. Watson, and A. Jones, High-concentration zeta potential measurements using light-scattering techniques. Philos. Transact. A Math. Phys. Eng. Sci. 368, 4439-51 (2010)

[36] T. Kodama, N. Tomita, S. Horie, N. Sax, H. Iwasaki, R. Suzuki, K. Maruyama, S. Mori, F. Manabu, Morphological study of acoustic liposomes using transmission electron microscopy. J. Electron. Microsc. (Tokyo) 259, 187-96 (2010)

[37] L. Zhang, S. Granick, How to stabilize phospholipid liposomes (using nanoparticles). Nano Lett. 6, 694-698 (2006)

[38] S.H. de Villiers, N. Lindblom, G. Kalayanov, S., Gordon, I. Baraznenok, A. Malmerfelt, M.M. Marcus, A.M. Johansson, and T.H. Svensson, Nicotine hapten structure, antibody selectivity and effect relationships: results from a nicotine vaccine screening procedure. Vaccine. 28, 2161-2168 (2010)

[39] M.L. Visciano, M. Tagliamonte, M.L. Tornesello, F.M. Buonaguro, L. Buonaguro, Effects of adjuvants on IgG subclasses elicited by virus-like particles. J. Transl. Med. 10, 4 (2012)

[40] U.S. FDA. U.S. Food and Drug Administration, Good Laboratory Practice Regulations for Nonclinical Laboratory Studies. CFR (April 1), (1988) p. 229–243.

[41] U.S. FDA. U.S. Food and Drug Administration. Good Laboratory Practice Regulations for Nonclinical Laboratory Studies. CFR (March 21), (1994). 56FR12300.

[42] NRC, Guide for the care and use of laboratory animals, National Academy Press, Washington, DC. (1996)

[43] T.F. Collins, R.L. Sprando, M.E. Shackelford, D.K. Hansen, J.J. Welsh, Food and Drug Administration proposed testing guidelines for developmental toxicity studies. Regul. Toxicol. Pharmacol. 30, 39-44 (1999)

[44] WHO guidelines on nonclinical evaluation of vaccines, WHO Technical Report Series. 17-21, November (2003). p. 9-12

[45] E. McNair, R. Bryson, Effects of nicotine on weight change and food consumption in rats. Pharmacol. Biochem. Behav. 18, 341-344 (1983)

[46] L.J. Pecora, B. Highman, Organ weights and histology of chronically thiamine-deficient rats and their pair-fed controls. J. Nutr. 51, 219-30 (1953)

[47] B.O. Iranloye, A.F. Bolarinwa, Effect of nicotine administration on weight and histology of some vital visceral organs in female albino rats. Niger. J. Physiol. Sci. 24, 7-12 (2009)

[48] R.D. Lillie, Histopathologic Technic. The Blakiston Co., Philadelphia, Pa. (1948)

[49] A. Hoffmann-Roder,, and M. Johannes. Synthesis of a MUC1-glycopeptide-BSA conjugate vaccine bearing the 3'-deoxy-3'-fluoro-Thomsen-Friedenreich antigen, Chem. Commun. (Camb.) 47, 9903-9905 (2011)

[50] F.Y. Huang, W.J. Chen, W.Y. Lee, S.T. Lo, T.W. Lee, J.M. Lo, In vitro and in vivo evaluation of lactoferrin-conjugated liposomes as a novel carrier to improve the brain delivery. Int. J. Mol. Sci. 14, 2862-2874 (2013)

[51] P. Benzinger, G. Martiniy-Baron, P. Reusch, G. Siemeister, J.T. Kley, D. Marmé, C., Unger and U. Massing, Targeting of endothelial KDR receptors with 3G2 immunoliposomes in vitro. Biochim. Biophys. Acta 1466, 71−78 (2000)

[52] C. Schwarz, W. Mehnert, J.S. Lucks, R.H. Muller, Solid lipid nanoparticles (SLN) for controlled drug delivery. I. Production, characterization and sterilization. J. Control. Release 30, 83-96 (1994)

[53] C. Alves, N., de Melo, L. Fraceto, D. de Araújo, M. Napimoga, Effects of 15d-$PGJ_2$-loaded poly(D,L-lactide-co-glycolide) nanocapsules on inflammation. Br. J. Pharmacol. 162, 623-632 (2011)

[54] M. G. Carstens, M. G. Camps, M. Henriksen-Lacey, K. Franken, T. H. Ottenhoff, Y. Perrie, J. A. Bouwstra,, F. Ossendorp, and W. Jiskoot, Effect of vesicle size on tissue localization and immunogenicity of liposomal DNA vaccines. Vaccine. 29, 4761-4770 (2011)

[55] M. Singh, M. Briones, G. Ott, and D. O'Hagan, Cationic microparticles: A potent delivery system for DNA vaccines. Proc. Natl. Acad. Sci. U.S.A. 97, 811-816 (2000)

[56] D. Pornpattananangkul, S. Olson, S. Aryal, M. Sartor, C.M. Huang, K. Vecchio, and L. Zhang. Stimuli-responsive liposome fusion mediated by gold nanoparticles. ACS Nano. 4, 1935-1942 (2010)

[57] B. Pietzyk, and K. Henschke. Degradation of phosphatidylcholine in liposomes containing carboplatin in dependence on composition and storage conditions. Int. J. Pharm. 196, 215-218 (2000)

[58] B. Stark, G. Pabst, and R. Prassl, Long-term stability of sterically stabilized liposomes by freezing and freeze-drying: Effects of cryoprotectants on structure. Eur. J. Pharm. Sci. 41, 546 -555(2010)

[59] P. Milla, F. Dosio, and L. Cattel, PEGylation of proteins and liposomes: a powerful and flexible strategy to improve the drug delivery. Curr. Drug Metab. 13, 105-119 (2012)

[60] K. Kishimoto, D. Altreuter, L. Johnston, P. Keller, L. Pittet. SEL-068® a fully synthetic nanoparticle vaccine for smoking cessation and relapse prevention. Society for Research on Nicotine and Tobacco's 18th Annual Meeting, Hilton Americas Hotel, Houston, Texas. Abstract Book, (2012) POS1-1.

[61] A. Jegerlehner, A. Tissot, F. Lechner, P. Sebbel, I. Erdmann, T. Kündig, T. Bächi, T. Storni, G. Jennings, P. Pumpens, W.A. Renner, M.F. Bachmann. A molecular assembly system that renders antigens of choice highly repetitive for induction of protective B cell responses. Vaccine. 20, 3104–3112 (2002)

[62] P. Maurer, G.T. Jennings, J. Willers, F. Rohner, Y. Lindman, K. Roubicek, W.A. Renner, P. Müller, M.F. Bachmann A therapeutic vaccine for nicotine dependence: preclinical efficacy, and Phase I safety and immunogenicity. Eur. J. Immunol. 35, 2031–2340 (2005)

[63] P.M. Ambühl, A.C. Tissot, A. Fulurija, P. Maurer, J. Nussberger, R. Sabat, V. Nief, C. Schellekens, K. Sladko, K. Roubicek, T. Pfister, M. Rettenbacher, H.D. Volk, F. Wagner, P. Müller, G.T. Jennings, M.F. Bachmann. A vaccine for hypertension based on virus-like particles: preclinical efficacy and phase I safety and immunogenicity. J. Hypertens. 25, 63–72 (2007)

[64] T.M. Kündig, G. Senti, G. Schnetzler, C. Wolf, B.M. Prinz Vavricka, A. Fulurija, F. Hennecke , K. Sladko, G.T. Jennings, M.F. Bachmann, Der p 1 peptide on virus-like particles is safe and highly immunogenic in healthy adults. J. Allergy Clin. Immunol. 117, 1470–1476 (2006)

[65] J. Cornuz, S. Zwahlen, W.F. Jungi, J. Cornuz, S. Zwahlen, W.F. Jungi, J. Osterwalder, K. Klingler, G. van Melle, Y. Bangala, I Guessous, P. Müller, J. Willers, P. Maurer, M.F. Bachmann, T.A Cerny. A vaccine against nicotine for smoking cessation: a randomized controlled trial. PLoS One 3, e2547 (2008)

[66] Banerjee K, Klasse PJ, Sanders RW, Pereyra F, Michael E, Lu M, Walker BD, Moore JP, IgG subclass profiles in infected HIV type 1 controllers and chronic progressors and in uninfected recipients of Env vaccines. AIDS Res. Hum. Retroviruses. 26, 445-458 (2010)

[67] Sokolovska A, Hem SL and HogenEsch H. Activation of Dendritic Cells and Induction of CD4(+) T Cell Differentiation by Aluminum-Containing Adjuvants. Vaccine. 25, 4575-85 (2007)

[68] O'Hagan DT and Rappuoli R, Novel Approaches to Vaccine Delivery. Pharm. Res. 21, 1519-1530 (2004)

[69] Rosenkrands I, Agger EM, Olsen AW, Korsholm KS, Andersen CS, Jensen KT, Andersen P, Cationic liposomes containing mycobacterial lipids: a new powerful Th1 adjuvant system. Infect. Immun. 73, 5817-5826 (2005)

[70] M. Becker, S. Reuter, P. Friedrich, F. Doener, A. Michel, T. Bopp, M. Klein, E. Schmitt, H. Schild, M.P. Radsak, B. Echtenacher, C. Taube, M. Stassen, Genetic variation determines mast cell functions in experimental asthma. J. Immunol. 186, 7225-7231 (2011)

[71] E. McNair, R. Bryson, Effects of nicotine on weight change and food consumption in rats. Pharmacol. Biochem. Behav. 18, 341-344 (1983)

[72] N.E. Grunberg, S.E. Winders, K.A. Popp, Sex differences in nicotine's effects on consummatory behavior and body weight in rats. Psychopharmacology (Berl.). 91, 221-225 (1987)

[73] J. Gross, M.L. Stitzer, J. Maldonado, Nicotine replacement: effects of postcessation weight gain. J. Consult. Clin. Psychol. 57, 87-92 (1989)

[74] C.E. Nabors, C.R. Ball. Spontaneous calcification in hearts of DBA mice. Anat. Rec. 164, 153-61 (1969)

[75] N. Goto, H. Kato, J. Maeyama, M. Shibano, T. Saito, J. Yamaguchi, S. Yoshihara, Local tissue irritating effects and adjuvant activities of calcium phosphate and aluminium hydroxide with different physical properties. Vaccine. 15, 1364-1371 (1997).

[76] N.W. Baylor, W. Egan, P. Richman, Aluminum salts in vaccines--US perspective. Vaccine. 20, S18-23 (2002)

[77] E.B. Lindblad. Aluminium adjuvants--in retrospect and prospect. Vaccine. 22, 3658-3668 (2004)

[78] N.R. Butler, M.A. Voyce, W.L. Burland, M.L. Hilton, Advantages of aluminium hydroxide adsorbed combined diphtheria, tetanus, and pertussis vaccines for the immunization of infants. Br. Med. J. 1, 663-666 (1969)

[79] L. Frost, P. Johansen, S. Pedersen, N. Veien, P.A. Ostergaard, M.H. Nielsen, Persistent subcutaneous nodules in children hyposensitized with aluminium-containing allergen extracts. Allergy. 40, 68-72 (1985)

[80] R.G.White, A.H. Coons. J.M.Connolly, Studies on antibody production. III. The alum granuloma. J. Exp. Med. 102, 73-82(1955)

[81] M. Erdohazi, R.L. Newman. Aluminium hydroxide granuloma. Br. Med. J. 3, 621-623 (1971)

[82] N. Goto, K. Akama, Histopathological studies of reactions in mice injected with aluminum-adsorbed tetanus toxoid. Microbiol. Immunol. 26, 1121-1132 (1982)

**Table 1.** Immunization scheme of mice (Balb/c). Each group had 8 mice. All vaccines (suspended in 100 µL saline) were administered subcutaneously with one primary immunization and two boosters two weeks apart.

| Group No. | Vaccine name | Dose of immunogen (µg) | Dose of Alum (mg) |
|---|---|---|---|
| **1** | Nic-BSA | 50 | 1.2 |
| **2** | Nic-BSA-LIP | 50 | - |
| **3** | Nic-BSA-LIP | 50 | 1.2 |
| **4** | Nic-BSA-NsL | 50 | - |
| **5** | Nic-BSA-NsL | 50 | 1.2 |
| **6** | LIP | - | 1.2 |
| **7** | NsL | - | 1.2 |

BSA: bovine serum albumin; LIP: liposome; NsL: nanohorn supported liposome.

**Table 2**. Determination of Nic-hapten density, Nic-BSA thiolation grade and AE and LC of Nic-BSA to NsL NPs.

| Molar ratio of additive (BSA:Nic:Traut's reagent: DSPE-Mal-PEG2000) | Approximate no. of amino groups used | Approximate no. of thiol groups used | AE (%) | LC (%) |
|---|---|---|---|---|
| **1: 50: 200: 4** | 15.1 (15) | 5.69 (5) | 50.4± 1.0 | 21.7±2.4 |
| **1: 50: 200: 8** | 15.1 (15) | 5.69 (5) | 65.8± 1.4 | 25.3±4.6 |

Results are expressed as means (SD) for n=3. AE: association efficiency; LC: loading capacity.

**Table 3.** Size distribution and zeta potential of nanohorn, DOTAP liposomes, NsL and Nic-BSA-NsL in 0.15 M pH 7.4 NaCl solution or ultrapure water.

| | Size (nm) | Zeta potential (mV) | Polydispersity |
|---|---|---|---|
| **nanohorn** | 107.8 ± 3.3 | -29.5 ± 1.29 | 0.18 ± 0.02 |
| **DOTAP liposomes** | 152.0 ± 6.0 | 42.8 ± 0.96 | 0.20 ± 0.03 |
| **NsL** | 164.9 ± 2.5 | 47.6 ± 1.10 | 0.23 ± 0.02 |
| **Nic-BSA-NsL** | 175.3 ± 3.2 | 52.2 ± 1.38 | 0.19 ± 0.01 |

Results are expressed as means ± SD (n=3).

**Table 4.** Th1:Th2 index for nicotine vaccine

| | Nic-BSA+Alum | Nic-BSA-LIP | Nic-BSA-LIP+Alum | Nic-BSA-NsL | Nic-BSA-NsL+Alum |
|---|---|---|---|---|---|
| **IgG1 (Th2)** | (3.18±0.48)× $10^3$ | (4.25±1.32)× $10^3$ | (5.99±1.37)× $10^3$ | (1.91±0.03)× $10^4$ | (2.94±0.07)× $10^4$ |
| **IgG2a (Th1)** | 16.3±4.5 | (1.49±0.29)× $10^3$ | (1.86±0.20)× $10^3$ | (2.17±0.45)× $10^3$ | (2.39±0.34)× $10^3$ |
| **IgG3 (Th1)** | 9.4±4.2 | 32.4±7.7 | 56.5±6.5 | (1.57±0.96)× $10^3$ | (2.85±0.92)× $10^3$ |
| **Th1/Th2 index** | 0.004 | 0.180 | 0.160 | 0.085 | 0.076 |

Results are expressed as mean ± SD, n=8.

**Table 5**. Effect of subcutaneous administration of nicotine vaccine on weight gains, feed consumption and water consumption of Balb/c mice.

| | Body Weight (g) | | | Food Consumption | Water Consumption |
|---|---|---|---|---|---|
| | Initial | Final | Change | (g/day) | (g/day) |
| **LIP+Alum** | 18.0±1.6 | 20.9±1.9 | 2.9±0.6 | 2.8±0.2 | 4.6 ±0.5 |
| **NsL+Alum** | 17.9±1.4 | 20.7±1.7 | 2.8±0.6 | 2.9±0.2 | 4.3±0.5 |
| **Nic-BSA+Alum** | 17.4±0.7 | 20.4±1.1 | 3.0±0.7 | 2.6±0.1 | 4.2 ±0.5 |
| **Nic-BSA-NsL** | 18.4±1.1 | 21.3±1.5 | 2.9±0.5 | 2.7±0.3 | 4.4± 0.6 |
| **Nic-BSA-NsL+Alum** | 19.0±0.9 | 21.7±2.3 | 2.7±1.7 | 2.8±0.3 | 4.3± 0..7 |
| **Nic-BSA-LIP** | 17.9±1.3 | 20.4±1.6 | 2.5±0.3 | 2.7±0.4 | 4.6± 0.7 |
| **Nic-BSA-LIP+Alum** | 18.2±1.4 | 21.0±1.4 | 2.8±0.9 | 2.7±0.2 | 4.4±0.6 |

Results of the mean body weight gains, feed consumption and water consumption of seven groups of mice are expressed as means ± SD. Data were analyzed by paired t tests and no differences were significant. (**P**＞0.05, n=8)

**Table 6.** Effect of of nicotine vaccines on body weight and organ/body weight ratio of Balb/c mice.

| | | Heart | Lung | Liver | Spleen | Kidney |
|---|---|---|---|---|---|---|
| **LIP+Alum** | 21.21±1.70 | 0.66±0.08 | 1.40±0.53 | 5.11±0.56 | 0.47±0.08 | 1.47±0.24 |
| **Nic-BSA+Alum** | 20.36±1.29 | 0.65±0.12 | 1.62±0.27 | 5.02±0.17 | 0.47±0.07 | 1.53±0.13 |
| **NsL+Alum** | 20.68±1.73 | 0.74±0.06 | 1.50±0.26 | 5.17±0.55 | 0.52±0.07 | 1.54±0.14 |
| **Nic-BSA-NsL** | 21.28±1.52 | 0.74±0.08 | 1.39±0.22 | 5.28±0.53 | 0.47±0.06 | 1.53±0.15 |
| **Nic-BSA-NsL+Alum** | 21.68±2.27 | 0.75±0.12 | 1.53±0.35 | 5.25±0.20 | 0.52±0.04 | 1.56±0.26 |
| **Nic-BSA-LIP** | 20.43±1.58 | 0.65±0.13 | 1.59±0.41 | 4.92±0.39 | 0.46±0.05 | 1.51±0.18 |
| **Nic-BSA-LIP+Alum** | 21.03±1.37 | 0.74±0.14 | 1.60±0.27 | 4.85±0.30 | 0.50±0.08 | 1.49±0.15 |

Results of the mean body weight and organ/body weight ratio of seven groups mice are expressed as means ± SD. Data were analyzed by paired t tests and no differences were significant. (**P**＞0.05, n=8)

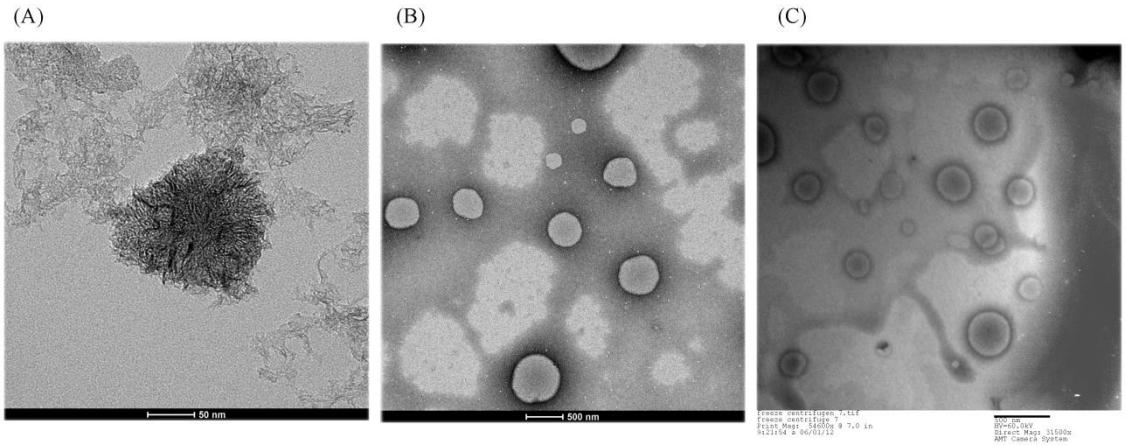


**Figure 1.** TEM images of (A) Nanohorn, (B) liposomes prepared with DOTAP, and (C) NsL. Scale bar in (A) =50 nm. Scale bar in (B) and (C) = 500 nm.

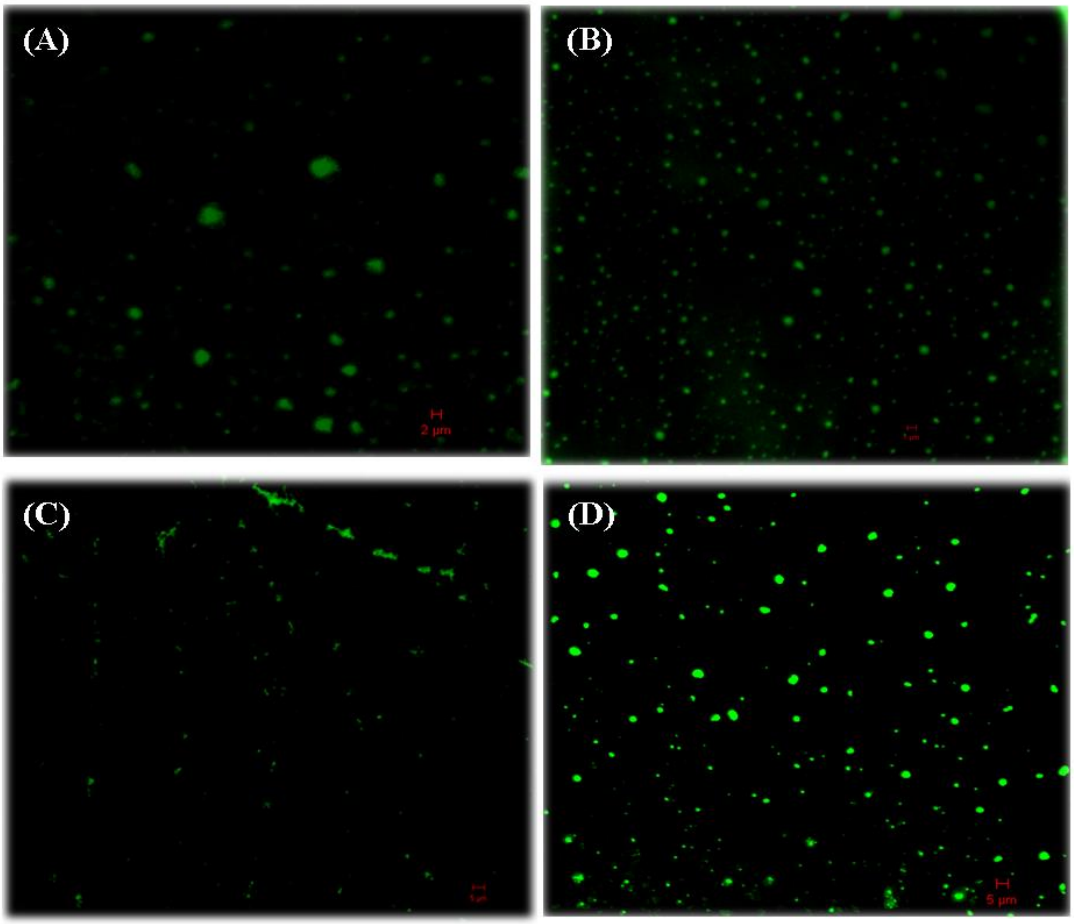


**Figure 2.** Confocal microscopic images of liposomes and nanohorn supported liposomes labeled with FITC (A) newly synthesized liposomes, (B) newly synthesized nanohorn supported liposomes, (C) liposomes after storage for 5 days, (D) nanohorn supported liposomes after storage for 5 days.

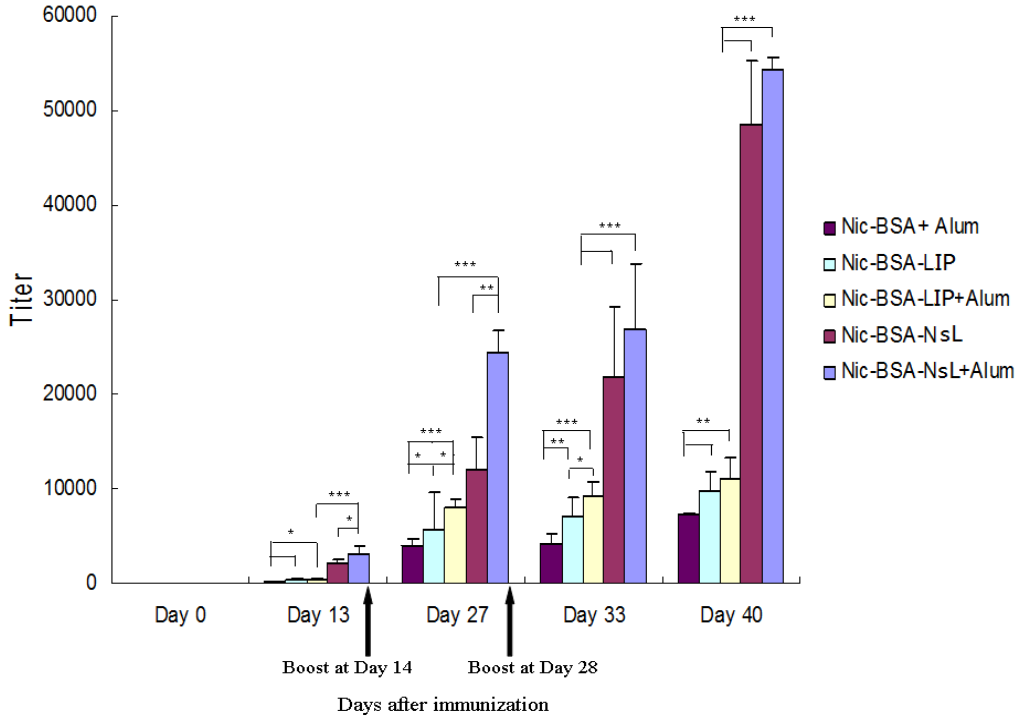


**Figure 3.** Time-course of IgG nicotine-specific response to subcutaneous immunization with nicotine vaccines. Mice were given 50 µg of Nic-BSA with Alum and Nic-BSA-LIP or Nic-BSA-NsL with or without Alum adjuvant on days 0, 14 and 28. Two groups of control animals received either LIP with Alum or NsL with Alum, respectively. Serum samples from eight animals per group were taken at two weekly intervals. Control animals showed no detectable nicotine-specific IgG. Mean nicotine-specific serum IgG antibody titers and the corresponding standard deviations are represented by columns and error bars (*$P$< 0.05; **$P$<0.01; ***$P$<0.001).

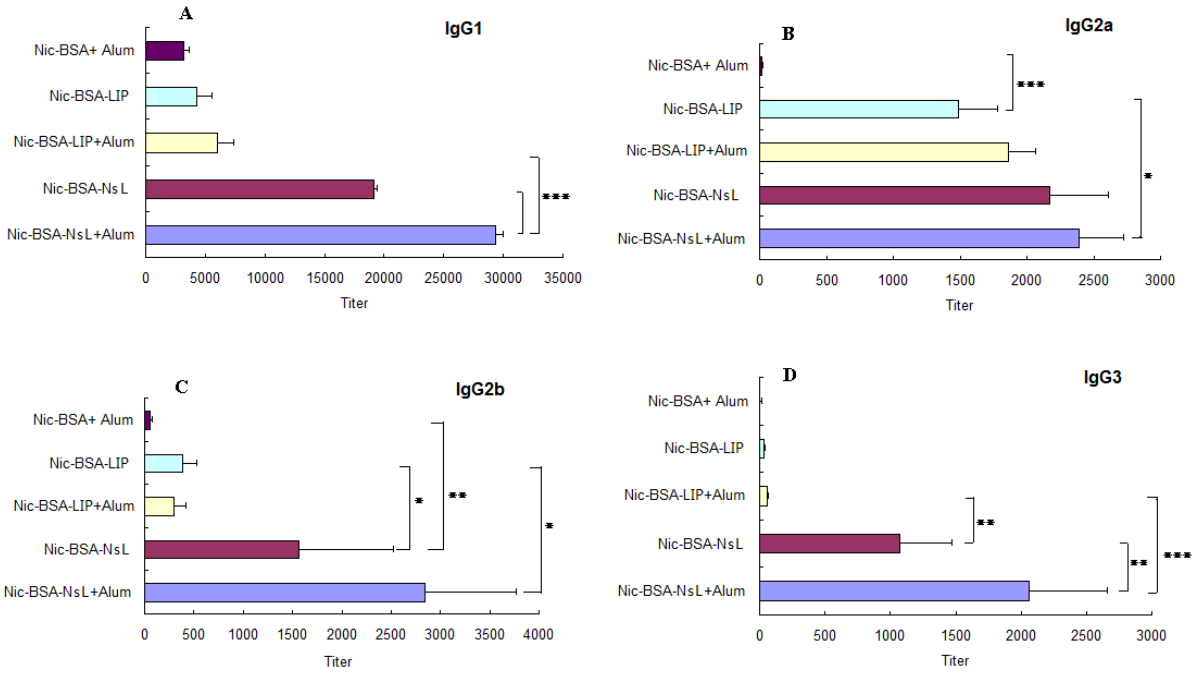


**Figure 4.** Responses of IgG subclasses to subcutaneous immunization with nicotine vaccines. Mice were given 50 µg of Nic-BSA with Alum and Nic-BSA-LIP or Nic-BSA-NsL with or without Alum adjuvant on days 0, 14 and 28. Serum samples from eight animals per group were taken on day 40. Mean nicotine-specific serum IgG subclass antibody titers and the corresponding standard deviations are represented by columns and error bars (**P*< 0.05; ***P*<0.01; ****P*<0.001).

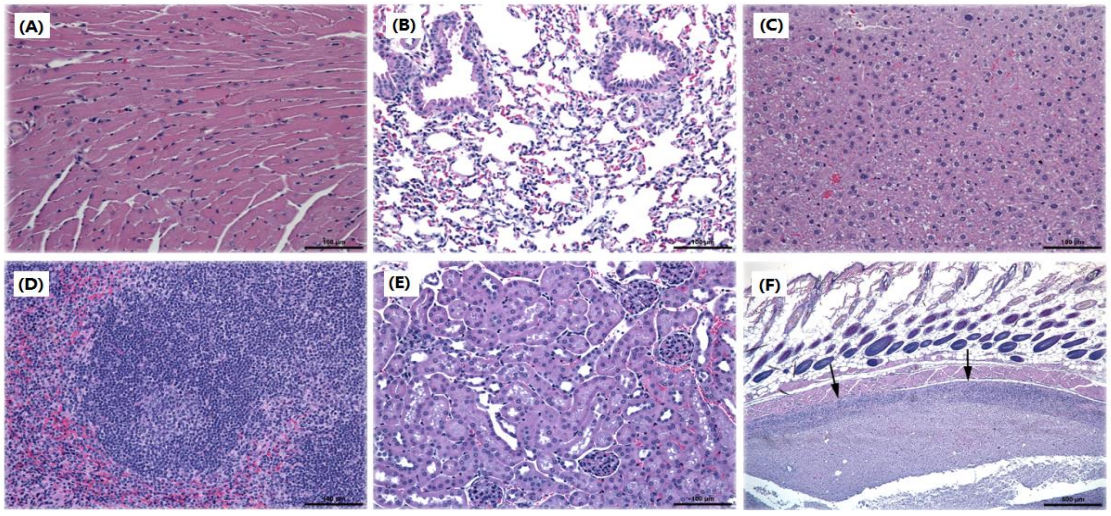


**Figure 5.** Representative histopathological images of different mouse tissues after subcutaneous administration of nicotine vaccines. No lesions were noted in (A) heart, (B) lung, (C) liver, (D) spleen, and (E) kidney. Figure 5F is from a mouse given a vaccine with Alum. Arrows indicate subcutaneous lesions. Scale bars in (A) - (E) are 100 µm; for (F) the scale bar is 500 µm.

# Chapter V (results): *In vitro* performance of lipid-PLGA hybrid nanoparticles as an antigen delivery system: lipid composition matters

Yun Hu,[1] Marion Ehrich,[2] Kristel Fuhrman,[3] Chenming Zhang[1]†

[1] Department of Biological Systems Engineering, Virginia Tech, Blacksburg, VA 24061, U.S.A.

[2] Department of Biomedical Sciences and Pathobiology, Virginia Tech, Blacksburg, VA 24061, U.S.A.

[3] Veterinary Medicine Experiment Station, Virginia Tech, Blacksburg, VA 24061

† To whom correspondence should be addressed. Office phone number: (540) 231-7601; E-mail address: chzhang2@vt.edu.

This article has been published in Nanoscale Research letters 2014, 9(1):434. Reprinted with permission of the publisher.

**Abstract**

Due to the many beneficial properties combined from both poly(lactic-co-glycolic acid) (PLGA) nanoparticles (NPs) and liposomes, lipid-PLGA hybrid NPs have been intensively studied as cancer drug delivery systems, bio-imaging agent carriers, as well as antigen delivery vehicles. However, the impact of lipid composition on the performance of lipid-PLGA hybrid NPs as a delivery system has not been well investigated. In this study, the influence of lipid composition on the stability of the hybrid NPs and *in vitro* antigen release from NPs under different conditions was examined. The uptake of hybrid NPs with various surface charges by dendritic cells (DCs) and the cytotoxicity of lipid-PLGA hybrid NPs with different lipid compositions to DC were carefully studied. The results showed that PLGA NPs enveloped

by a lipid shell with more positive surface charges could improve the stability of the hybrid NPs, enable better controlled release of antigens encapsulated in PLGA NPs, as well as enhance uptake of NPs by DC.

**Keywords**

Hybrid NP; lipid composition; PLGA; surface charge; vaccine; antigen delivery

## 1. Introduction

Nanoparticles made from poly(lactic-co-glycolic acid) (PLGA) or lipids have been used as drug delivery systems for many years. PLGA and liposome nanoparticles (NPs) share some common merits, such as long circulation time, biocompatibility, tunable size, and high drug loading capacity [1, 2]. Meanwhile, both PLGA and liposome NPs have their own unique advantages. For example, the degradation rate of PLGA NPs can be flexibly controlled by adjusting the molar ratio between glycolic acid and lactic acid [3], and substances with distinct physiochemical properties, including proteins, anticancer drugs, nucleic acids, and even metal NPs can be easily incorporated into PLGA NPs. On the other hand, liposome NPs can entrap hydrophobic drugs between lipids layer, while encapsulate hydrophilic payloads in the aqueous core. In addition, the surface chemistry of liposomes can be easily tuned to meet different requirements by simply adjusting the types or concentrations of lipids, and the inclusion of certain lipid molecules with terminal reactive groups offers great flexibility in conjugating target molecules with different chemical properties [4]. It is even possible to formulate liposomes that are sensitive to a wide range of external stimuli, such as heat, light, ultrasound, pH, to allow highly controlled release of payloads [5]. However, PLGA and liposome NPs also have their own limitations. For instance, the fabrication process for liposomes of accurate size is cumbersome [6], and they are also plagued by storage instability and burst release of the payload [7]. PLGA NPs, on the other hand, tend to

have short half-life during circulation *in vivo* [7], and the surface chemistry of PLGA NPs cannot be easily modified. Therefore, it would be attractive to fabricate lipid-PLGA hybrid NPs, which combine the desirable characteristics of both liposome and PLGA NPs, meanwhile mitigate or even avoid the aforementioned limitations.

Indeed, in the past decade, lipid-PLGA hybrid NPs have exhibited great potentials as a delivery system for cancer drugs, antigens, as well as *in vivo* imaging agents. They may play an important role in overcoming the increasingly prevalent multidrug resistance (MDR) [8]. Encapsulation of anticancer drugs in both the PLGA core and the lipid layer allows the release of drugs in a step-wise manner, resulting in improved therapeutic index with reduced toxicity [9]. In vaccine application, vaccines delivered by hybrid NPs demonstrated enhanced immunogenicity [10]. Antigens can be either conjugated on the surface of the lipid layer, or encapsulated inside the PLGA core, or both. In addition, molecular adjuvants such as Monophosphoryl Lipid A (MPLA), CpG oligodeoxynucleotides (CpG OND) can be co-delivered with antigens to further enhance immune response and reduce systemic toxicity [11].

Despite the broad applications of lipid-PLGA NPs, some fundamental questions have not been well addressed. Among them, the surface chemistry of the hybrid NPs that is governed by lipid composition and concentration, including surface charge, hydrophobicity, fluidity, permeability, and steric shielding effect of polyethylene glycol (PEG) [12], could greatly impact the performance of the NPs as a delivery vehicle. The understanding of how a lipid shell affects the efficacy of drug or antigen delivery may provide basis for more rational design of hybrid NPs. Therefore, in this study, lipid-PLGA NPs, which are composed of a PLGA core and a lipid shell with variable lipid compositions, were prepared. In order to evaluate the performance of the hybrid NPs as an antigen delivery system, a model antigen, keyhole limpet hemocyanin (KLH), was enclosed inside the PLGA core. The influence of different lipids compositions on the surface charge, size and stability of hybrid NPs was evaluated. Furthermore, the

release of KLH from the hybrid NPs in phosphate buffered saline (PBS), fetal bovine serum (FBS), and human serum were studied. The *in vitro* uptake of the hybrid NPs with different surface properties by dendritic cells (DCs) was also studied. It was found that lipid shells made from cationic lipids could improve the stability of NPs, enable more controlled release of antigen, and enhance the uptake of the NPs by DCs. In addition, hybrid NPs, regardless of the lipid composition, showed excellent safety to DCs. These results should provide guidance to future design of hybrid NPs for improving drug or antigen delivery.

## 2. Materials and methods

### 2.1 Materials

Lactel® 50:50 PLGA was purchased from Durect Corporation (Cupertino, CA). Lipids, including 1,2-dioleoyl-3-trimethylammonium-propane (DOTAP), 1,2-dioleoyl-sn-glycero-3-phosphocholine (DOPC), 1,2-distearoyl-sn-glycero-3-phosphoethanolamine-N-[amino(polyethylene glycol)-2000] (ammonium salt) (DSPE-PEG2000), and 1,2-diphytanoyl-sn-glycero-3-phosphoethanolamine-N-(7-nitro-2-1,3-benzoxadiazol-4-yl) (ammonium salt) (NBD PE) were purchased from Avanti Polar Lipids, Inc. (Alabaster, AL). KLH, poly(vinyl alcohol) (PVA, Mw 89,000-98,000), dichloromethane, rhodamine B, sodium deoxycholate (DOC), trichloroacetic acid (TCA), sodium dodecyl sulfate (SDS), paraformaldehyde, Triton™X-100 were purchased from Sigma-Aldrich Inc. (Saint Louis, MO). 1-ethyl-3-[3-dimethylaminopropyl] carbodiimide hydrochloride (EDC) was purchased from Thermo Fisher Scientific Inc. (Rd, Rockford, IL). JAWSII (ATCC® CRL-11904™) immature DCs were purchased from ATCC (Manassas, VA). Fetal Bovine Serum (FBS), GM-CSF recombinant mouse protein, minimum essential medium (MEM) α, trypsin/EDTA, HCS CellMask™ Blue Stain were purchased from Life Technologies Corporation (Grand Island, NY).

### 2.2 Fabrication of PLGA-KLH (PK) nano-complex

PLGA-KLH nano-complex was prepared using double emulsion solvent evaporation method [13]. Briefly, PLGA of 200 mg was dissolved in 5 mL dichloromethane, followed by mixing with 300 µL of 10 mg/mL KLH using vortex mixer for 2 min. The resulting mixture emulsified via sonication at 20% amplitude for 20 s using a sonic dismembrator (Model 500; Fisher Scientific, Pittsburg, PA). The primary emulsion was added dropwise into 200 mL 1% (w/v) PVA, and stirred for 10 min at 500 rpm. The above suspension was emulsified through sonication at 50% amplitude for 120 s. The secondary emulsion was stirred overnight to allow organic solvent to evaporate. After settling in room temperature for 30 min, precipitant was removed. NPs in suspension were collected by centrifuge at 20000 g, 4 °C for 30 min (Beckman Coulter Avanti J-251, Brea, CA). Pellet was washed using ultrapure water for 3 times. The final suspension was freeze-dried (LABCONCO Freezone 4.5, Kansas City, MO) and stored at 2 °C for later use.

### 2.3 Assembly of liposome-PK (LPK) nano-complex

Lipid film of 20 g with various lipid composition was hydrated with 15 mL hydration buffer (0.9% saline, 5% dextrose, and 10% sucrose). After vigorous mixing with vortex for 2 min, the resulting solution was incubated in a 55 °C water batch for 5 min and cooled to room temperature. PK NPs of 200 mg was added into liposome solution and pre-homogenized for 15 min using Branson 2510 bath sonicator (Danbury, CT), followed by sonication in ice bath at 15% amplitude for 5 min (pulse on 20 s, pulse off 50 s) using a sonic dismembrator (Model 500; Fisher Scientific, Pittsburg, PA). The formed LPK NPs were collected by centrifuge at 20000 g, 4 °C for 30 min and stored at 2 °C after being lyophilized.

### 2.4 Labeling KLH with rhodamine B fluorescence

Ten mg of EDC dissolved in 700 µL ultrapure water (pH 6.8) was mixed with 300 µL of 2 mg/mL rhodamien B. After incubation at 0 °C for 10 minutes, the mixture was added with 10 mg KLH (10 mg/mL) and stirred in darkness at room temperature for 12 hours. Fluorescently labeled KLH was purified using

Microcon centrifugal filter units (50,000 MWCO) from EMD Millipore (Billerica, MA) and stored at 2 °C after freeze dry.

### 2.5 Physicochemical properties characterization of NPs

5 mg of NPs was dispersed in 20 mL ultrapure water (pH 7.0) using a water bath sonicator for 5 min. Each sample was diluted by 10 folds using ultrapure water. Particle size (diameter, nm), surface charge (zeta potential, mV) were measured using a Malvern Nano-ZS zetasizer (Malvern Instruments Ltd, Worcestershire, United Kingdom) at room temperature.

### 2.6 Imaging of NPs using transmission electrical microscope (TEM)

NPs suspended in ultrapure water (5mg/mL) were dropped onto a 300-mesh Formvar-coated copper grid. After 10 min standing, the remaining suspension was carefully removed with wipes, and the samples were negatively stained using fresh 1% phosphotunstic acid for 60 s and washed by ultrapure water twice. The dried samples were imaged on a JEOL JEM 1400 Transmission Electron Microscope (JEOL Ltd., Tokyo, Japan).

### 2.7 Confocal imaging of LPK NPs

Fluorescent LPK NPs were formed using the above described methods, except that KLH were labeled with rhodamine B and 0.5 mg of NBD PE were added into existing lipids (DOPC: DSPE-PEG = 16 mg : 4 mg). 100 µL of NPs suspension (1 mg/mL) was placed onto a glass slide and covered with a cover glass (thickness: 0.16 to 0.19 mm) from Fisher Scientific (Pittsburg, PA). The sample was imaged using Zeiss LSM 510 Laser Scanning Microscope (LSM) (Carl Zeiss, German).

### 2.8 In vitro stability of NPs

20 mg of NPs was suspended in 20 mL 10% (v/v) human serum (pH 7.4), 10% (v/v) FBS, 10 mM phosphate buffered saline (PBS), respectively. The suspensions were constantly mixed on a shaker in room temperature for 9 days. 150 µL samples were diluted in 2 mL ultrapure water at different time

points, and the particle size was measured by Malvern Nano-ZS zetasizer. The measurements were performed in triplicate at room temperature.

### 2.9 Determination of KLH content in NPs

KLH in NPs was quantified using a modified method [14]. Briefly, 10 mg of NPs was dissolved in 1 mL of 0.1 M NaOH solution, and incubated at 2 °C for 12 h. The solution pH was adjusted to 7.0 using 1 M HCl. Two hundred μL of DOC (0.15, w/v) was added and the final volume was adjust to 2 mL using ultrapure water. After sitting at room temperature for 15 min, the mixture was added with 200 μL of TCA (80%, w/v) and incubated for 5 min. Samples were vortexed for 2 min and centrifuged at 5000 g for 20 min at room temperature. Pellets were dissolved in 500 μL of SDS (5%, w/v) containing 0.01 M NaOH. Following the protocol from supplier, KLH concentration was determined using Micro BCA Protein Assay Kit (Thermal Scientific, Rockford, IL).

### 2.10 In vitro release of KLH from NPs in human plasma

5 mg of NPs containing rhodamine B labeled KLH were suspended in 1 mL of 10% (v/v) human serum (pH 7.4), and incubated in darkness (covered by foil) at 37 °C. Samples were centrifuged at 10000 g for 15 min at determined time points. The supernatant (200 μL) was added into a blank 96 well plate (Thermal Scientific, Rockford, IL), and measured using Synergy HT Multi-Mode Microplate Reader (BioTek Instruments, Inc., Winooski, VT) with excitation at 530 nm and emission at 590 nm. The pellets were re-suspended in 1 mL of 10% (v/v) human serum. Release of KLH at certain time points was calculated by using following equation: KLH release% = Absorbance at certain time point/Total absorbance×100.

### 2.11 Flow cytometry measurement of endocytosis of NPs by DCs

JAWSII (ATCC® CRL-11904™) immature DCs from ATCC were cultured with alpha minimum essential medium (80%v) including ribonucleosides, deoxyribonucleosides, 4 mM L-glutamine, 1 mM sodium pyruvate and 5 ng/ml murine GM-CSF, and fetal bovine serum (20%v) at 37 °C, 5% $CO_2$ in 24 well

plates (CORNING, Tewksbury, MA). NPs were assembled according to the above mentioned method, except that KLH was labeled with rhodamine B and 0.5 mg of NBD PE was added to existing lipids. 1 mg of NPs suspended in 2 mL complete medium with a final concentration of 0.5 mg/mL was added into each well containing $10^6$ cells, and incubated for 1 h, 2 h, and 3 h, respectively. After incubation, the medium was immediately removed and cells were washed with ultrapure water for 5 times. Cells were detached from culture plate using trypsin/EDTA solution and centrifuged at 200 g for 10 min, and cell pellets were re-suspended in 10 mM PBS (pH 7.4). Cell samples were immediately analyzed using flow cytometer (BD FACSAria Ⅰ, BD, Franklin Lakes, NJ).

### 2.12 LSM imaging of endocytosis of NPs by DCs

Cells were cultured in 4 well chamber slide (Thermo Fisher Scientific Inc., Rd, Rockford, IL) using the same method described above. NP (0.1 mg) suspended in 500μL complete medium with a final concentration of 0.2 mg/mL was incubated with $10^5$ cells for certain time (1 h, 2 h, and 3 h) at 37 °C, 5% $CO_2$. After incubation, medium was immediately removed and cells were washed with ultrapure water for 5 times. Freshly prepared 4% (w/v) paraformaldehyde (500 μL) was added into each well, and cells were fixed for 15 min and washed 3 times using PBS (10 mM, pH 7.4). Fixed cells were permeabilized using 500 μL of 0.1% (v/v) Triton™ X-100 for 15 min at room temperature, and washed 3 times using PBS (10 mM, pH 7.4). Cells were stained using 500 μL of freshly diluted 1X HCS CellMask™ Blue Stain for 15 min, and washed 3 times using PBS (10 mM, pH 7.4). Cell samples were covered with a glass cover and sealed by nail polish. Images were acquired using Zeiss LSM 510 Laser Scanning Microscope (Carl Zeiss, German). Each step was carried out in darkness as much as possible to avoid fluorescence quenching.

### 2.13 Statistical analysis

All experiments were performed with at least triplicate. Results were expressed as mean ± standard deviation. Different treatment groups in stability test were compared by one-way ANOVA

following Tukey test using the JMP pro 10 (SAS, Cary, NC). Differences were considered significant at p-values that were less than or equal to 0.05.

## 3. Results and discussion

### 3.1 Characterization of PK NPs and LPK NPs

PK NPs (Schematically illustrated in Figure 1 A) were prepared through double emulsion and evaporation technique, and LPK NPs (Schematically illustrated in Figure 1 B) were generated from sonication aided fusion of PK NPs into liposomes. The physicochemical properties, including particle size, polydispersity, surface charge, and antigen content of the NPs were characterized. In PK NP preparation, 3 mg of KLH was added into 200 mg PLGA during the primary emulsion, and the results indicated that around 75% of the KLH was entrapped inside PLGA. The KLH contents in LPK NPs were slightly less (Table 1), and the decrease is possibly due to the extra weight from liposome and loss of KLH during LPK NP preparation. Table 1 also shows that PK NPs have a size of 191.0±15.3 nm, while all LPK NPs, ranging from 208±12.0 nm to 232±34.5 nm, are slightly bigger. Such an increase in size is probably caused by the addition of a lipid layer on surface of the PLGA NP [15]. Nevertheless, all NPs are well smaller than 500 nm, a size that has been shown to enable the NPs to be efficiently uptaken by DCs for vaccine applications [16]. The low polydispersity value (lower than or equal to 0.240±0.019) for each NP indicates that the size distributions of all NPs are in a very narrow range, reflecting high effectiveness and robustness of the preparation method. Surface charge of LPK NPs expressed as zeta potential is largely dependent on the composition of lipid layer. PK NPs with carboxyl groups on the surface showed the lowest zeta potential (-9.7±1.1 mV) among all NPs. Compared to PK NPs, $LPK^{--}$ NPs exhibited positively shifted zeta potential, which might be attributed to the shielding effect of DSPE-PEG (2000) and the small amount of ammine groups on PEG molecules [17]. The positive zeta potentials of $LPK^{++}$ and $LPK^{+}$ NPs are probably attributed to the positive charges carried by DOTAP. The results from zeta potential

measurement demonstrated that the surface charges of hybrid NPs can be flexibly controlled by modulating the lipids composition.

Incorporation of long chain PEG molecules on the surface of NPs is of significant importance as they can not only protect NPs from degradation by enzymes during *in vivo* circulation [18], increasing the stability of NPs and prolonging circulation time [19], but also allow the inclusion of reactive groups in PEG molecules to offer flexible conjugation of various antigens [20]. For targeted delivery purposes, antibodies or affinity ligands against receptors of target cells or tissues may be conjugated to the surface of NPs via PEG chains [21, 22].

The morphology of NPs was studied using TEM. Consistent with the particle size measured using dynamic light scattering (DLS) (Table 1), both PK NPs (Figure 1 C) and LPK NPs (Figure 1 D) displayed a highly uniform particle size (around 200 nm) and narrow size distribution. Most of the NPs showed a smooth surface and were of a spherical shape. Compared to PK NPs, there is a grey membrane covering LPK NPs (Figure1D), demonstrating the successful hybridization of PK NPs and liposomes. The thickness of the membrane is around 20 nm, which is equal to the thickness of a lipid bilayer [15].

To further confirm that PK NPs were successfully hybridized with lipids, LPK NPs comprising PK NPs (KLH was labeled with rhodamine B (red color)) and lipids layer (lipids were labeled with nitro-2-1,3-benzoxadiazole (NBD) (green color)) were examined using confocal LSM. Figure 2 shows the hybrid NPs are marked with both red and green fluorescence, confirming that there is a lipid membrane layer on the surface of PK NPs. It is worth noting that the majority of NPs are double-color labeled, indicating the high efficiency of sonication induced hybridization of PLGA NPs and liposomes.

### 3.2 Stability of NPs in PBS, FBS and human serum

For vaccines, having a desirable stability could ensure prolonged circulation in blood and sustained induction of immune response. Size stability of NPs in various solution, (A) 10 mM PBS, (B) 10%

(v/v) FBS, and (C) 10% (v/v) human serum, was evaluated by DLS (Figure 3). All the NPs, especially LPK NPs were highly stable during incubation in 10 mM PBS (Figure 3 A): no significant size change of LPK NPs was detected over 8 days of test; the size of PK NPs did not increase until day 7. In both FBS (Figure 3 B) and human serum (Figure 3 C), marked size change was detected for PK NPs after 4 h of incubation. In contrast, all the LPK NPs stayed stable for at least 2 days in both FBS and human serum. Especially $LPK^{++}$ NPs kept constant size in FBS for 7 days and in human serum for 8 days. Interestingly, size stability of LPK NPs appears to be related to lipid compositions; NPs with more positive charges exhibited higher stability compared to those with less positive charges. Higher stability of positively charged hybrid NPs may be resulted from strong electrostatic attraction between cationic lipid layer and anionic PLGA core [22, 23].

### 3.3 In vitro release of antigen from NPs

The evaluation of *in vitro* antigen release from NPs in human serum could simulate the antigen release *in vivo*. In agreement with other reports that a lipid shell could help retain molecules loaded inside PLGA cores [15], in this work, LPK NPs displayed more controlled and delayed release of the payload, KLH. As shown in Figure 4, a burst release was observed between 10 h and 12 h for PK NPs, and more than 70% of KLH was released in the first 16 h. In contrast, more than 50% of the KLH was released between 16 h and 96 h for LPK NPs, and in particular, only 35% and 37% percent of KLH were released in the first 16 h for $LPK^{++}$ and $LPK^{+}$ NPs, respectively. The regulated release of KLH in LPK NPs is probably due to the presence of a lipid bilayer that acts as a barrier to reduce KLH diffusion from the PLGA core to the bulk solution, and the PEG shield that delays the enzymatic degradation of NPs [24]. Consistent with the results from size stability study, antigen release from NPs with more positive surface charges was slower than the release from NPs with less positive charges. The slower antigen release may be attributed to the tighter association of the lipid layer with the PLGA core, which reduces the diffusion of KLH from NPs into the bulk solution. Delayed antigen release from NPs may reduce loss of antigen during circulation and increase bioavailability of antigen to DCs, thereby enhancing immune response.

### 3.4 Endocytosis of NPs by DCs

Dendritic cell is the most professional antigen presenting cell that can initiate and regulate adaptive immune response [25, 26]. Higher internalization efficiency of NPs by DCs may lead to more activated T helper cells, resulting in enhanced immune response. Fluorescently marked NPs were added into immature DCs from mouse to study the uptake of NPs by DCs. Results from flow cytometry measurement (Figure 5) showed that higher internalization efficiency was observed in all LPK NPs compared to PK NPs. In the first hour after NP treatment, only 28% of DCs had taken up PK NPs, and while 77%, 63%, 39%, and 50% of DCs had taken up $LPK^{++}$, $LPK^{+}$, $LPK^{--}$, and $LPK^{-}$ NPs, respectively. After 3 h of incubation, more than 90% of DCs have internalized LPK NPs in all four groups; however, only 52% of DCs have taken up PK NPs. Evidently, surface charge has a great impact on NP uptake. For example, 77% of DCs ingested $LPK^{++}$ NPs in the first hour of incubation, but only 39% for $LPK^{--}$ NPs. Faster uptake of NPs by DCs is important because it should reduce the clearance of NPs by reticuloendothelial system (RES), avoid premature degradation by enzymes, and increase the availability of antigens to the immune system. LSM images (Figure 6) also confirmed that LPK NPs had superior uptake efficiency in comparison to PK NPs. In the first hour after NPs treatment, only few PK NPs were internalized by DCs; in contrast, both $LPK^{++}$ and $LPK^{--}$ NPs with large quantities were taken up by DCs (Figure 6 A). After 2 h, the internalized PK NPs located in a small area of the cell, while LPK NPs were widely distributed in cells (Figure 6 B). Faster uptake of LPK NPs by DCs is probably due to the coating lipid bilayer that could mimic cell membrane to fuse with plasma membrane of DCs. Consistent with the results from flow cytometry study, more $LPK^{++}$ NPs were ingested by DCs than $LPK^{--}$ NPs within the same period of time, suggesting DCs could more efficiently capture NPs with more positive surface charges. The faster uptake of $LPK^{++}$ NPs may be due to the electrostatic attraction between positive surface charges on $LPK^{++}$ and negative charges on plasma membrane of DCs.

## 4. Conclusions

In summary, lipid-PLGA hybrid NPs with variable lipid compositions were constructed. As a potential antigen delivery system, lipid-PLGA NPs exhibited superior quality in comparison to PLGA NPs in terms of stability, antigen release, and particle uptake by DCs. The *in vitro* performance of lipid-PLGA NPs was highly influenced by the composition of the lipid layer, which dictates the surface chemistry of hybrid NPs. Hybrid NPs enveloped by lipids with more positive surface charges demonstrated higher stability, better controlled release of antigen, and more efficient uptake by DC than particles with less positive surface charges. The results should provide basis for future design of lipid-PLGA hybrid NPs intended for antigen delivery.

## Acknowledgment

This work was financially supported by National Institutes of Health, more specifically, National Institute on Drug Abuse (R21 DA030083).

## References

[1] Grottkau BE, Cai X, Wang J, Yang X, Lin Y. Polymeric nanoparticles for a drug delivery system. Current drug metabolism. 2013;14:840-6.

[2] Mallick S, Choi JS. Liposomes: versatile and biocompatible nanovesicles for efficient biomolecules delivery. Journal of nanoscience and nanotechnology. 2014;14:755-65.

[3] Danhier F, Ansorena E, Silva JM, Coco R, Le Breton A, Preat V. PLGA-based nanoparticles: an overview of biomedical applications. Journal of controlled release : official journal of the Controlled Release Society. 2012;161:505-22.

[4] Nobs L, Buchegger F, Gurny R, Allemann E. Current methods for attaching targeting ligands to liposomes and nanoparticles. Journal of pharmaceutical sciences. 2004;93:1980-92.

[5] Ganta S, Devalapally H, Shahiwala A, Amiji M. A review of stimuli-responsive nanocarriers for drug and gene delivery. Journal of controlled release : official journal of the Controlled Release Society. 2008;126:187-204.

[6] Takara K, Hatakeyama H, Kibria G, Ohga N, Hida K, Harashima H. Size-controlled, dual-ligand modified liposomes that target the tumor vasculature show promise for use in drug-resistant cancer therapy. Journal of controlled release : official journal of the Controlled Release Society. 2012;162:225-32.

[7] Tan S, Li X, Guo Y, Zhang Z. Lipid-enveloped hybrid nanoparticles for drug delivery. Nanoscale. 2013;5:860-72.

[8] Mandal B, Bhattacharjee H, Mittal N, Sah H, Balabathula P, Thoma LA, et al. Core-shell-type lipid-polymer hybrid nanoparticles as a drug delivery platform. Nanomedicine : nanotechnology, biology, and medicine. 2013;9:474-91.

[9] Sengupta S, Eavarone D, Capila I, Zhao G, Watson N, Kiziltepe T, et al. Temporal targeting of tumour cells and neovasculature with a nanoscale delivery system. Nature. 2005;436:568-72.

[10] Moon JJ, Suh H, Polhemus ME, Ockenhouse CF, Yadava A, Irvine DJ. Antigen-displaying lipid-enveloped PLGA nanoparticles as delivery agents for a Plasmodium vivax malaria vaccine. PloS one. 2012;7:e31472.

[11] Krishnamachari Y, Geary SM, Lemke CD, Salem AK. Nanoparticle delivery systems in cancer vaccines. Pharmaceutical research. 2011;28:215-36.

[12] Salmaso S, Caliceti P. Stealth properties to improve therapeutic efficacy of drug nanocarriers. Journal of drug delivery. 2013;2013:374252.

[13] Yang YY, Chia HH, Chung TS. Effect of preparation temperature on the characteristics and release profiles of PLGA microspheres containing protein fabricated by double-emulsion solvent extraction/evaporation method. Journal of controlled release : official journal of the Controlled Release Society. 2000;69:81-96.

[14] Brown RE, Jarvis KL, Hyland KJ. Protein measurement using bicinchoninic acid: elimination of interfering substances. Analytical biochemistry. 1989;180:136-9.

[15] Zhang L, Chan JM, Gu FX, Rhee JW, Wang AZ, Radovic-Moreno AF, et al. Self-assembled lipid--polymer hybrid nanoparticles: a robust drug delivery platform. ACS nano. 2008;2:1696-702.

[16] Foged C, Brodin B, Frokjaer S, Sundblad A. Particle size and surface charge affect particle uptake by human dendritic cells in an in vitro model. International journal of pharmaceutics. 2005;298:315-22.

[17] Takahashi T, Yamada Y, Kataoka K, Nagasaki Y. Preparation of a novel PEG-clay hybrid as a DDS material: dispersion stability and sustained release profiles. Journal of controlled release : official journal of the Controlled Release Society. 2005;107:408-16.

[18] Zou W, Liu C, Chen Z, Zhang N. Preparation and Characterization of Cationic PLA-PEG Nanoparticles for Delivery of Plasmid DNA. Nanoscale research letters. 2009;4:982-92.

[19] Romberg B, Hennink WE, Storm G. Sheddable coatings for long-circulating nanoparticles. Pharmaceutical research. 2008;25:55-71.

[20] Roberts MJ, Bentley MD, Harris JM. Chemistry for peptide and protein PEGylation. Advanced drug delivery reviews. 2002;54:459-76.

[21] Cruz LJ, Tacken PJ, Fokkink R, Figdor CG. The influence of PEG chain length and targeting moiety on antibody-mediated delivery of nanoparticle vaccines to human dendritic cells. Biomaterials. 2011;32:6791-803.

[22] Chun KW, Yoo HS, Yoon JJ, Park TG. Biodegradable PLGA microcarriers for injectable delivery of chondrocytes: effect of surface modification on cell attachment and function. Biotechnology progress. 2004;20:1797-801.

[23] Even-Chen S, Barenholz Y. DOTAP cationic liposomes prefer relaxed over supercoiled plasmids. Biochimica et biophysica acta. 2000;1509:176-88.

[24] Cai Q, Shi G, Bei J, Wang S. Enzymatic degradation behavior and mechanism of poly(lactide-co-glycolide) foams by trypsin. Biomaterials. 2003;24:629-38.

[25] Hamdy S, Haddadi A, Hung RW, Lavasanifar A. Targeting dendritic cells with nano-particulate PLGA cancer vaccine formulations. Advanced drug delivery reviews. 2011;63:943-55.

[26] Cruz LJ, Tacken PJ, Rueda F, Domingo JC, Albericio F, Figdor CG. Targeting nanoparticles to dendritic cells for immunotherapy. Methods in enzymology. 2012;509:143-63

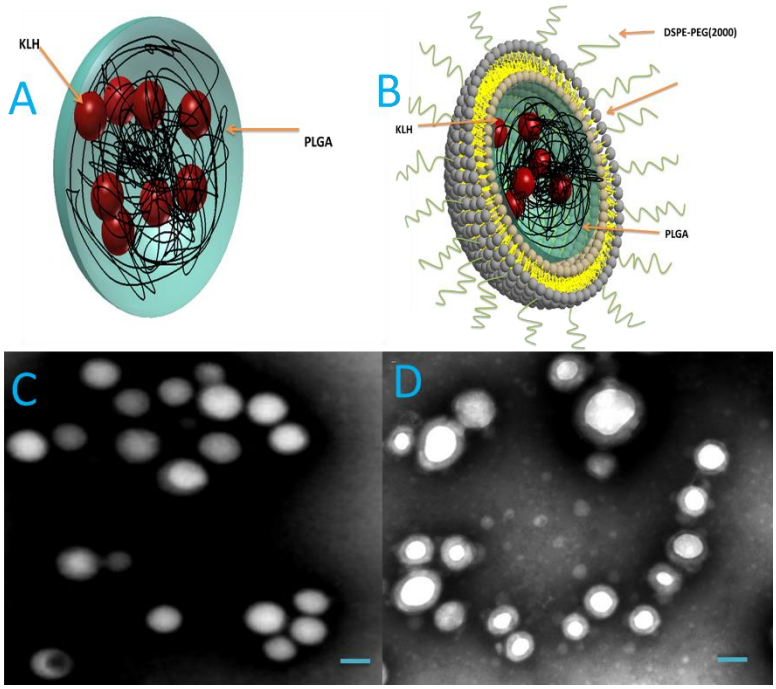


**Figure 1.** TEM images of hybrid NPs. (A) Schematic illustration of PK NP. (B) Schematic illustration of LPK NP. (C) TEM image of PK NPs, which highlights the uniform size and spherical shape of PK NPs. (D) TEM image of hybrid LPK NPs, which shows the lipid bilayer enclosed PK NPs. The scale bars represent 200 nm.

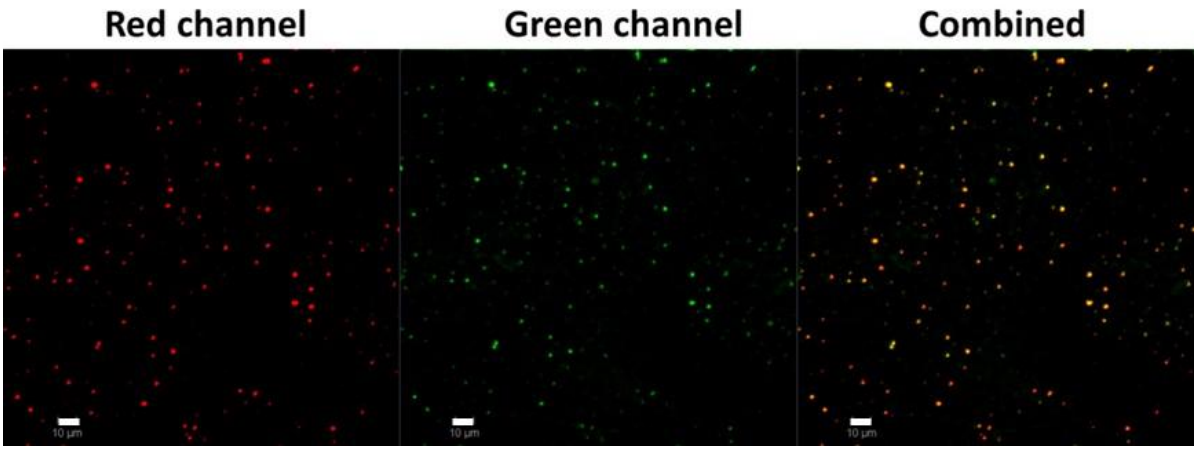


**Figure 2.** Confocal images of LPK NPs, in which KLH was labeled with rhodamine B (red) and liposome was labeled with NBD (green), confirmed that PK NPs was enclosed by liposome. Scale bars represent 10 μm.

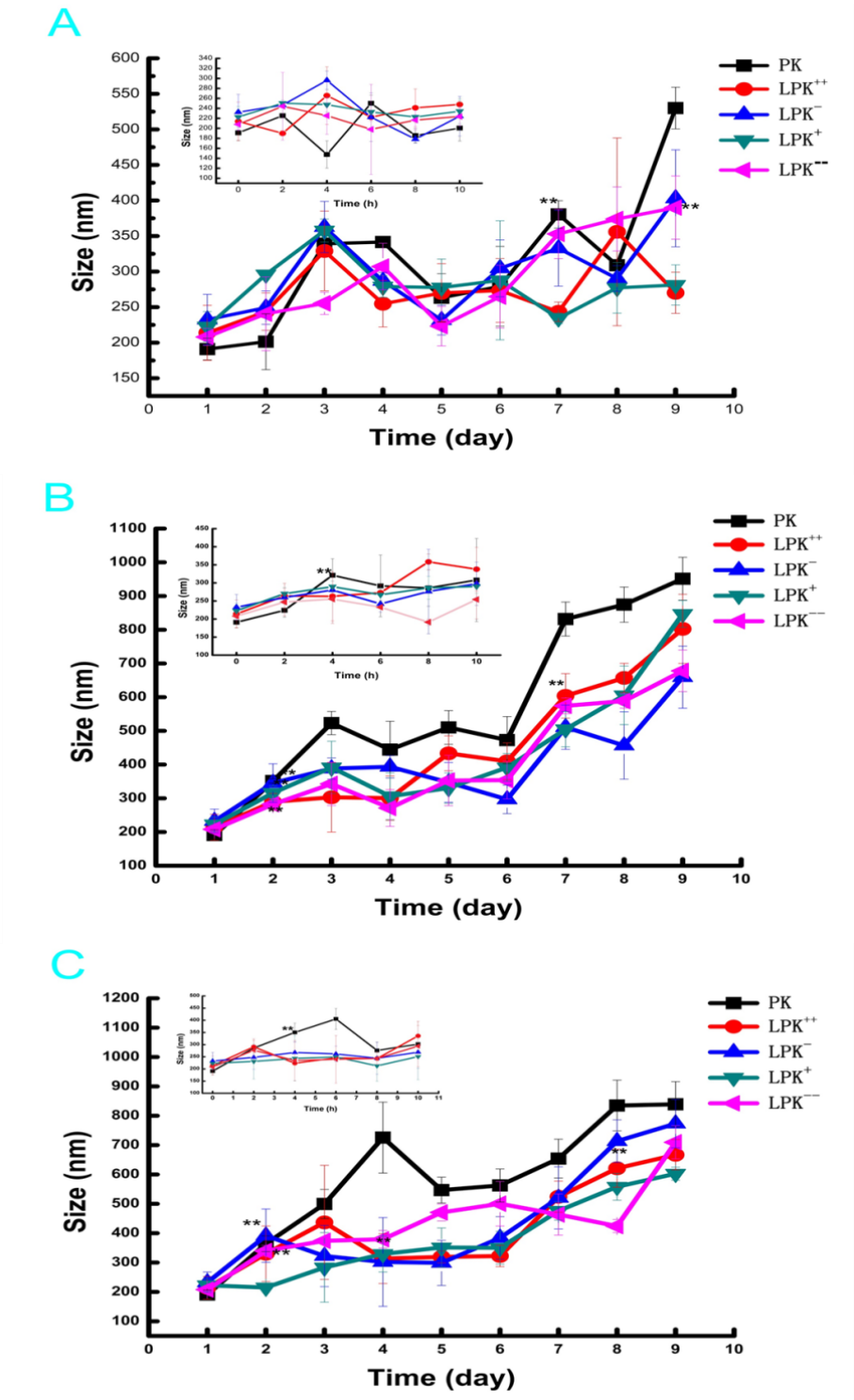


**Figure 3.** In vitro stability of NPs: (A) 10 mM PBS, (B) 10% (v/v) FBS, and (C) 10% (v/v) human serum. Sizes of all NPs, except PK NPs were stable in PBS over 9 days' incubation. LPK NPs demonstrated superior stability compared to PK NPs in the three solutions. In both FBS and human serum, sizes of all NPs increase more quickly compared to that in PBS. The inset pictures show antigen release from NPs

within 10 hours incubation.** indicates that the size of NPs at this point was significantly higher compared to that at 0 h (P-value<0.05).

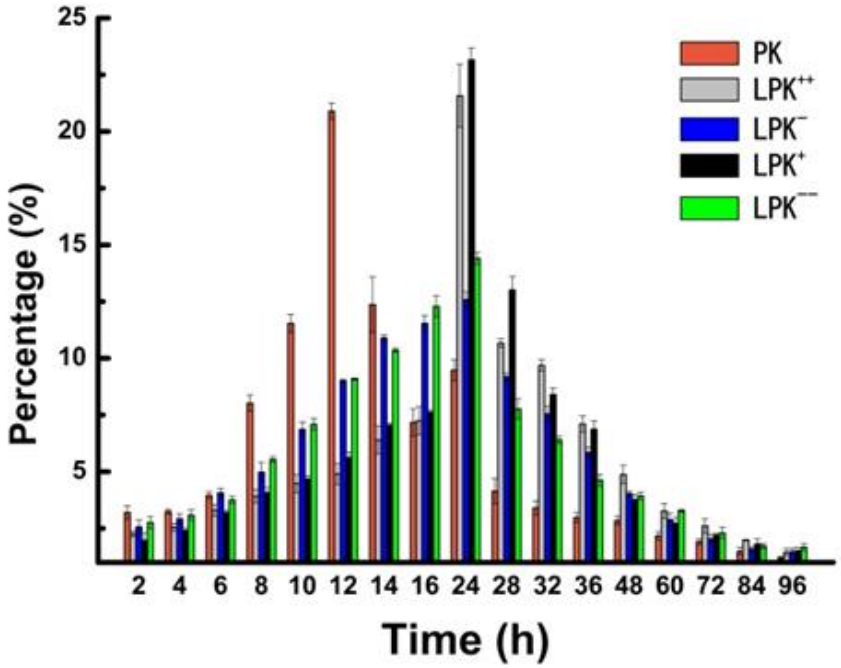


**Figure 4.** Release of KLH contained in NPs in 10% human serum (pH 7.4) at 37 $^{0}$C. All NPs exhibited a prolonged release of KLH. PK NPs showed a burst release of KLH between 8 h and 10 h. LPK displayed a delayed release profile, in which the largest percentage release occurred between 16 h and 24 h. The extent of release was also dependent on the composition and charged of the NPs.

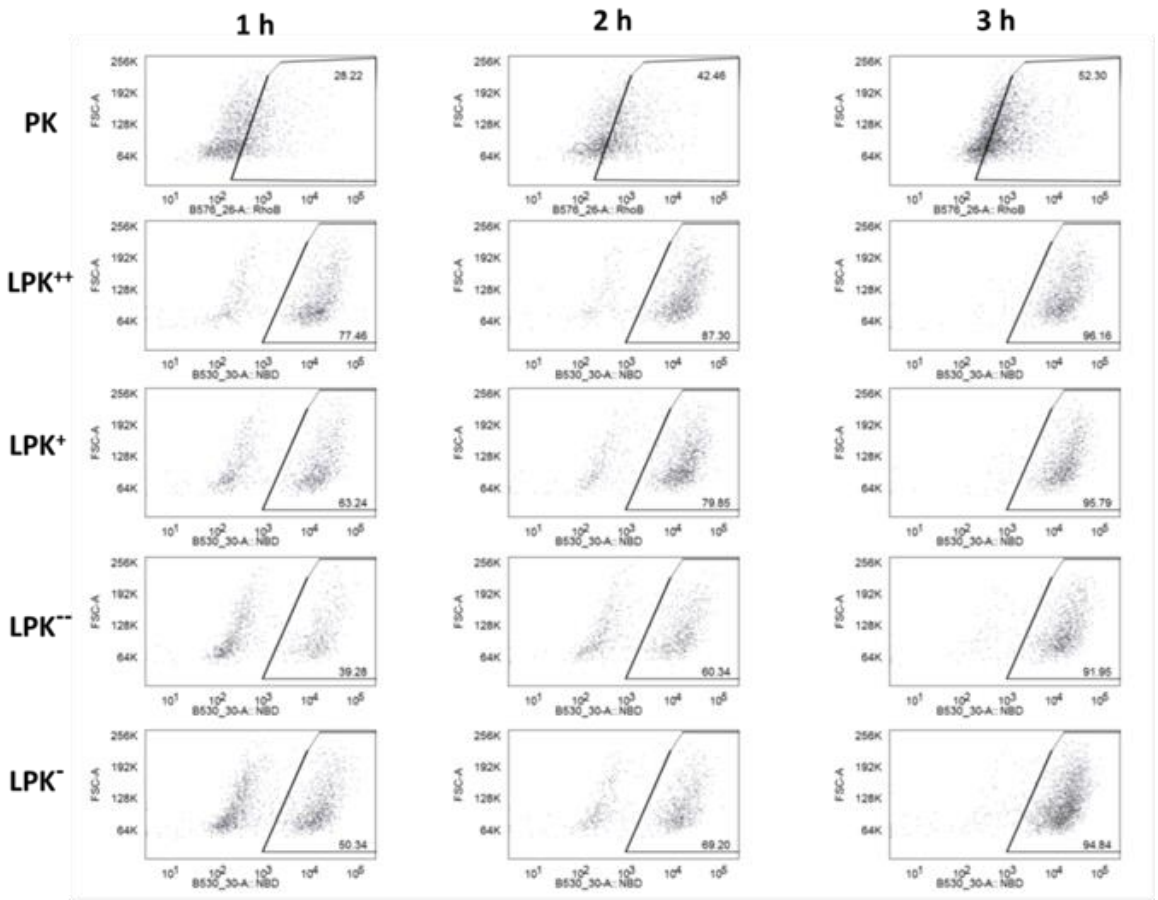


**Figure 5.** Flow cytometer measurement of uptake of PK NPs, and LPK NPs by JAWS Ⅱ DCs. 1 mg of NPs was incubated with $10^6$ cells for 1 h, 2 h, and 3 h, respectively. As time lapsed, more NPs were ingested by cells. Enhanced uptake of LPK NPs by DCs was observed compared to PK NPs. DCs are more readily to uptake positively charged NPs compared to negatively charged NPs. Most of the cells (>90%) had taken up LPK NPs in 3 h, and while only 52% of the cells had taken up PK NPs.

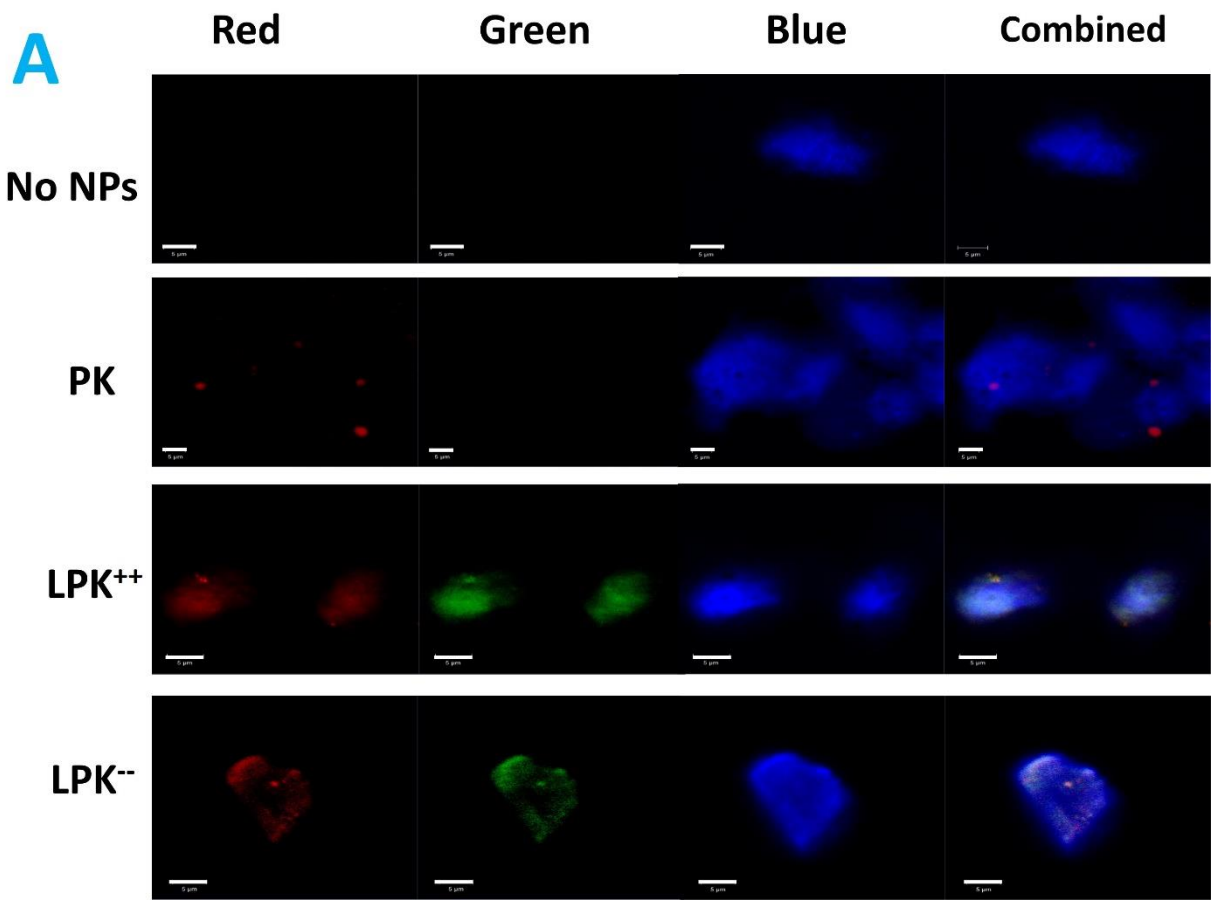
A
Red
Green
Blue
Combined
No NPs
PK
LPK++
LPK--

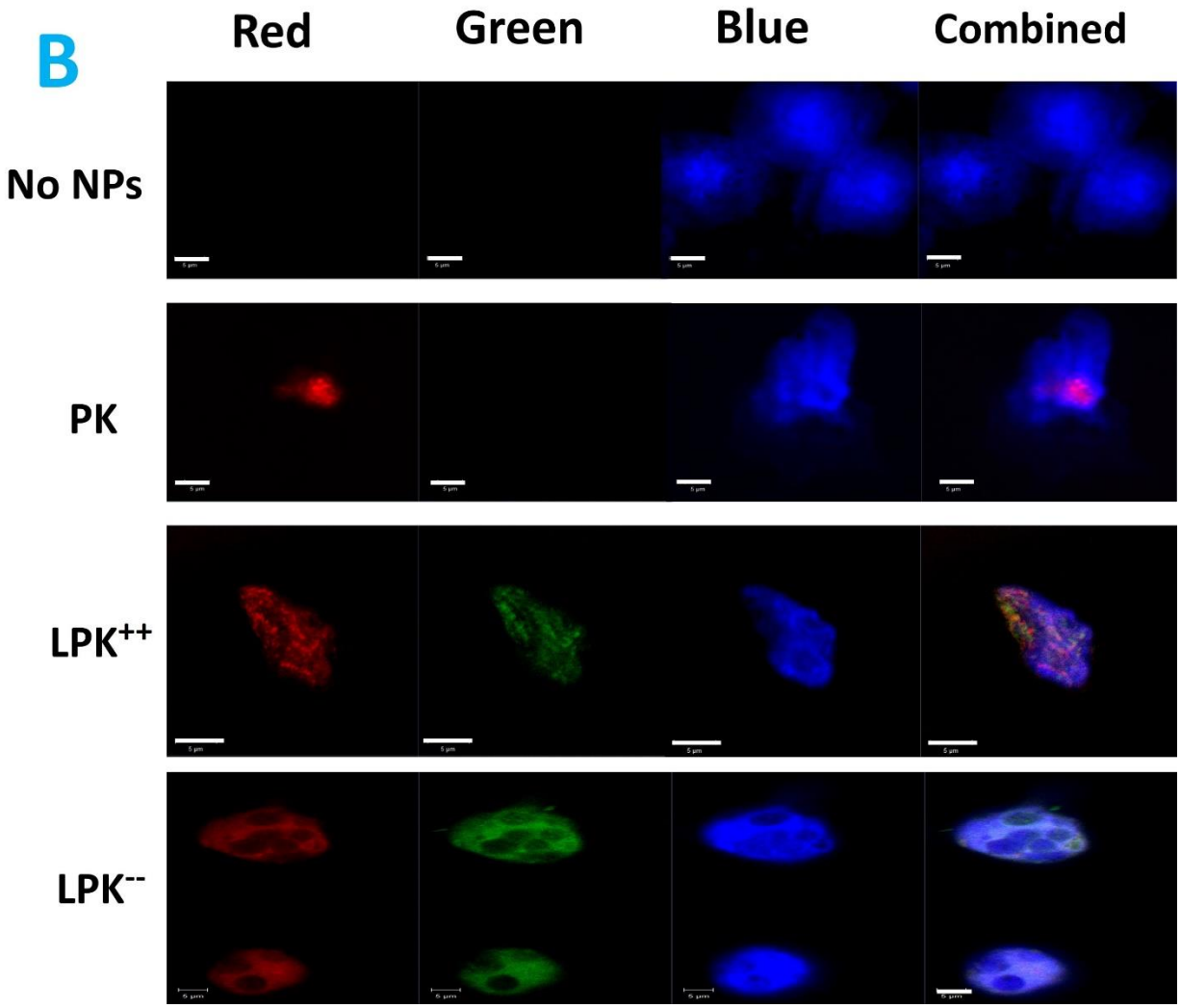
B
Red
Green
Blue
Combined
No NPs
PK
LPK++
LPK--

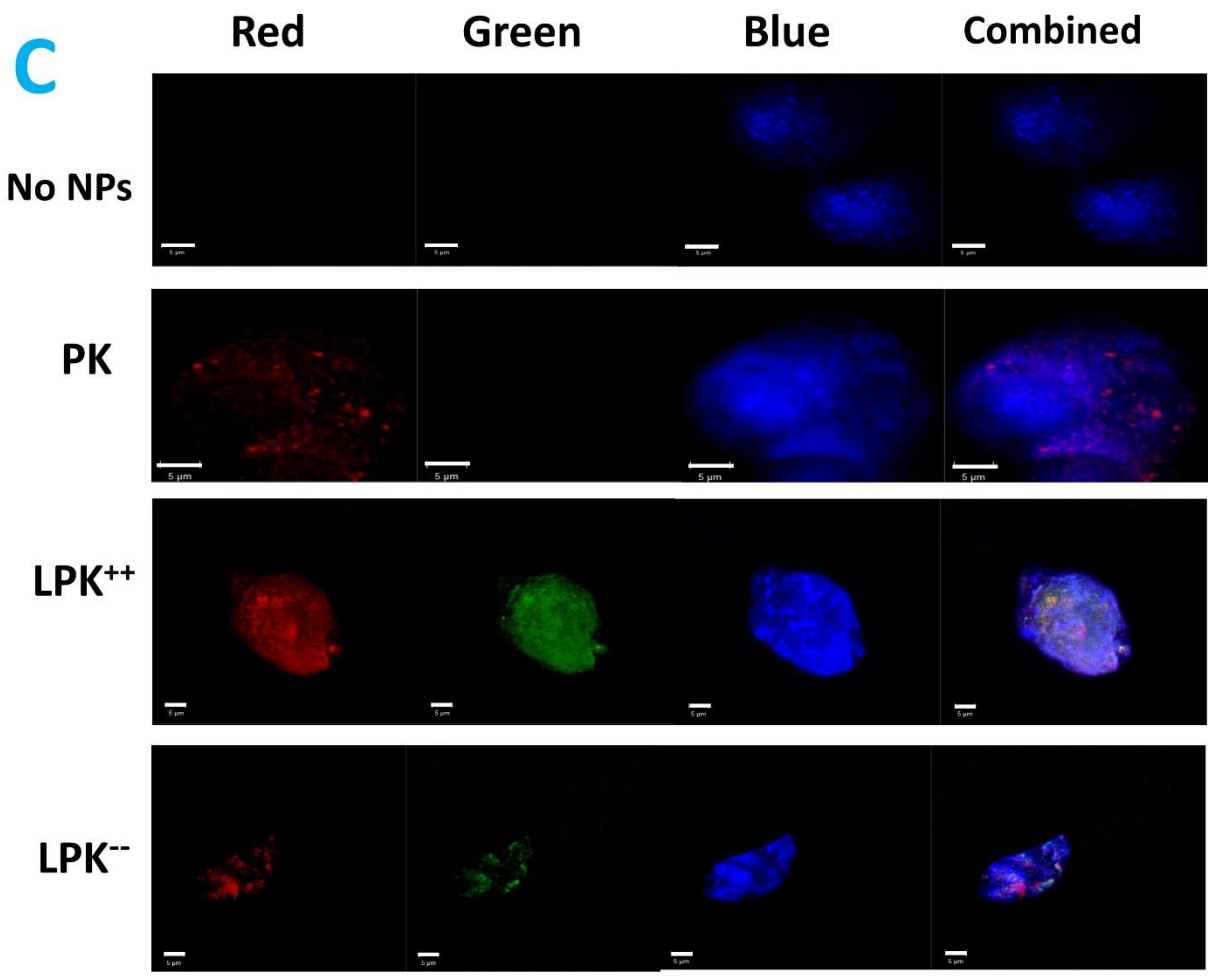


**Figure 6.** Confocal images of internalization of PK NPs, and LPK NPs by JAWS II DCs. $10^5$ cells were incubated with 0.1 mg NPs for 1 h (A), 2 h (B), and 3 h (C), respectively. Red color is rhodamine B, which was used to label KLH; green color is NBD PE, which was used to label lipid layer; blue color is CellMask™ Blue Stain, which was used to label cell membrane. Both positively charged LPK NPs and negatively charged LPK NPs were internalized more readily by cells than PK NPs. Scale bars represent 5 µm.

**Table 1.** Components, physicochemical properties and the KLH content of various NPs.

| Group | Components of NPs (mg) | | | | | Size (dm. nm) | Polydispersity | Zeta potential (mV) | KLH content (%) |
|---|---|---|---|---|---|---|---|---|---|
| | PLGA | KLH | DOTAP | DOPC | DSPE-PEG | | | | |
| **PK** | 200 | 3 | 0 | 0 | 0 | 191.0±15.3 | 0.199±0.012 | -9.7±1.1 | 1.12±0.21 |
| **LPK$^{++}$** | 200 | 3 | 16 | 0 | 4 | 213±38.7 | 0.231±0.022 | 13.9±1.3 | 1.11±0.22 |
| **LPK$^{-}$** | 200 | 3 | 2 | 14 | 4 | 232.4±34.5 | 0.248±0.018 | -3.6±1.4 | 1.05±0.10 |
| **LPK$^{+}$** | 200 | 3 | 14 | 2 | 4 | 222.6±21.0 | 0.240±0.019 | 6.4±1.1 | 0.92±0.15 |
| **LPK$^{--}$** | 200 | 3 | 0 | 16 | 4 | 208.0±12.0 | 0.219±0.023 | -5.5±0.9 | 0.84±0.03 |

# Chapter VI (results): Controlled release of antigen in dendritic cells using pH-sensitive liposome-polymeric hybrid nanoparticles

Yun Hu[1], Zongmin Zhao[1], Marion Ehrich[2], Kristel Fuhrman[3], Chenming Zhang[1*]

[1] Department of Biological Systems Engineering, Virginia Tech, Blacksburg, VA 24061, U.S.A.

[2] Department of Biomedical Sciences and Pathobiology, Virginia Tech, Blacksburg, VA 24061, U.S.A.

[3] Veterinary Medicine Experiment Station, Virginia Tech, Blacksburg, VA 24061, U.S.A.

[*] Corresponding author

Email: chzhang2@vt.edu

**Abstract**

The ability for a nano delivery system to remain stable during circulation *in vivo*, as well as enable rapid release of the encapsulated antigens in dendritic cells (DCs) would be of great value in vaccine development. Hybrid nanoparticles (NPs) have been extensively studied as antigen delivery vehicles, but very few of those particles were able to realize intracellular controlled release of antigens in DC. Here, a nano hybrid particle consisting of a pH sensitive lipid shell and a poly (lactic-co-glycolic) acid (PLGA) core was constructed. This NP has mean size of 120.1±8.8 nm and positively charged surface (zeta potential of 14.2±1.4 mV). The lipid shell of the hybrid NP was quickly disintegrated in response to a low pH challenge, which resembles the acidic environment of endosomes in DC. The hybrid NPs exhibited minimal antigen release in human serum at physiological pH, but a faster release of antigen from this NP compared to non-pH sensitive NPs was observed in DC.

Keeping all the favorable characteristics of traditional hybrid NPs as well as facilitating controlled release of antigen in DC make this hybrid NP a promising antigen delivery system for vaccine development.

**Keywords:** Dendritic cell; Hybrid nanoparticle; Liposome; PLGA; pH-sensitive lipid; Vaccine

## 1. Introduction

As the most professional antigen presenting cell (APC), dendritic cells (DCs) play a critical role in adaptive immune response.[1] Immature DCs are widely and sparsely distributed in the periphery tissues, including skin, nose and lungs, scanning surrounding areas for invading foreign materials. [2] Upon internalizing antigens, DCs will be activated, commence maturation and start to migrate into the nearest lymph node, where the processed antigen peptides associated with MHC molecules can be presented to naïve T cells, triggering their subsequent activation.[3] The maturation of DCs is of particular importance to vaccine development, because rapid maturation may lead to rapid activation of naïve T cells, and the degree of maturation can also affect the magnitude of the immune response via the expression of MHC molecules, costimulatory molecules, and cytokines by DC.[4]

Currently, NP based vaccine delivery systems are considered to hold great promise for enhancing the immunogenicity of conventional antigens due to their advantages of more pathogen-like morphology, co-delivery of adjuvants, high antigen loading capacity, protection of antigens such as proteins, peptides, and DNAs from degradation during circulation, and sustained release of antigens.[5-7] Normally, NPs are designed to be stable enough to avoid premature release of the enclosed effector molecules. However, it is possible that such stability may overprotect antigens from enzymatic processing in endosomes after uptake by DCs, resulting in slow and incomplete induction of an immune response, thus compromising the efficacy of the vaccine. It is reasonable to believe that the timely release of antigens and adjuvants contained in NPs after internalization may facilitate the maturation of DCs and promote an immune response. Therefore, it is desirable to devise a delivery system that could not only protect the antigen

from premature degradation, but also enable the timely release of antigens and adjuvants in the endosomes of DCs.

In addition to the common advantages enjoyed by NPs as mentioned above, NPs made from poly(lactic-co-glycolic) acid (PLGA) or lipids have been extensively used as vaccine and drug delivery systems due to their biocompatibility and biodegradable characteristics.[8-10] Hybrid NPs composed of PLGA and lipids have been constructed to improve cancer drug delivery and imaging diagnosis [11, 12]. Previous work in our lab (data not published) showed that liposome-polymeric hybrid NPs could potentially be applied as a vaccine delivery system due to their large antigen loading capacity, tunable physiochemical properties, and excellent stability in human plasma. However, previous researchers mainly focused their work on how to improve the stability of NPs for antigen delivery,[13, 14] while ignoring the possibility that "overprotection" may occur to delay the release of antigens in target cells.[15]

In order to devise a NP for vaccine delivery that can minimize the loss of the enclosed antigens during circulation as well as enable timely release of the antigens in immune cells, a lipid-PLGA hybrid NP was constructed in our laboratory. The hybrid NP on one hand exhibited excellent stability in human plasma to enable extended circulation of NPs, and on the other hand allowed rapid release of the enclosed antigen in response to acidification in endosomes after uptake by DCs. These features should enable antigens delivered by this NP to induce a rapid and complete immune response as well as produce prolonged immunity. This hybrid nanosystem consists of a shell made from pH sensitive lipids and an inner PLGA core. The physicochemical properties of the nano hybrid were evaluated in terms of size, surface charge, morphology, *in vitro* release profile of the enclosed antigen, its uptake by DCs, and intracellular release of the enclosed antigen. All nanoparticles tested exhibited good stability under physiological pH. However, in contrast to non-pH sensitive hybrid NPs, the lipid shell of pH sensitive NPs

could be readily disintegrated to allow rapid release of the enclosed antigens in response to a low pH challenge (**Scheme**). All results to date suggest that the pH sensitive hybrid NPs are particularly suitable for addressing the "overprotection" and are capable of controlling the release of the enclosed antigens.

## 2. Materials and methods

### 2.1 Materials

Lactel® 50:50 PLGA was purchased from Durect Corporation (Cupertino, CA). Fetal bovine serum (FBS), GM-CSF recombinant mouse protein, minimum essential medium (MEM) α, trypsin/EDTA, CellMask™ Orange Plasma membrane Stain, Alexa Fluor® 647 hydrazide, tris(triethylammonium) salt were purchased from Life Technologies Corporation (Grand Island, NY). Lipids, including 1,2-dioleoyl-3-trimethylammonium-propane (DOTAP), 1,2-dioleoyl-sn-glycero-3-phosphocholine (DOPC), cholesteryl hemisuccinate (CHEMS), 1,2-dioleoyl-sn-glycero-3-phosphoethanolamine (DOPE), 1,2-distearoyl-sn-glycero-3-phosphoethanolamine-N-[amino(polyethylene glycol)-2000] (ammonium salt) (DSPE-PEG2000), and 1,2-diphytanoyl-sn-glycero-3-phosphoethanolamine-N-(7-nitro-2-1,3-benzoxadiazol-4-yl) (ammonium salt) (NBD PE) were purchased from Avanti Polar Lipids, Inc. ( Alabaster, AL). Keyhole limpet hemocyanin (KLH), poly (vinyl alcohol) (PVA, Mw 89,000-98,000), dichloromethane (DCM), rhodamine B (Rhod B), paraformaldehyde, Triton™X-100 were purchased from Sigma-Aldrich Inc. (Saint Louis, MO). 1-Ethyl-3-[3-dimethylaminopropyl] carbodiimide hydrochloride (EDC) was purchased from Thermo Fisher Scientific Inc. (Rd, Rockford, IL). JAWSII (ATCC® CRL-11904™) immature dendritic cells were purchased from ATCC (Manassas, VA). All other chemicals were of analytical grade.

### 2.2 Methods

#### 2.2.1 Synthesis of KLH containing PLGA (PK) NPs

PK NPs were prepared using a reported double emulsion solvent evaporation method with modifications.[16] Briefly, PLGA (20 mg) was dissolved in DCM (2 mL), followed by mixing with 50 μL of

KLH (10 mg/mL) using a vortex for 2 min. The resultant mixture was emulsified via sonication at 20% amplitude for 20 s using a sonic dismembrator (Model 500; Fisher Scientific, Pittsburg, PA). The primary emulsion was added dropwise into 100 mL PVA (1% (w/v)), and continuously stirred for 10 min at 500 rpm. The above suspension was emulsified through sonication at 50% amplitude for 120 s. The secondary emulsion was stirred overnight to allow DCM to evaporate. Large particles were removed after the mixture stood at room temperature for 30 min. NPs in suspension were collected by centrifugation at 20,000 g, 4 °C for 30 min (Beckman Coulter Avanti J-251, Brea, CA). The pellet was washed 3 times using ultrapure water. The final suspension was freeze-dried (LABCONCO Freezone 4.5, Kansas City, MO), and NPs were stored at 2 °C for later use.

### 2.2.2 Assembly liposome-PK (LPK) hybrid NPs

A lipid film (10 mg) containing given lipids was hydrated with 5 mL, 55°C pre-warmed hydration buffer (0.9% saline, 5% dextrose, and 10% sucrose). The resulting suspension was vigorously mixed using a vortex for 2 min, followed by incubation at 55 °C for 5 min and cooling to room temperature. PK NPs (10 mg) were added into the liposome suspension and pre-homogenized for 15 min using a Branson 2510 bath sonicator (Danbury, CT), followed by sonication on ice bath at 15% amplitude for 5 min (pulse on 20 s, pulse off 50 s) using a sonic dismembrator (Model 500; Fisher Scientific, Pittsburg, PA). The formed LPK NPs were collected by centrifugation at 20,000 g, 4 °C for 30 min, lyophilized, and stored at 2 °C.

### 2.2.3 Labeling KLH with Rhod B or Alexa Fluor® 647 hydrazide

The coupling of fluorescent dyes to KLH was done by a method described in a previous study.[17] Ten mg of EDC dissolved in 700 µL ultrapure water (pH 6.8) were mixed with 300 µL of 2 mg/mL Rhod B. After incubation at 0 °C for 10 minutes, the product was mixed with 5 mg KLH (10 mg/mL) and stirred in darkness at room temperature for 12 h. For Alexa Fluor® 647 hydrazide labeling, 5 mg of EDC in 800 µL

ultrapure water (pH 6.8) was incubated with 5 mg KLH (10 mg/mL) at 0 °C for 10 minutes, followed by reaction with 100 μg Alexa Fluor® 647 hydrazide in darkness at room temperature for 10 h. Fluorescently labeled KLH was purified using Microcon centrifugal filter units (50,000 MWCO, EMD Millipore, Billerica, MA), freeze-dried, and stored at 2 °C.

### 2.2.4 Characterizing physicochemical properties of NPs

One mg of NPs was dispersed in 5 mL ultrapure water (pH 7.0) using a bath sonicator for 5 min. Each sample was diluted by 10 fold using ultrapure water, and the particle size (diameter, nm) and surface charge (zeta potential, mV) were measured using a Malvern Nano-ZS zetasizer (Malvern Instruments Ltd, Worcestershire, United Kingdom) at room temperature.

### 2.2.5 In vitro size stability of NPs under low pH

For these experiments, all the NPs were synthesized in the same batch. One mg of NPs was suspended in 5 mL, 10 mM phosphate buffered saline (PBS) with initial pH of 7.4, and then the pH was lowered to 5.5 for each group. The original particle size in pH 7.4 and that after being treated with pH 5.5 for 10 min were measured.

### 2.2.6 In vitro KLH release from NPs treated with low pH human plasma

Five mg of LPK NPs containing Rhod B labeled KLH were suspended in 10 mL (5% v/v) human plasma (pH 7.4) and continuously stirred at room temperature. After 24 h incubation, the pH was lowered to 5.5 for each group and treated for another 48 h. The released KLH was separated from NPs via centrifugation at 20,000 g for 30 min at indicated time points. The NPs were re-suspended in human plasma and the released KLH in supernatant was measured using Synergy HT Multi-Mode Microplate Reader (BioTek Instruments, Inc., Winooski, VT) with excitation at 530 nm and emission at 590 nm. The percentage of released KLH at given time points was calculated using the following equation: % KLH released = Absorbance at a given time point/Total absorbance×100.

### 2.2.7 Imaging NPs using transmission electrical microscopy (TEM)

NP suspensions (1 mg/mL) before and after pH 5.5 treatment were dropped onto a 300-mesh Formvar-coated copper grid. After standing 10 min, the remaining suspension was carefully removed with wipes, and the samples were negatively stained using fresh 1% phosphotunstic acid for 60 s and washed by ultrapure water twice. The dried samples were imaged on a JEOL JEM 1400 Transmission Electron Microscope (JEOL Ltd., Tokyo, Japan).

### 2.2.8 Imaging LPK NPs using confocal laser scanning microscope (LSM)

A Zeiss LSM 510 Laser Scanning Microscope (Carl Zeiss, German) was used to image pH sensitive NPs containing Alexa Fluor® 647 hydrazide labeled KLH and NBD PE labeled lipid shells.

### 2.2.9 Fourier transform infrared (FT-IR) spectroscopy analysis of NPs

The spectrum of freeze-dried pH sensitive liposome, PLGA NPs, and the hybrid NPs were recorded on a Thermo Nicolet 6700 FT-IR spectrometer (Thermo Fisher Scientific Inc., Waltham, MA). The spectrum was taken from 4000 to 400 $cm^{-1}$.

### 2.2.10 Flow cytometry measurement of endocytosis of NPs by DCs

JAWSII (ATCC® CRL-11904™) immature dendritic cells from ATCC were cultured with alpha minimum essential medium (80%v) including ribonucleosides, deoxyribonucleosides, 4 mM L-glutamine, 1 mM sodium pyruvate and 5 ng/mL murine GM-CSF, and fetal bovine serum (20%v) at 37 °C, 5% $CO_2$ in 24 well plates (CORNING, Tewksbury, MA). NPs were assembled according to the above mentioned method, except 0.25 mg NBD PE was added into the existing lipids. Two hundred μg of NPs were added into each well containing $2\times10^6$ cells, and incubated for 5 h. After incubation, the medium was immediately removed and cells were washed 5 times with ultrapure water. Cells were detached from culture plate using trypsin/EDTA solution and centrifuged at 200 g for 10 min, then cell pellets were re-

suspended in 10 mM PBS (pH 7.4). Cell samples were immediately analyzed by flow cytometry (BD FACSAria Ⅰ, BD, Franklin Lakes, NJ).

### 2.2.11 Imaging endocytosis of NPs by DCs using LSM

Cells were cultured in a 4 well chamber slide (Thermo Fisher Scientific Inc., Rd, Rockford, IL) using the same method described above. One hundred μg NPs were incubated with $2\times10^5$ cells for 8 h at 37 °C, 5% $CO_2$. After incubation, the medium was immediately removed and cells were washed 5 times with ultrapure water. Freshly prepared 4% (w/v) paraformaldehyde (500 μL) was added into each well, and cells were fixed for 15 min. This was followed by washing 3 times with PBS (10 mM, pH 7.4). Fixed cells were permeabilized using 500 μL of 0.1% (v/v) Triton™ X-100 for 15 min at room temperature, and washed 3 times using PBS (10 mM, pH 7.4). Cells were stained using 500 μL of freshly diluted 1X CellMask™ Orange Plasma membrane Stain for 15 min, and washed 3 times using PBS (10 mM, pH 7.4). Cell samples were covered with a glass cover and sealed by nail polish. Images were acquired using a Zeiss LSM 510 Laser Scanning Microscope (Carl Zeiss, Germany).

### 2.2.12 Imaging distribution of NPs in DCs using TEM

Petri dishes containing $4\times10^6$ immature DCs were supplemented with 500 μg of the three types of NPs. After 5 h incubation, the medium containing un-internalized NPs was removed and cells were washed with 5 times with ultrapure water. Cell samples were prepared for TEM using the following procedure: Cells were washed 2 times in 0.1 M Na-Cacodylate for 15 minutes each, and then post-fixed in 1% $OsO_4$ in 0.1 M Na-Cacodylate for one hour. $OsO_4$ was discarded, and the samples were washed two times for 10 minutes each in 0.1 M Na-Cacodylate. Cell samples were dehydrated in solutions containing increasing ethanol concentration as follows: 15%, 30%, 50%, 70%, 95%, and 100% (15 minutes in each ethanol solution). Dehydration was completed by submerging cell samples in propylene oxide for 15 minutes. Cells were infiltrated with a 50:50 solution of propylene oxide:Poly/Bed 812 for 6-24 hours,

then embedded using freshly prepared 100% Poly/Bed 812 in flat embedding molds, and placed in a 60 $^{o}$C oven for at least 48 hours to cure. Images were acquired using a JEOL JEM 1400 Transmission Electron Microscope (JEOL Ltd., Tokyo, Japan).

### 2.2.13 Statistical analysis

All experiments were performed in at least triplicate. Data were expressed as mean ± standard deviation (SD). Significant tests were conducted using one-way ANOVA followed by Tukey test (JMP pro 10). Differences were considered significant at P-values that were less than or equal to 0.05.

## 3. Results

### 3.1 Characterization of the physicochemical properties of LPK hybrid NPs

The hydrodynamic size and ploydispersity of various NPs were characterized using dynamic light scattering (DLS), and the results are shown in Table 1. The average sizes for negatively charged LPK ($LPK^{-}$), positively charged ($LPK^{+}$), and pH sensitive ($LPK^{pH}$) NPs are 127.5±5.2 nm, 123.0±7.4 nm, and 120.1±8.8 nm mean ± SD, respectively. Surface charges, measured in term of zeta potential, were -11.7±1.8 mV, 24.7±0.5 mV, and 14.2±1.4 mV, respectively, which evidently depends on the lipid composition of NPs. The polydisperisty of NPs ranges between 0.18±0.04 and 0.21±0.02 for the three different types of particles. The hybridization of lipids and PLGA NPs containing KLH was verified via confocal microscopy, in which the lipid shell was labeled with NBD PE (green) and KLH was labeled with Alexa Fluor® 647 hydrazide (red), respectively. As shown in **Figure 1**, all particles that were labeled with red (left panel) were concomitantly stained with green fluorescence (middle panel), indicating a lipid shell was successfully formed outside PK NPs. Moreover, no disassociated liposomes in the merged image were detected, suggesting that liposomes could be readily coated onto PK NPs. The size and narrow size distribution of NPs displayed in the confocal images were consistent with the size and small polydispersity of NPs measured by DLS. In order to further confirm that pH sensitive lipids were coated

onto PLGA NPs, the FTIR spectrums of pH-sensitive liposomes, PLGA NP, and pH sensitive liposome-PLGA ($LP^{pH}$) hybrid NP were taken. As shown in **Figure 2**, a peak of $LP^{pH}$ NP was observed at 1081 nm, which includes contributions by the peaks at 1062 nm and 1089 nm of the liposome and PLGA NP, respectively. Compared to the other two NPs, an increased peak is shown at 1228 nm for $LP^{pH}$ NPs, due to the contributions of the peaks at 1220 nm and 1234 nm of the liposome and PLGA NPs, respectively. A combined peak also occurs at 1739 nm with $LP^{pH}$ NPs. In addition, a unique peak belonging to liposome at 2852 nm is shown in hybrid NPs. Similarly, a peak at 3297 nm, which only occurs with PLGA NPs, was also detected in hybrid NPs. Considering all the evidence together, the results from FTIR analysis prove that the pH sensitive liposome was successfully hybridized with PLGA NPs.

The morphology of PK NPs and LPK NPs was studied using TEM (**Figure 3**). PK NP is schematically illustrated in **Figure 3A**, and its TEM image is displayed in **Figure 3C**. Agreeing with the illustration presented in the Scheme, PK NP is a spherical particle with a diameter around 100 nm. In contrast, LPK NP has a lipid shell outside PK NP, as illustrated in **Figure 3B**, and its TEM image (**Figure 3D**) confirms that there is a lipid layer coating the white spherical PK NP.

### 3.2 Stability of NPs in response to a low pH treatment

The stability of NPs was evaluated by measuring the change of their size. The size distributions for each particle before and after the low pH treatment are shown in **Figure 4**. Neither $LPK^-$ NPs (**Figure 4A**) nor $LPK^+$ NPs (**Figure 4B**) underwent significant size changes after being treated with pH 5.5 PBS buffer for 10 min. The average sizes with and without the low pH treatment were 123.6±1.8 nm and 122.6±2.0 nm, 122.9±2.0 nm and 120.7±3.7 nm for $LPK^-$ NPs (**Figure 4A**) and $LPK^+$ NPs (**Figure 4B**), respectively. In contrast, significant size changes under conditions of low pH were detected for pH sensitive LPK NPs. The average size of $LPK^{pH}$ NPs increased from 118.4±2.3 nm to 146.6±1.5 nm after 10 min of the low pH treatment (**Figure 4C**). Evidently, the size distribution curve of $LPK^{pH}$ NPs shifted to the

right after a low pH challenge, which was consistent with the increase in average size of $LPK^{pH}$ NPs. The stability of NPs was also studied using TEM, and the morphologies of NPs in both pH 7.4 and pH 5.5 PBS buffer were compared (**Figure 5**). The three NPs share strong resemblance in their morphology in pH 7.4 PBS buffer: there is an apparent lipid shell (grey layer) coating the PK NPs (white core). The size distribution, which centers around 100 nm, is also in agreement with those obtained by DLS and confocal microscopy. Not surprisingly, non-pH sensitive NPs remained intact after being suspended in pH 5.5 PBS buffer for 10 min (**Figure 5A and Figure 5B**), but pH sensitive NPs disassembled in the low pH environment (**Figure 5C**). Formerly regularly shaped lipid shells can be seen to disintegrate into thread-like lipid aggregates (blue arrow), and PK NPs (red square) were released and distributed around the debris of lipid shells.

### 3.3 In vitro release of KLH from LPK NPs

To mimic the conditions *in vivo*, NPs underwent two phases of pH treatment, in which NPs were treated with pH 7.4 human serum for the first 24 h and pH 5.5 human serum for an additional 48 h. In the first 24 h, all NPs exhibited a similarly sustained and slow KLH release profile, of which less than 20% of the KLH was released for all NPs, reflecting the high stability of LPK hybrid NPs under pH 7.4. However, significantly different KLH release profiles of the LPK NPs were observed after the pH was lowered to 5.5 at the 24 h time point. In the first 8 h after the pH change, 40% of the KLH was released from $LPK^{pH}$ NPs, while only 11% and 14% of KLH were released from $LPK^{+}$ NPs and $LPK^{-}$ NPs, respectively. The true percentage of KLH released from non-pH sensitive NPs should be smaller than the values shown in **Figure 6** because the KLH release rates were still noticeably high even at 72 h. The sharp increase in KLH release of $LPK^{pH}$ NPs was likely due to the removal of the protection provided by the lipid shell after low pH treatment. Between 32h and 72h, sustained release of KLH continued for all NPs, except the release rates were considerably higher than those during the first 24 h. When approaching 72h, $LPK^{pH}$ NPs displayed a nearly flat release curve, indicating $LPK^{pH}$ NPs had almost depleted their payload. The other

two NPs showed considerably higher release rates, suggesting that a large amount of KLH was still retained in the NPs.

### 3.4 The uptake of LPK NPs by DCs

The uptake rates of the three NPs by DCs were compared using flow cytometry. Two hundred μg of NPs labeled with NBD were incubated with $2\times10^6$ DCs for 5 h, and the fluorescence intensity in the cells was measured. The results (**Figure 7**) show that DCs internalized more $LPK^+$ NPs than either $LPK^{pH}$ or $LPK^-$ NPs. The mean fluorescence intensities of the internalized NPs were 9164, 7448, 5631, respectively. To some degree, the uptake rate of the NPs by DCs appears to be related to their surface charge, implying that positive surface charge might facilitate NP uptake.

The internalization of NPs by DCs was also measured using confocal microscopy. KLH was labeled with Alexa Fluor® 647, the lipid shell was labeled with NBD, and cells were labeled with CellMask™ Orange Plasma Membrane Stain. As shown in **Figure 8**, all three NPs were internalized by DCs, indicated by the presence of both red and green fluorescence in the cells. However, the state of NPs and their distribution in cells differed from one to another. The green fluorescence in $LPK^-$ NPs (**Figure 8A**) was obviously weaker than that of the either $LPK^+$ NPs (**Figure 8B**) or $LPK^{pH}$ (**Figure 8C**), suggesting that less $LPK^-$ NPs was internalized by DCs compared to the other two NPs. This is consistent with the results obtained from flow cytometry. As shown in Alexa Fluor® 647 panels, most $LPK^+$ and $LPK^-$ NPs existed as distinct and intact particles, while the red fluorescence in $LPK^{pH}$ NPs spread over the whole cell, suggesting that most of the non-pH sensitive NPs remained stable in cells, but pH sensitive NPs underwent significant degradation, resulting in the release of KLH into the entire cell.

The endocytosis of NPs by DCs was further examined with TEM (**Figure 9**). No endosome vesicles were formed in the control group, to which no NPs were added (**Figure 9A**). On the other hand, numerous endosomes (blue arrow) were observed in DCs treated with the three NPs (**Figure 9 B, C, and**

**D**). Consistent with previous results, DCs internalized less $LPK^-$ NPs (**Figure 9B**) than either $LPK^+$ (**Figure 9C**) or $LPK^{pH}$ NPs (**Figure 9D**). In particular, two huge rod-like endosomes containing considerable numbers of $LPK^+$ NPs were present in DCs, implying that positively charged NPs might induce the formation of larger endosomes for NPs uptake. Another interesting and important phenomenon was that the NPs in endosomes of DCs treated with either of the non-pH sensitive NPs retained a regular spherical shape, while the morphology of the NPs in the pH sensitive group could not be defined, indicating that $LPK^{pH}$ NPs might have been degraded by acidification in endosomes.

## 4. Discussion

Lipid-PLGA hybrid NPs have been widely accepted as outstanding systems for delivery of cancer chemotherapeutic agents.[18] In a previous study, we found that lipid-PLGA hybrid NPs may also be used as vaccine delivery systems due to their high antigen loading capacity, ability in co-delivering both antigen and adjuvants, and desired stability for long term storage.[19] However, to be an excellent vaccine delivery system, the above mentioned features of lipid-PLGA NPs are not enough. A desirable delivery system needs to meet at least three criteria: the first is that antigen-containing NPs can maintain high stability during circulation, reducing the loss of payloads; the second is that NPs are able to readily disassemble to release the payloads upon internalization by the target cells, maximizing their efficacy; the last is that NPs can be easily taken up by antigen presenting cells (APCs).

The main findings of this study were that 1) a lipid-PLGA hybrid NP with a pH-sensitive lipid layer can be constructed via sonication mediated fusion, 2) this pH-sensitive hybrid NP exhibited high sensitivity to low pH challenge, 3) DCs could effectively encapsulate pH-sensitive hybrid NPs, and 4) antigen was released more rapidly from pH-sensitive hybrid NPs than non pH-sensitive hybrid NPs after internalization by DCs.

Dendritic cell is the most professional antigen presenting cell that plays a core role in eliciting immune response.[20] To delivery vaccine components using a vehicle that favors DC maturation would be beneficial to development of immune response. In this study, rapid disintegration of hybrid nano-structure of $LPK^{pH}$ NPs in low pH environment was observed. This disintegration probably resulted from poor stability of DOPE in the lipid layer under low pH condition.[21] Lipid layer of the hybrid NP can protect antigens and adjuvants from premature release during circulation. However, it may also hinder the release of antigen and adjuvants after uptake by DCs, resulting in slow or even incomplete maturation of DCs. Therefore, the rapid disassociation of lipid layer from PLGA core in response to low pH challenge is of great significance. It may allow rapid release of antigens and adjuvants, providing DCs strong stimuli for their rapid and complete maturation.

Also, a burst release of antigen was detected in $LPK^{pH}$ NPs after switching pH from 7.4 to 5.5. It is known that PLGA is subject to continuous bulk erosion in aqueous solution.[22] The stored antigen in PLGA core may consistently be released during PLGA degradation. However, due to the existence of the lipid layer, the released antigen may be retained in the inter-space between the PLGA core and the lipid layer. And, the removal of the lipid layer caused burst release of antigen.

It is also important to note that $LPK^{pH}$ NPs displayed outstanding stability as the other two NPs did in human serum at pH 7.4. This stability might be attributed to the protection offered by the long PEG chains placed on the surface of the particles and reduced diffusion of enzymes from the human serum into the inner core of NPs due to the barrier provided by the lipid shell.[23, 24] As a matter of fact, PEG molecules have been routinely used in biodegradable NPs to improve stability of NPs.[25] Reducing the release of the enclosed antigens or adjuvant during circulation is of great value, because it can not only reduce the loss of effector molecules that target immune cells, but also minimize the potential systemic toxicity caused by adjuvants.[26]

We also noticed that surface charges played a significant role in the uptake of NPs by DCs, as NPs with the more positive surface charges could be more effectively encapsulated by DCs. This finding was consistent with the results from a previous study.[19] As we know that cell membrane is negatively charged, therefore, the positive surface charge of NPs may improve cellular uptake via electrostatic interactions between immune cells and NPs. It was also shown that positive charges on the surface of NPs could promote the DCs maturation and enhance vaccine induced immune response.[27] In addition to the positive surface charges, the presence of fusion-promoting DOPE molecules in the lipid shell may also contribute to the faster uptake of $LPK^{pH}$ NPs than $LPK^{-}$ NPs.[28] The fast uptake of NPs based vaccine is meaningful in at least three aspects: 1) it may allow fast development of immune response, 2) it may enable immune system to use vaccine components more efficiently, and 3) it reduces the potential systemic toxicity from adjuvants that may be released from NPs after long term circulation.

The fate of NPs in DCs after internalization is of particular interest to vaccine researchers, because NP degradation and trafficking may have profound impact on the types and magnitude of immune responses.[29, 30] An intense and sustained stimulation of DCs by the antigens and adjuvants released from NPs may lead to a strong and prolonged adaptive immune response. In this study, we observed rapid release of antigen from NPs after internalization by DCs. As discussed above, the burst antigen release may come from the antigen accumulated in the inter-space between PLGA core and lipid layer. Such a burst release of antigen may result in more processed antigenic peptides. These antigenic peptides could subsequently associate with MHC molecules, form peptide-MHC (pMHC) complexes, and be transported to the membrane surface of DC for T cell activation.[31] To prime naive T cells, there has to be a sufficient number of interactions between T cell receptors and pMHC complexes. Higher density of pMHC complexes may, therefore, increase the likelihood of such interactions.[32] Therefore, burst release of antigen from pH-sensitive hybrid NPs in DCs may promote the magnitude of immune response.

The results of the present experiment suggested that shortly after being internalized by DCs, the lipid shell of $LPK^{pH}$ would be removed, leading to a burst release of KLH, followed by sustained and prolonged release. Such a two phase antigen release in DCs may initially enable a strong immune response as well as provide prolonged stimulation to the immune system.

## 5. Conclusion

This study describes preparation and characterization of a pH sensitive liposome-polymeric hybrid NP, which would remain stable under physiological pH, but readily disassemble in response to a low pH challenge. The nano-range size, positive surface charges, and hydrophobic lipid shell enhance its internalization by DC. The rapid release of the enclosed antigens in DCs may enable the hybrid NPs to serve as a potential delivery system of antigens and adjuvants for rapid and complete activation of the immune system.

## Competing interests

The authors declare that they have no competing interests.

## Author's contributions

Yun Hu participated in experimental design, carried out the experiments, and drafted the manuscript. Zongmin Zhao participated in experiments. Chenming Zhang participated in experiment design, coordinated the experiments, and conducted manuscript revision. Marion Ehrich participated in experimental design. Kristel Fuhrman participated in experiments related to dendritic cell culture. All authors read and approved the final manuscript.

## Acknowledgment

This work was financially supported by National Institutes of Health (R21 DA030083).

**Abbreviations**

Dendritic cells: DCs

Nanoparticles: NPs

Poly (lactic-co-glycolic) acid: PLGA

Antigen presenting cell: APC

Dynamic light scattering: DLS

pH sensitive liposome-PLGA nanoparticle: $LP^{pH}$ NP

Fetal bovine serum: FBS

1,2-dioleoyl-3-trimethylammonium-propane: DOTAP

1,2-dioleoyl-sn-glycero-3-phosphocholine: DOPC

Cholesteryl hemisuccinate: CHEMS

1,2-dioleoyl-sn-glycero-3-phosphoethanolamine: DOPE

1,2-distearoyl-sn-glycero-3-phosphoethanolamine-N-[amino(polyethylene glycol)-2000] (ammonium salt): DSPE-PEG2000

1,2-diphytanoyl-sn-glycero-3-phosphoethanolamine-N-(7-nitro-2-1,3-benzoxadiazol-4-yl) (ammonium salt): NBD PE

Keyhole limpet hemocyanin: KLH

Poly (vinyl alcohol): PVA

Dichloromethane: DCM

Rhodamine B: Rhod B

1-Ethyl-3-[3-dimethylaminopropyl] carbodiimide hydrochloride: EDC

peptide-MHC: pMHC

## References

[1] Caminschi I, Shortman K. Boosting antibody responses by targeting antigens to dendritic cells. Trends in immunology. 2012;33:71-7.

[2] Shortman K, Lahoud MH, Caminschi I. Improving vaccines by targeting antigens to dendritic cells. Experimental & molecular medicine. 2009;41:61-6.

[3] Hamdy S, Haddadi A, Hung RW, Lavasanifar A. Targeting dendritic cells with nano-particulate PLGA cancer vaccine formulations. Advanced drug delivery reviews. 2011;63:943-55.

[4] Banchereau J, Steinman RM. Dendritic cells and the control of immunity. Nature. 1998;392:245-52.

[5] Park YM, Lee SJ, Kim YS, Lee MH, Cha GS, Jung ID, et al. Nanoparticle-Based Vaccine Delivery for Cancer Immunotherapy. Immune network. 2013;13:177-83.

[6] Smith DM, Simon JK, Baker JR, Jr. Applications of nanotechnology for immunology. Nature reviews Immunology. 2013;13:592-605.

[7] Date AA, Destache CJ. A review of nanotechnological approaches for the prophylaxis of HIV/AIDS. Biomaterials. 2013;34:6202-28.

[8] Martin-Banderas L, Duran-Lobato M, Munoz-Rubio I, Alvarez-Fuentes J, Fernandez-Arevalo M, Holgado MA. Functional PLGA NPs for oral drug delivery: recent strategies and developments. Mini reviews in medicinal chemistry. 2013;13:58-69.

[9] Gregory AE, Titball R, Williamson D. Vaccine delivery using nanoparticles. Frontiers in cellular and infection microbiology. 2013;3:13.

[10] Joshi VB, Geary SM, Salem AK. Biodegradable particles as vaccine delivery systems: size matters. The AAPS journal. 2013;15:85-94.

[11] Chan JM, Zhang L, Yuet KP, Liao G, Rhee JW, Langer R, et al. PLGA-lecithin-PEG core-shell nanoparticles for controlled drug delivery. Biomaterials. 2009;30:1627-34.

[12] Valencia PM, Basto PA, Zhang L, Rhee M, Langer R, Farokhzad OC, et al. Single-step assembly of homogenous lipid-polymeric and lipid-quantum dot nanoparticles enabled by microfluidic rapid mixing. ACS nano. 2010;4:1671-9.

[13] Galindo-Rodriguez SA, Allemann E, Fessi H, Doelker E. Polymeric nanoparticles for oral delivery of drugs and vaccines: a critical evaluation of in vivo studies. Critical reviews in therapeutic drug carrier systems. 2005;22:419-64.

[14] Prasad S, Cody V, Saucier-Sawyer JK, Fadel TR, Edelson RL, Birchall MA, et al. Optimization of stability, encapsulation, release, and cross-priming of tumor antigen-containing PLGA nanoparticles. Pharmaceutical research. 2012;29:2565-77.

[15] Pelosi A, Shepherd R, Walmsley AM. Delivery of plant-made vaccines and therapeutics. Biotechnology advances. 2012;30:440-8.

[16] Yang YY, Chia HH, Chung TS. Effect of preparation temperature on the characteristics and release profiles of PLGA microspheres containing protein fabricated by double-emulsion solvent extraction/evaporation method. Journal of controlled release. 2000;69:81-96.

[17] Hu Y, Zheng H, Huang W, Zhang C. A novel and efficient nicotine vaccine using nano-lipoplex as a delivery vehicle. Human vaccines & immunotherapeutics. 2013;10:64-72.

[18] Zhang LF, Chan JM, Gu FX, Rhee JW, Wang AZ, Radovic-Moreno AF, et al. Self-assembled lipid−polymer hybrid nanoparticles: a robust drug delivery platform. ACS nano. 2008;2:1696-1702.

[19] Hu Y, Ehrich M, Fuhrman K, Zhang C. In vitro performance of lipid-PLGA hybrid nanoparticles as an antigen delivery system: lipid composition matters. Nanoscale research letters. 2014;9:1-10.

[20] Liu YJ, Kanzler H, Soumelis V, Gilliet M. Dendritic cell lineage, plasticity and cross-regulation. Nature immunology. 2001;2:585-589.

[21] Hafez I, Ansell S, Cullis P. Tunable pH-sensitive liposomes composed of mixtures of cationic and anionic lipids. Biophysical journal. 2000;79:1438-46.

[22] Chan JM, Zhang LF, Yuet KP, Liao G, Rhee JW, Langer R, et al. PLGA–lecithin–PEG core–shell nanoparticles for controlled drug delivery. Biomaterials. 2009;30:1627-1634.

[23] Gindy ME, Ji S, Hoye TR, Panagiotopoulos AZ, Prud'homme RK. Preparation of poly(ethylene glycol) protected nanoparticles with variable bioconjugate ligand density. Biomacromolecules. 2008;9:2705-11.

[24] Martins S, Sarmento B, Ferreira DC, Souto EB. Lipid-based colloidal carriers for peptide and protein delivery--liposomes versus lipid nanoparticles. International journal of nanomedicine. 2007;2:595-607.

[25] Li, SD, Huang L. Stealth nanoparticles: high density but sheddable PEG is a key for tumor targeting. Journal of controlled release. 2010;145:178.

[26] Montomoli E, Piccirella S, Khadang B, Mennitto E, Camerini R, De Rosa A. Current adjuvants and new perspectives in vaccine formulation. Expert review of vaccines. 2011;10:1053-61.

[27] Ma Y, Zhuang Y, Xie X, Wang C, Wang F, Zhou D, et al. The role of surface charge density in cationic liposome-promoted dendritic cell maturation and vaccine-induced immune responses. Nanoscale. 2011;3:2307-14.

[28] Huth US, Schubert R, Peschka-Suss R. Investigating the uptake and intracellular fate of pH-sensitive liposomes by flow cytometry and spectral bio-imaging. Journal of controlled release. 2006;110:490-504.

[29] Cubas R, Zhang S, Kwon S, Sevick-Muraca EM, Li M, Chen C, et al. Virus-like particle (VLP) lymphatic trafficking and immune response generation after immunization by different routes. Journal of immunotherapy. 2009;32:118-28.

[30] Wallace A, West K, Rothman AL, Ennis FA, Lu S, Wang S. Post-translational intracellular trafficking determines the type of immune response elicited by DNA vaccines expressing Gag antigen of Human Immunodeficiency Virus Type 1 (HIV-1). Human vaccines & immunotherapeutics. 2013;9:2095-102.

[31] Lanzavecchia A, Sallusto F. Regulation of T cell immunity by dendritic cells. Cell. 2001;106:263-6.

[32] Anikeeva N, Gakamsky D, Scholler J, Sykulev Y. Evidence that the density of self peptide-MHC ligands regulates T-cell receptor signaling. PloS one. 2012;7:e41466.

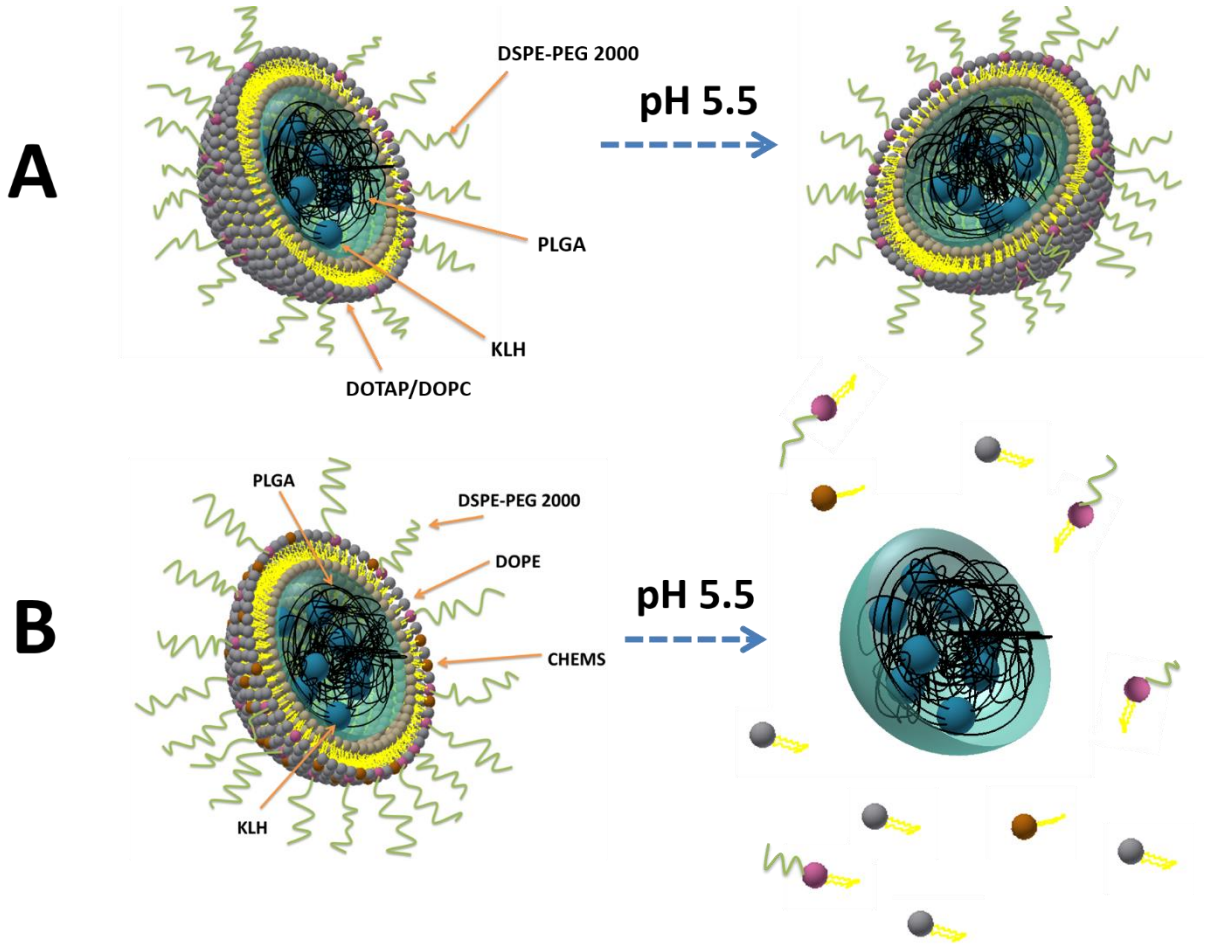


**Scheme**. Illustration of non-pH sensitive NPs (A) and pH sensitive NPs (B) in response to a low pH challenge.

**Table 1.** Compositions and physicochemical properties of LPK hybrid NPs.

| LPK NPs | Lipid composition | Surface charge (mV ± SD) | Size (nm ± SD) | Polydispersity |
|---|---|---|---|---|
| $LPK^{-}$ | DOPC:cholesteral:DSPE-PEG2000 (w/w 8:0.5:1.5) | -11.7±1.8 | 127.5±5.2 | 0.18±0.04 |
| $LPK^{+}$ | DOTAP:cholesteral:DSPE-PEG2000 (w/w 8:0.5:1.5) | 24.7±0.5 | 123.0±7.4 | 0.20±0.05 |
| $LPK^{pH}$ | DOPE:CHEMS:DSPE-PEG2000 (w/w 6.5:2.0:1.5) | 14.2±1.4 | 120.1±8.8 | 0.21±0.02 |

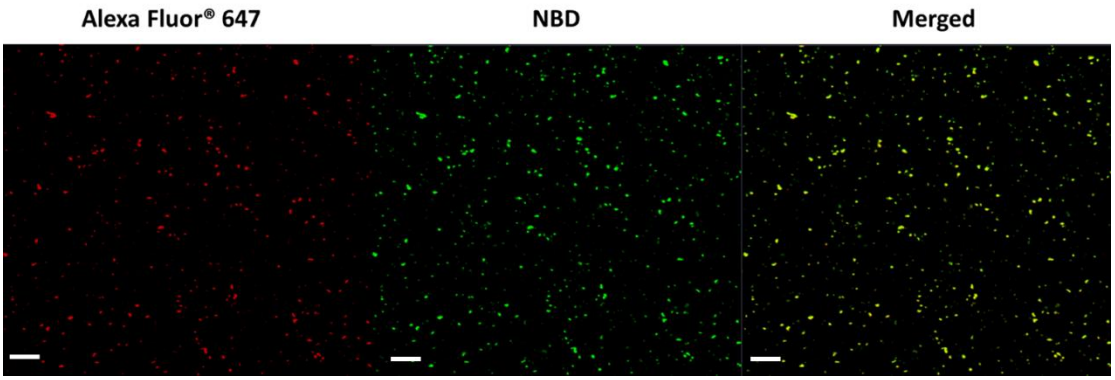


**Figure 1.** Confocal LSM images of LPK$^{pH}$ NPs, in which KLH was labeled with Alexa Fluor® 647, and lipids were labeled with NBD. The images show that hybrid nanoparticle composed of a PLGA core and a lipid layer were formed. The scale bars represent 10 µm.

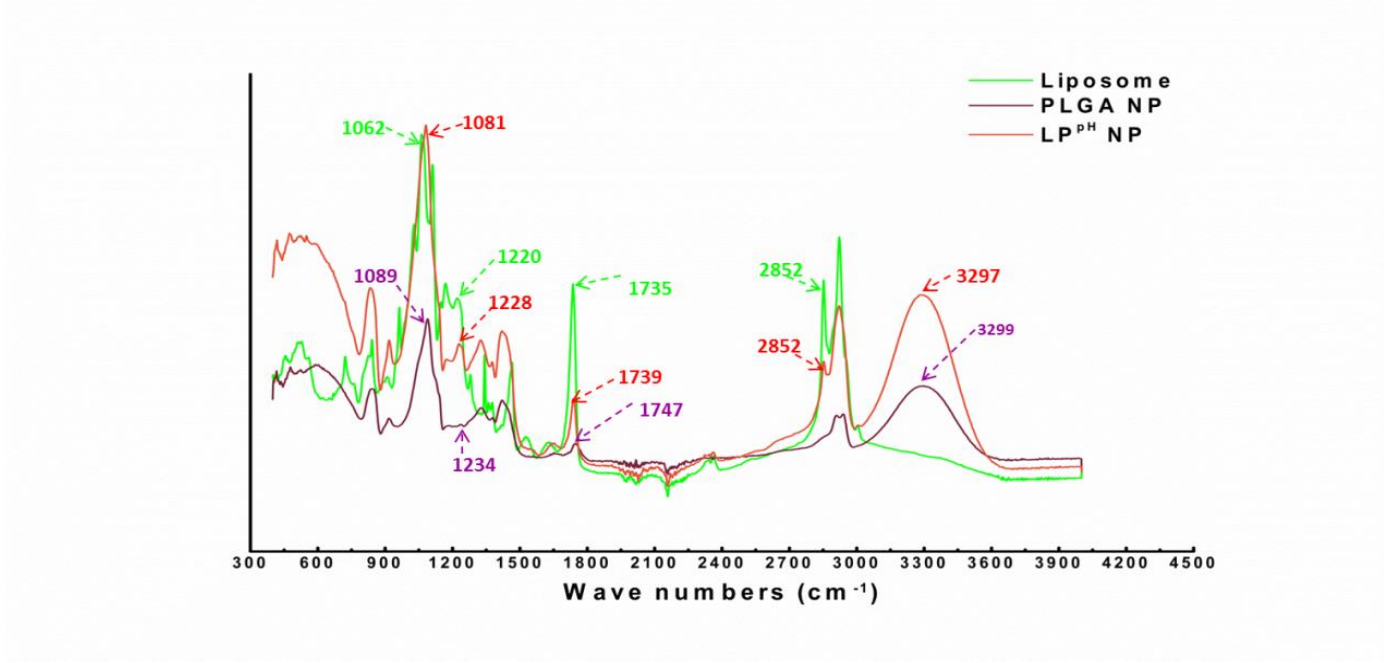


**Figure 2.** FTIR spectra of the pH sensitive liposome, PLGA NP, and LP$^{pH}$ hybrid NP. A unique peak belonging to liposome at 2852 nm is shown in LP$^{pH}$ hybrid NP. Similarly, a peak at 3297 nm, which only occurs with PLGA NPs, is also shown in hybrid NPs.

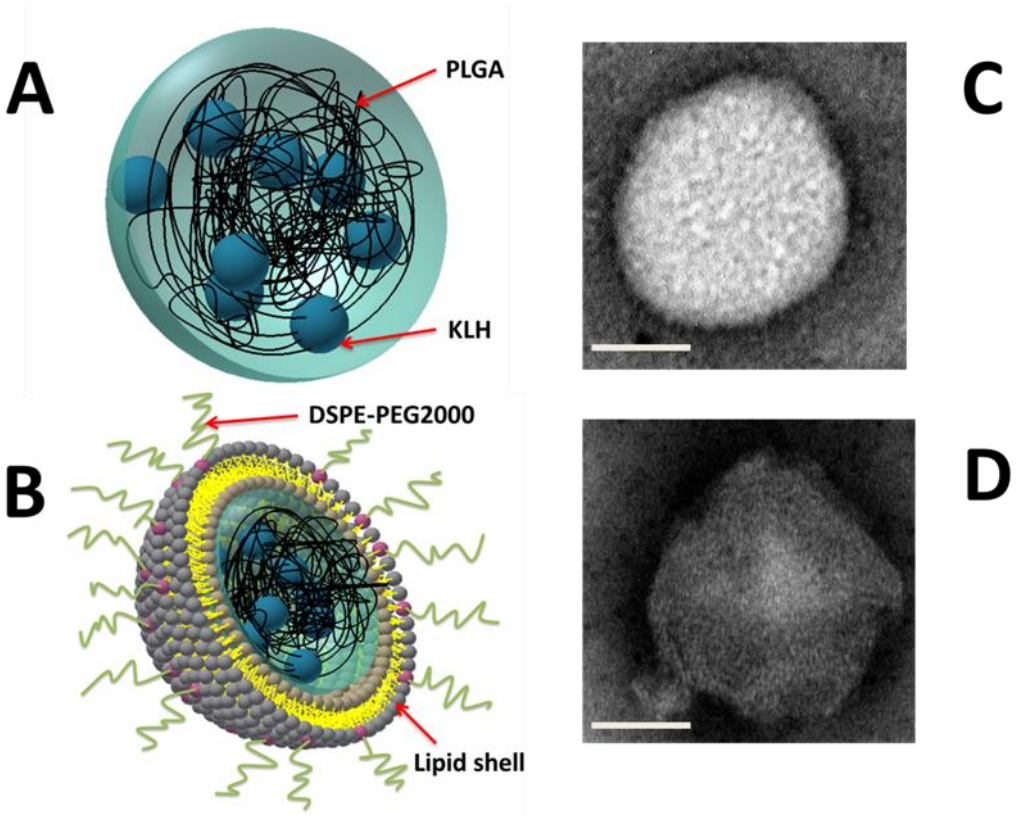


**Figure 3.** Schematic illustration of PK NP (A) and LPK NP (B). TEM images of PK NP (C) and LPK NP (D). PK NP is a spherical particle (white) with a diameter around 100 nm. In contrast, LPK NP has a lipid shell (grey) outside PK NP core (white). The scale bars represent 50 nm.

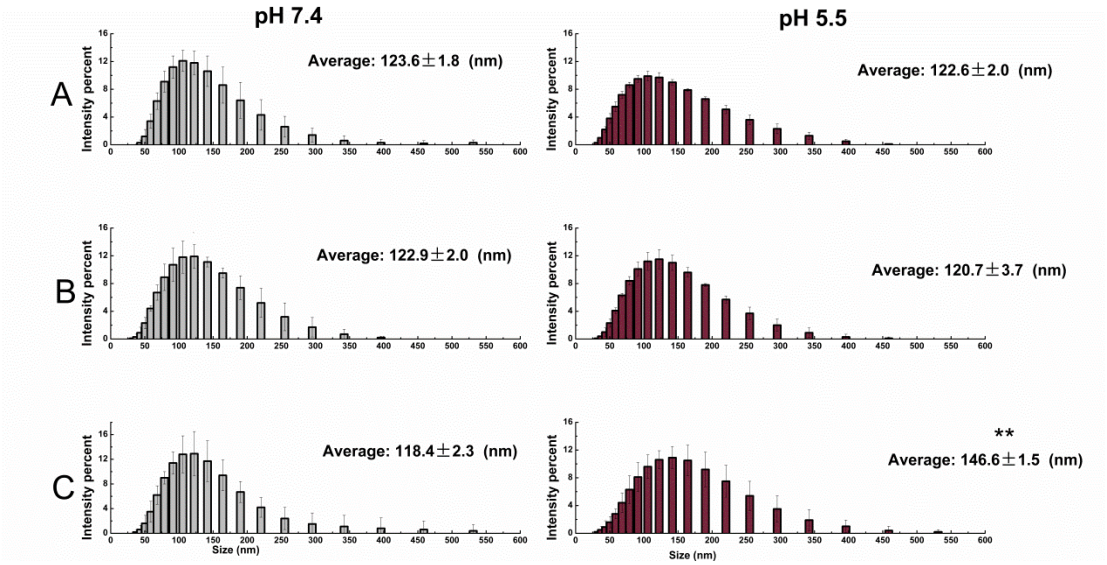


**Figure 4.** The stability (size) of the three LPK NPs in response to a pH 5.5 treatment for 10 minutes. (A) $LPK^-$ NPs, (B) $LPK^+$ NPs, (C) $LPK^{pH}$ NPs. ** indicates that significant size increase occurred after $LPK^{pH}$ NPs were treated with pH 5.5 PBS buffer (P-value<0.05).

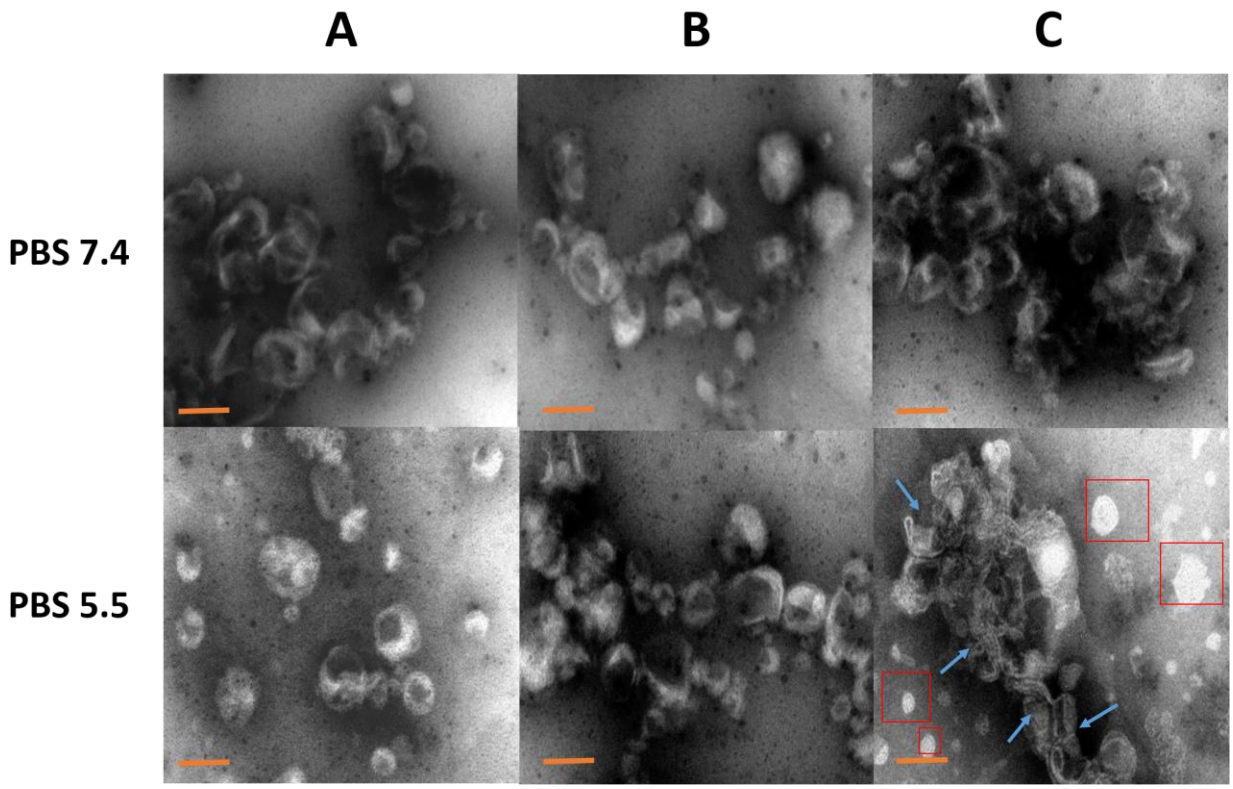


**Figure 5.** TEM images of the three LPK NPs in both pH 7.4 and pH 5.5 PBS buffer. (A) $LPK^{-}$ NPs, (B) $LPK^{+}$ NPs, (C) $LPK^{pH}$ NPs. In contrast to other two NPs, $LPK^{pH}$ NP in Figure 5C underwent significant morphology change after low pH treatment. The blue arrows in the lower panel of Figure 5C show the degraded lipid layer, and red boxes show the released PK NPs. The scale bars represent 100 nm.

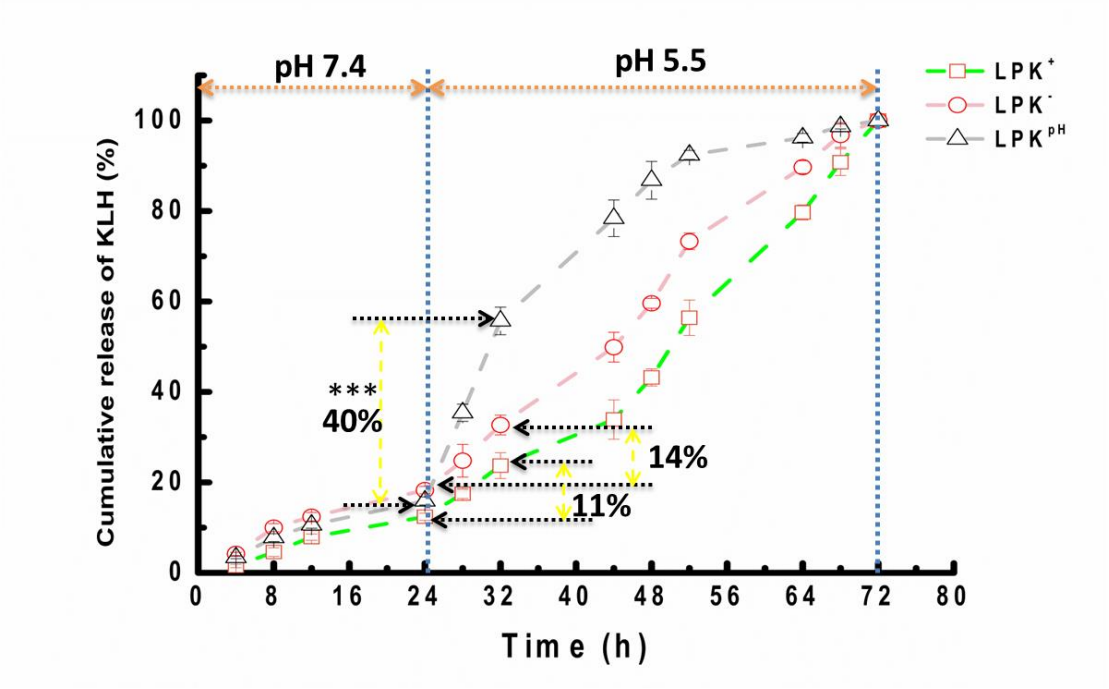


**Figure 6.** KLH release profile of LPK NPs in human serum with two phases of pH treatment, in which from 0 to 24 h, pH was 7.4, and from 24 to 72 h, pH was 5.5. *** indicates that the percentage of KLH released from $LPK^{pH}$ between 24 h and 32 h was significantly higher than that from either $LPK^{-}$ NPs or $LPK^{+}$ NPs (P-value <0.01).

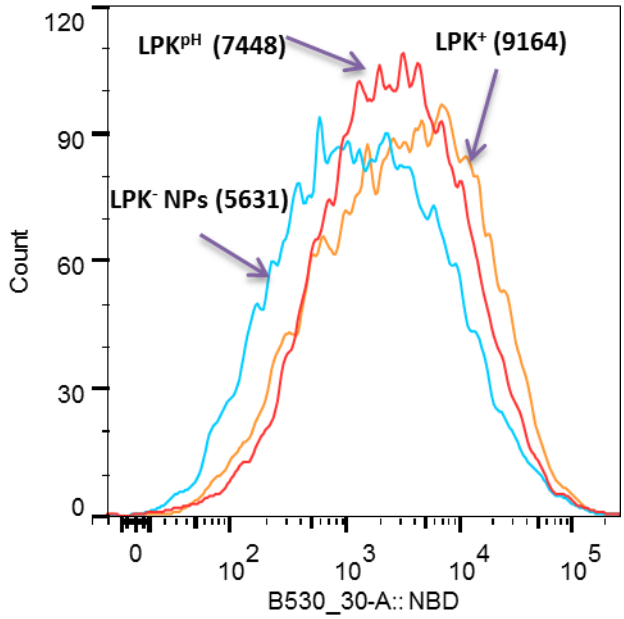


**Figure 7.** The intensity of NBD fluorescence in DCs, all of which internalized the three LPK NPs, respectively. LPK$^{+}$ NPs exhibited the fastest uptake rate by DCs, while LPK$^{pH}$ NP could be more readily taken up by DCs in comparison to LPK$^{-}$ NPs. The numbers in parentheses represent the mean NBD intensity.

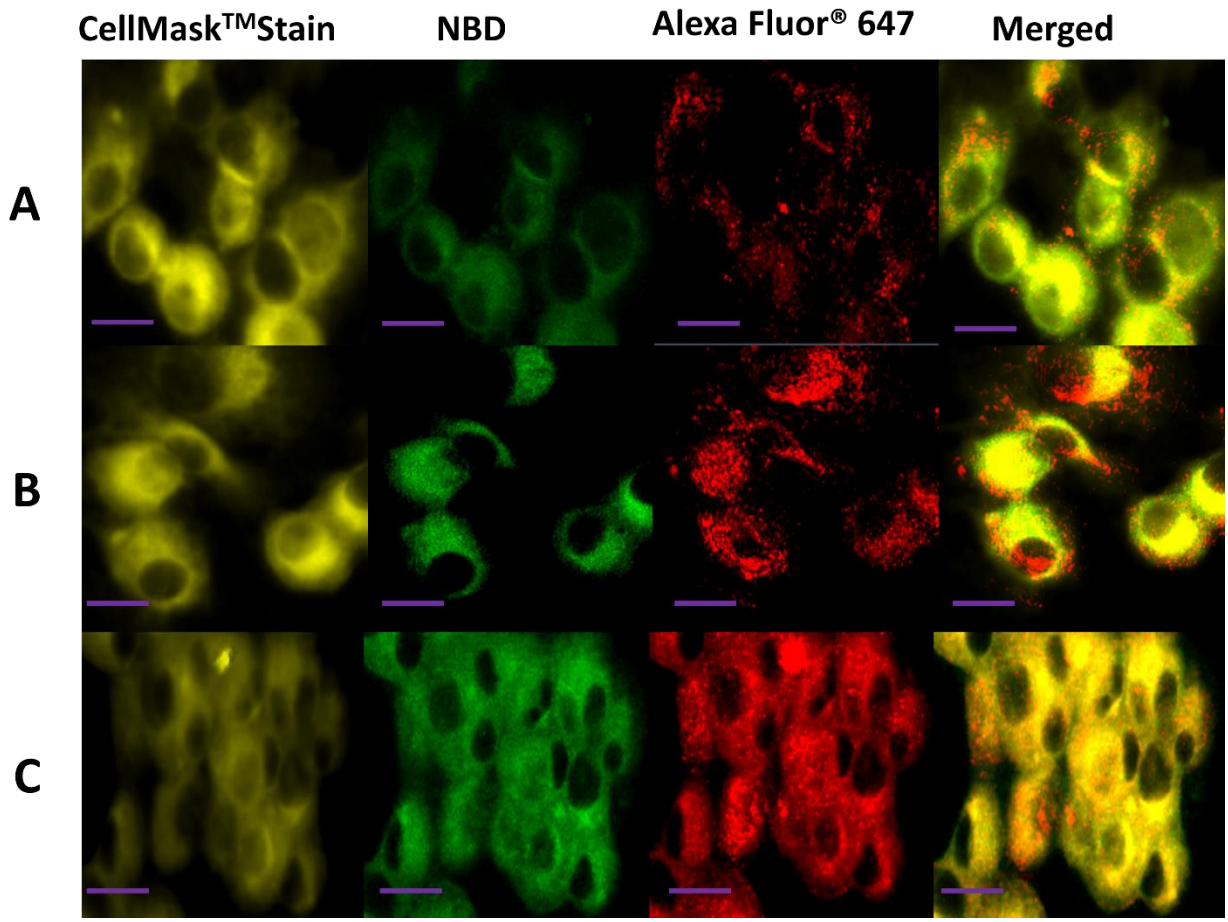


**Figure 8.** Confocal LSM images of DCs after LPK NP uptake, in which KLH was labeled with Alexa Fluor® 647, and lipids were labeled with NBD. Dendritic cells were treated with (A) $LPK^{-}$ NPs, (B) $LPK^{+}$ NPs, and (C) $LPK^{pH}$ NPs, respectively. The intracellular release of KLH from $LPK^{pH}$ NPs was faster than those in other two NPs. The scale bars represent 10 µm.

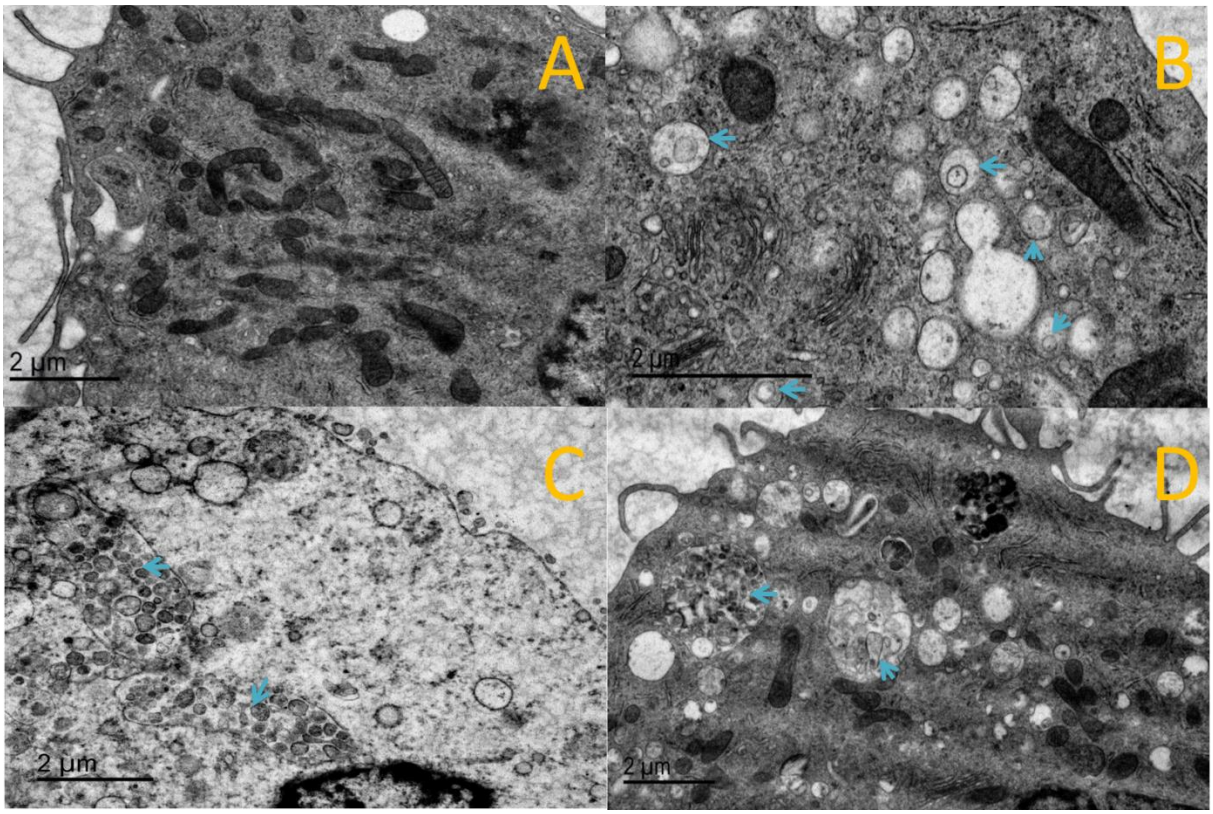


**Figure 9.** TEM images of DCs after LPK NPs internalization. (A) Control group, (B) $LPK^{-}$ NPs, (C) $LPK^{+}$ NPs, (D) $LPK^{pH}$ NPs. Blue arrows show the position of endosomes, which were more numerous in groups treated with NPs compared to the control group, and $LPK^{pH}$ NPs underwent significant degradation in endosomes. Scale bars represent 2 µm.

# Chapter VII (results): Engineering the lipid layer of lipid-PLGA hybrid nanoparticles for enhanced *in vitro* cellular uptake and improved stability

Yun Hu[1], Marion Ehrich[2], Chenming Zhang[1]†

[1] Department of Biological Systems Engineering, Virginia Tech, Blacksburg, VA 24061, U.S.A.

[2] Department of Biomedical Sciences and Pathobiology, Virginia Tech, Blacksburg, VA 24061

† To whom correspondence should be addressed. Office phone number: (540) 231-7601; E-mail address: chzhang2@vt.edu.

## Abstract

Lipid-polymer hybrid nanoparticles (NPs), consisting of a polymeric core and a lipid shell, have been intensively examined as a delivery system for cancer drugs, imaging agents, and vaccines. However, the influence of lipid composition on the performance of hybrid NPs has not been well studied. In this study, we demonstrate that higher concentrations of cholesterol in the lipid layer enable slower and more controlled antigen release from lipid- poly(lactide-co-glycolide) acid (lipid-PLGA) NPs in human serum and phosphate buffered saline (PBS). Higher concentrations of cholesterol also promoted *in vitro* cellular uptake of hybrid NPs, improved the stability of the lipid layer, and protected the integrity of the hybrid structure during long- term storage. However, stabilized hybrid structures of high cholesterol content tended to fuse with each other during storage, resulting in significant size increases and lower cellular uptake. Additional experiments demonstrated that PEGylation of NPs could effectively minimize fusion-caused size increases after long term storage, leading to improved cellular uptake.

## *1.* Introduction

In the past decade, lipid-polymer hybrid NPs have been increasingly recognized as promising drug delivery vehicles due to their multiple advantageous features [1]. Hybrid NPs are capable of carrying both hydrophobic and hydrophilic drugs with high loading capacity [2]; they also allow step-wise release of multiple drugs of distinct properties and purposes [3]. Furthermore, pharmacokinetics of delivered drugs can be easily modified by tuning physiochemical properties of hybrid NPs [4]. In addition, targeted delivery of drugs can be performed by introducing site specific antibodies or other targeting molecules to the exterior surface of hybrid NPs [5].

Lipid-polymer hybrid NPs consist of two major components. The inner part is a polymer core, which is capable of encapsulating both hydrophilic and hydrophobic drugs as well as offering rigid support for the hybrid entity. The outer part is a lipid layer coating the external surface of the polymer core, and it can function as (i) a biocompatible shield to avoid fast clearance of NPs by the reticuloendothelial system (RES), (ii) a template for surface modifications, enabling targeted delivery of drugs, and (iii) a barrier preventing the fast leakage of water-soluble drugs, allowing prolonged and controlled release of drugs [2].

Previous studies mainly focused on developing methods for fabricating hybrid NPs and potential applications of hybrid NPs for delivery of various kinds of drugs [1]. However, the impact of the composition of the lipid layer on the performance of hybrid NPs has not been well studied. It has been clearly elucidated that lipid composition has a significant influence on the efficacy of drugs delivered by liposomes. For example, 1,2-dioleoyl-sn-glycero-3-phosphoethanolamine (DOPE)-based liposomes were markedly more stable in 20% serum than 1,2-distearoyl-sn-glycero-3-phosphoethanolamine (DSPE)-based liposomes [6]. It was also reported that the presence or the absence of 1,2-distearoyl-sn-glycero-3-phosphoethanolamine-N-[(polyethylene glycol)-2000] (DSPE–PEG2000) had a great impact on lipid

transition temperature and drug release, and increasing the molar percentage of 1-myristoyl-2-stearoyl-sn-glycero-3-phosphocholine (MSPC) in temperature sensitive liposomes led to faster initial doxorubicin release [7].

Among lipid constituents, cholesterol plays an unique as well as essential role as a main membrane-stabilizing material, and has been extensively investigated and utilized in the majority of liposome products on the market [8]. In addition to its ability to improve lipid bilayer stability, cholesterol can also reduce the permeability of liposomal bilayers. For instance, addition of cholesterol in liposomes resulted in increased free energy barriers of the membranes, which were primarily responsible for the reduced water permeability [9]. For anti-cancer drug delivery, reduced permeability of lipid membranes should reduce leakage of enclosed drugs during circulation, minimizing side effects and improving bioavailability of drugs. For vaccine delivery, in addition to the reduced loss of vaccine effector molecules, the bi-directionally lowered permeability should also minimize interactions between antigenic proteins and external water molecules or serum proteinases, avoiding their premature degradation.

In this study, lipid-PLGA hybrid NPs of various cholesterol concentrations were prepared to evaluate the influence of cholesterol content on the stability of long-term stored hybrid NPs, the release of antigen from NPs in human serum and PBS buffer, and *in vitro* uptake of NPs by dendritic cells (DCs). DSPE-PEG (2000) amine was later introduced into lipids to reduce aggregation of hybrid NPs at higher concentrations of cholesterol.

## 2. Materials and methods

### 2.1 Materials

Lactel® 50:50 PLGA was purchased from Durect Corporation (Cupertino, CA). Fetal bovine serum (FBS), Granulocyte macrophage-colony stimulating factor (GM-CSF) recombinant mouse protein, Alpha minimum essential medium, trypsin/EDTA, Alexa Fluor® 647 hydrazide, and tris(triethylammonium) salt were purchased from Life Technologies Corporation (Grand Island, NY). Lipids, including 1,2-dioleoyl-3-trimethylammonium-propane (DOTAP), 1,2-distearoyl-sn-glycero-3-phosphoethanolamine-N-[amino(polyethylene glycol)-2000] (ammonium salt) (DSPE-PEG2000) amine, cholesterol, and 1,2-diphytanoyl-sn-glycero-3-phosphoethanolamine-N-(7-nitro-2-1,3-benzoxadiazol-4-yl) (ammonium salt) (NBD PE) were purchased from Avanti Polar Lipids, Inc. (Alabaster, AL). Poly (vinyl alcohol) (PVA, MW 89,000-98,000), dichloromethane (DCM), rhodamine B (Rhod B), and bovine serum albumin (BSA) were purchased from Sigma-Aldrich Inc. (Saint Louis, MO). 1-Ethyl-3-[3-dimethylaminopropyl] carbodiimide hydrochloride (EDC) was purchased from Thermo Fisher Scientific Inc. (Rockford, IL). JAWSII (ATCC® CRL-11904™) immature dendritic cells were purchased from ATCC (Manassas, VA). All other chemicals were of analytical grade.

### *2.2 Synthesis of BSA-containing PLGA NPs*

PLGA NPs were prepared using a reported double emulsion solvent evaporation method with modifications [10]. Briefly, PLGA (100 mg) was dissolved in DCM (3 mL), followed by mixing with 500 µL of BSA (10 mg/mL) for 2 min using a vortex. (In the study of uptake of hybrid NP by DCs using TEM, BSA was replaced with iron NP.) The resultant mixture was emulsified in Branson B1510DTH Ultrasonic Cleaner (Branson, Danbury, CT) for 10 min. The primary emulsion was added drop-wise into 100 mL PVA (1% (w/v)), and continuously stirred for 10 min at 500 rpm. The above suspension was emulsified through sonication using a sonic dismembrator (Model 500; Fisher Scientific, Pittsburg, PA) at 50%

amplitude for 120 s. The secondary emulsion was stirred overnight to allow DCM to evaporate. Large particles were removed after the mixture set undisturbed at room temperature for 30 min. NPs in suspension were collected by centrifugation at 10,000 g, 4 °C for 60 min using an Eppendorf centrifuge. (Eppendorf, Hauppauge, NY). The pellet was washed 3 times using ultrapure water. The final suspension was freeze-dried using LABCONCO Freezone 4.5 (LABCONCO Kansas City, MO), and NPs were stored at 2 °C for later use. For measurement of encapsulation efficiency of BSA by PLGA NPs, various amounts of BSA (0.5 mg, 1 mg, 5 mg, and 10 mg) were emulsified with 100 mg of PLGA. After the second emulsion, non-encapsulated BSA in PVA solution were separated from PLGA-entrapped BSA through centrifugation at 10,000 g, 4 °C for 60 min, and the concentration of BSA in PVA solution was measured using the Micro BCA Protein Assay Kit (Thermo Fisher Scientific, Grand Island, NY). Encapsulation efficiency was calculated using the follow equation**: Encapsulation efficiency (%)= [Concentration of BSA in PVA solution (μg/mL)*100 mL*0.001/ BSA (mg) initially added]*100.**

### 2.3 Assembly of lipid-PLGA hybrid NPs

A lipid film (10 mg) containing the lipids identified above was hydrated with 10 mL, 55°C pre-warmed phosphate buffered saline (PBS) buffer. The resulting liposome suspension was vigorously mixed using a vortex for 2 min, followed by 5 min sonication using a Branson B1510DTH Ultrasonic Cleaner (Branson, Danbury, CT) and cooling to room temperature. PLGA NPs (50 mg) were added into the liposome suspension and pre-homogenized for 15 min using a Branson B1510DTH Ultrasonic Cleaner, followed by 5 min sonication in an ice bath using a sonic dismembrator at 15% amplitude (pulse on 20 s, pulse off 50 s). The formed lipid-PLGA NPs were collected by centrifugation at 10,000 g, 4 °C for 60 min, lyophilized, and stored at 2 °C.

### 2.4 Labeling BSA with rhodamine B (Rhod B) or Alexa Fluor® 647 hydrazide

The coupling of fluorescent dyes to BSA was done using a method described in a previous study [11]. Ten mg of EDC dissolved in 700 µL ultrapure water (pH 6.8) were mixed with 300 µL of 2 mg/mL Rhod B. After incubation at 0 °C for 10 minutes, the product was mixed with 10 mg BSA (20 mg/mL) and stirred in darkness at room temperature for 6 h. For Alexa Fluor® 647 hydrazide labeling, 10 mg of EDC in 800 µL ultrapure water (pH 6.8) was incubated with 10 mg BSA (20 mg/mL) at 0 $^{0}$C for 10 minutes, followed by reaction with 100 µg Alexa Fluor® 647 hydrazide in darkness at room temperature for 6 h. Fluorescently labeled BSA was purified using Microcon centrifugal filter units (10,000 MWCO, EMD Millipore, Billerica, MA), freeze-dried, and stored at 2 $^{0}$C.

### 2.5 Characterization of physicochemical properties of NPs

One mg of NPs was dispersed in 5 mL ultrapure water (pH 7.0), and each sample was diluted by 10 fold using ultrapure water, before the particle size (diameter, nm) and surface charge (zeta potential, mV) were measured at room temperature using a Malvern Nano-ZS zetasizer (Malvern Instruments Ltd, Worcestershire, United Kingdom).

### 2.6 *In vitro* BSA release from NPs in human serum and PBS buffer

Ten mg of lipid-PLGA NPs containing Rhod B-labeled BSA were suspended in 10 mL (5% v/v) human plasma (pH 7.4) and continuously stirred at room temperature in darkness. After 24 h incubation, the NPs were centrifuged at 10,000 g, 4 °C for 60 min. The supernatant was transferred to a 50 ml tube, and the NP pellet was suspended in 10 mL (5% v/v) human plasma (pH 7.4). 200 µL of supernatant or NP suspension were added into wells of a black 96-well plate, and the fluorescence intensity was measured using a Synergy HT Multi-Mode Microplate Reader (BioTek Instruments, Inc., Winooski, VT) with excitation at 530 nm and emission at 590 nm. The percentage of released BSA in human serum was calculated using the following equation: **BSA released (%) =Fluorescence intensity (supernatant)/**

**[Fluorescence intensity (supernatant) + Fluorescence intensity (pellet suspension)] x 100**. For measurement of BSA release in PBS buffer, 20 mg of lipid-PLGA NPs, which enclosed Rhod B-labeled BSA, were suspended in 20 mL PBS buffer (pH 7.4) at room temperature in darkness, and the released BSA was separated from NPs via centrifugation at 10,000 g, 4 °C for 60 min at indicated time points. The NPs were re-suspended in PBS buffer and fluorescence intensity of 200 μL of the released BSA in supernatant was measured using a Synergy HT Multi-Mode Microplate Reader (BioTek Instruments, Inc., Winooski, VT) with excitation at 530 nm and emission at 590 nm. Meanwhile, as a control group, 20 mg of the above Rhod B-labeled BSA containing lipid-PLGA NPs were suspended in 20 mL PBS buffer (pH 7.4), and the fluorescence intensity of 200 μL of the suspension was measured using the method described above. The percentage of released BSA at given time points was calculated using the following equation: **BSA released (%) = Fluorescence intensity (supernatant)/ Fluorescence intensity (control) x 100.**

### 2.7 Imaging NPs using transmission electrical microscopy (TEM)

NP suspensions (1 mg/mL) were dropped onto a 300-mesh Formvar-coated copper grid. After standing 10 min, the remaining suspension was carefully removed with wipes, and the samples were negatively stained using fresh 1% phosphotunstic acid for 20 s and washed with ultrapure water twice. The dried samples were imaged on a JEOL JEM 1400 Transmission Electron Microscope (JEOL Ltd., Tokyo, Japan).

### 2.8 Imaging hybrid NPs using confocal laser scanning microscopy (CLSM)

A Zeiss LSM 510 Laser Scanning Microscope (Carl Zeiss, German) was used to image lipid-PLGA NPs containing Rhod B labeled BSA and NBD PE labeled lipid shells.

### 2.9 Fourier transform infrared (FTIR) spectroscopy analysis of NPs

The spectrum of freeze-dried liposomes (i) with molar ratio of DOTAP: DSPE-PEG(2000) Amine: cholesterol = 80%: 5% : 15%, (ii) PLGA NPs, and (iii) lipid-PLGA NPs with molar ratio of DOTAP: DSPE-PEG

(2000) Amine: cholesterol = 80%: 5% : 15% were recorded on a Thermo Nicolet 6700 FTIR spectrometer (Thermo Fisher Scientific Inc., Waltham, MA). The spectrum was taken from 4000 to 400 $cm^{-1}$.

**2.10 Flow cytometry measurement of endocytosis of lipid-PLGA hybrid NPs by dendritic cells (DCs)**

JAWSII (ATCC® CRL-11904™) immature DCs from ATCC were cultured with alpha minimum essential medium (80%v) including ribonucleosides, deoxyribonucleosides, 4 mM L-glutamine, 1 mM sodium pyruvate and 5 ng/mL murine GM-CSF, along with fetal bovine serum (20%v) at 37 °C, 5% $CO_2$ in 24 well plates (CORNING, Tewksbury, MA). Alexa Fluor® 647 hydrazide-labeled lipid-PLGA hybrid NPs of varied lipid compositions were assembled according to the above mentioned method. Two hundred μg of NPs were added into each well containing $2\times10^6$ cells, and incubated for 90 min. After incubation, the medium was immediately removed and cells were washed 5 times with ultrapure water. Cells were detached from culture plate using trypsin/EDTA solution and centrifuged at 200 g for 10 min, before cell pellets were re-suspended in 10 mM PBS (pH 7.4). Cell samples were immediately analyzed by flow cytometry (BD FACSAria Ⅰ, BD, Franklin Lakes, NJ).

**2.11 Imaging endocytosis of lipid-PLGA hybrid NPs by DCs using CLSM**

Cells were cultured in a 4 well chamber slide (Thermo Fisher Scientific Inc., Rd, Rockford, IL) using the same method described above. To investigate the effect of the content of cholesterol on the uptake of hybrid NPs by DCs, 100 μg of freshly made hybrid NPs (labeled with Alexa Fluor® 647 hydrazide) were incubated with $3\times10^5$ cells for 5 h at 37 °C, 5% $CO_2$. To study the influence of content of DSPE-PEG (2000) amine on endocytosis of hybrid NPs (stored in pH 7.4 PBS for 30 days) by DCs, 100 μg hybrid NPs (labeled with both NBD PE and Alexa Fluor® 647 hydrazide) were incubated with $3\times10^5$ cells for 30 min at 37 °C, 5% $CO_2$. After incubation, the medium was immediately removed and cells were washed 5 times with ultrapure water. Freshly prepared 4% (w/v) paraformaldehyde (500 μL) was added into each well, and cells were fixed for 15 min. This was followed by washing 3 times with PBS buffer

(10 mM, pH 7.4). Fixed cells were permeabilized using 500 µL of 0.1% (v/v) Triton™ X-100 for 15 min at room temperature, and washed 3 times using PBS buffer (10 mM, pH 7.4). Cell samples were covered with a glass cover and sealed by nail polish. Images were acquired using a Zeiss LSM 510 Laser Scanning Microscope (Carl Zeiss, Germany).

### 2.12 Imaging endocytosis of lipid-PLGA hybrid NPs in DCs using transmission electron microscopy (TEM)

To view the uptake of hybrid NPs, which contained various concentrations of cholesterol, petri dishes containing $2\times10^6$ immature DCs were supplemented with 200 µg of hybrid NPs. After 90 min incubation, the medium containing un-internalized NPs was removed and cells were washed 5 times with ultrapure water. Cell samples were prepared for TEM using the following procedure: Cells were washed 2 times in 0.1 M Na-Cacodylate for 15 minutes each, and then post-fixed in 1% $OsO_4$ in 0.1 M Na-Cacodylate for one hour. OsO4 was discarded, and the samples were washed 2 times for 10 minutes each in 0.1 M Na-Cacodylate. Cell samples were dehydrated in solutions containing increasing ethanol concentration as follows: 15%, 30%, 50%, 70%, 95%, and 100% (15 minutes in each ethanol solution). Dehydration was completed by submerging cell samples in propylene oxide for 15 minutes. Cells were infiltrated with a 50:50 solution of propylene oxide:Poly/Bed 812 for 6-24 hours, then embedded using freshly prepared 100% Poly/Bed 812 in flat embedding molds, and placed in a 60 °C oven for at least 48 hours to cure. Images were acquired using a JEOL JEM 1400 Transmission Electron Microscope (JEOL Ltd., Tokyo, Japan).

### 2.13 Statistical analysis

All experiments were performed in at least triplicate. Data were expressed as mean ± standard deviation (SD). Tests for significance were conducted using one-way ANOVA followed by Tukey's test (JMP pro 10). Differences were considered significant at P-values that were less than or equal to 0.05.

## 3. Results and discussion

### 3.1 Fabrication of lipid-PLGA NPs

As shown schematically in **Fig. 1A**, lipid-PLGA hybrid NPs consisted of a PLGA core, in which BSA as a model antigen was encapsulated, and a lipid layer composed of DOTAP, DSPE-PEG (2000) amine, and cholesterol. Fabrication of lipid-PLGA NPs was performed in two steps. In the first step, PLGA NPs were formed using a widely applied double emulsion and evaporation method [12]. Various amounts of BSA (0.5 mg, 1 mg, 5 mg, and 10 mg) were emulsified with 100 mg PLGA, and the encapsulation efficiency of BSA was measured. As shown in **Fig. 1B**, encapsulation efficiency amounted to 98.3% when 0.5 mg of BSA was added, and although encapsulation efficiency dropped as the amount of added BAS increased, it was still as high as 88.5% when 10 mg of BSA was added. High encapsulation efficiency is of particular importance for drug or vaccine delivery, because lower amounts of NPs are needed to carry certain cargo quantities. This could reduce the potential side effects of NPs, increase treatment efficacy, and lower cost. In the second step, liposomes consisting of given molar ratio of lipids were hybridized with PLGA NPs via sonication-aided fusion. The size and zeta potential of hybrid NPs containing various molar ratios of cholesterol (cholesterol ranged from 5% to 20%; the remaining lipid was DOTAP) were evaluated. As shown in **Fig. 1B**, sizes of all hybrid NPs were around 144 nm, largely attributable to the size of PLGA NPs. (The size of PLGA NPs formed using the above mentioned method was around 120 nm.) It is worth noting that the polydispersity indexes (shown with blue numbers) of all hybrid NPs were very low, indicating that the sizes of hybrid NPs were narrowly distributed and the aforementioned methods for NP fabrication were highly robust. Zeta potential of hybrid NP decreased with the increased concentration of cholesterol, which can be explained by the decreased concentration of positively charged DOTAP in the lipid layer. Nevertheless, even at a cholesterol molar ratio of 20%, the surface of

the hybrid NP was still positively charged, which was indicated by the positive value of zeta potential. It has been reported that positively charged NPs were taken up by cells with higher efficiency compared with neutral NPs or those with negative surface charge [13, 14]. To confirm that a hybrid structure was successfully formed, hybrid NPs, in which PLGA core was labeled with Rhod B (red color) and a lipid layer that was labeled with NBD PE (green color), were imaged using confocal microscopy. As shown in **Fig. 1C**, hybrid NPs display both red color and green color, indicating that PLGA NPs and liposomes were indeed hybridized. Moreover, the vast majority of NPs in **Fig. 1C** were hybrid NPs, implying the high efficiency of hybridization achieved by the sonication-aided fusion. In addition, by comparing the FTIR spectra of liposomes, PLGA NP, and hybrid NP, liposomes and hybrid NPs evidently share peaks at wavenumbers of 2854 $cm^{-1}$ and 2923 $cm^{-1}$, and PLGA NPs show the same peaks at wavenumbers of 1270 $cm^{-1}$ and 1132 $cm^{-1}$ as hybrid NPs, further demonstrating that the lipid layer was coated onto the PLGA core.

### 3.2 *In vitro* release of BSA from hybrid NPs in human serum and PBS buffer

Others reported that a lipid layer can act as a molecular fence and contribute to keeping anti-cancer drug molecules in a PLGA core while keeping $H_2O$ out of the core, decreasing hydrolysis of the PLGA polymer as well as decreasing erosion and undesired drug release [15]. In this study, to investigate how cholesterol concentration in the lipid layer of hybrid NPs influences their performance and subsequent antigen release, hybrid NPs containing a range of cholesterol concentrations (5%, 10%, 15%, and 20%) were fabricated. BSA as a model antigen was enclosed in the PLGA core. Performance of NPs in human serum is an important criterion for their application as vaccine delivery vehicle *in vivo*. In human serum, the amount of released BSA was inversely correlated with cholesterol concentration (**Fig. 2A**). At 5% cholesterol, 34.2% of BSA was released from NPs in 24 h. However, the amount of released BSA was significantly reduced to 27.7% when cholesterol concentration was increased by 5%. At 20% cholesterol level, only 15.6% of BSA was released from NPs. Early studies demonstrated that incorporation of cholesterol in a liposome formulation could remarkably increase the stability and

reduce the permeability of liposomal bilayers [16, 17]. In this study, the decreased BSA release from hybrid NPs with higher cholesterol content when put in serum probably resulted from slowed diffusion of BSA out of the lipid layer as well as reduced influx of water and serum enzymes into the PLGA core. To compare long-term antigen release among NPs without the confounding factors associated with incubation in serum, hybrid NPs formulated with various concentrations of cholesterol were incubated in PBS buffer. The antigen release profiles (**Fig. 2B**) show that the rate of BSA release was also reversely correlated with the concentration of cholesterol in the lipid layer. Although sustained BSA release profiles were observed among all tested hybrid NPs, slower and steadier BSA release was achieved by hybrid NPs with higher cholesterol concentrations. After 168 h of incubation in PBS buffer, 51.5% BSA was released from NPs containing 20% cholesterol in its lipid layer. In contrast, 76.8% of BSA was released from NPs with 5% cholesterol, demonstrating a significant impact of cholesterol on retaining antigen in hybrid NPs.

### 3.3 *In vitro* uptake into DCs of hybrid NPs with varied cholesterol concentrations

To understand how cholesterol concentration in lipid layer affects the uptake of lipid-PLGA hybrid NPs by DCs, freshly produced hybrid NPs containing different molar ratios of cholesterol (5%, 10%, 15%, and 20%) in lipid layer were added to DCs. After 5 h of incubation, the *in vitro* cellular uptake of hybrid NPs by DCs was investigated using confocal microscopy and TEM. In **Fig. 3A**, fluorescence from the hybrid NPs (labeled with Alexa Fluor® 647 ) internalized in DCs (nucleus was labeled with DAPI, which displays blue color) is shown. Qualitative examination of the CLSM images of cellular uptake demonstrated that red fluorescence with wider distribution and brighter color was observed in DCs treated with hybrid NPs containing higher concentrations of cholesterol. This suggests that increasing cholesterol concentration in the lipid layer could remarkably enhance the internalization of hybrid NPs by DCs. A quantitative study of cellular uptake was performed by measuring the percentage of DCs that internalized hybrid NPs (Alexa Fluor® 647 labeled) as well as the fluorescence intensity of NPs

internalized into DCs after incubating 200 μg of NPs with $2\times10^6$ cells for 90 min. As shown in **Fig. 3B**, 24.9%, 35.1%, 46.7%, and 62.4% of DCs have entrapped hybrid NPs with cholesterol concentrations of 5%, 10%, 15%, and 20%, respectively. The significant increase in number of DCs that internalized NP at higher cholesterol concentrations demonstrates that increasing cholesterol content in the lipid layer could considerably facilitate the uptake of hybrid NPs by DCs. Others proposed that *in vitro* cellular uptake of lipid-polymer hybrid NP was mediated by carrier endocytosis and cell fusion [18]. In this study, the enhancing effect of cholesterol on cellular uptake may result from the fact that cholesterol can improve the stability of the lipid bilayer [19], and the improved integrity of the hybrid structure promotes NP uptake by DCs. In addition, as shown in **Fig. 3C**, increasing cholesterol concentrations resulted in significantly higher fluorescent intensities in DCs, suggesting that more NPs of higher cholesterol content were internalized. Analysis of the fluorescence intensity demonstrates that DCs internalized 150% more hybrid NP of 20% cholesterol concentration compared internalization in NP of 5% cholesterol concentration.

Cellular uptake of hybrid NP of various cholesterol content was further examined with TEM. In order to increase the contrast of TEM image and better locate distribution of NPs in DCs, iron NPs were encapsulated in lipid-PLGA hybrid NPs. In addition to the physiochemical characterization of hybrid NP in **Fig. 1**, the morphologies of PLGA NP and lipid-PLGA hybrid NP were studied using TEM. A representative TEM image of PLGA NP is shown in **Fig. 4A**. The NP is of a spherical shape with a diameter around 160 nm, and the particle surface is smooth. As shown in **Fig. 4B**, although the size and morphology of lipid-PLGA hybrid NP are highly similar to that of PLGA NP, one lipid layer with thickness of 10-20 nm is seen to closely surround the PLGA core. The comparison of **Fig. 4A** and **Fig. 4B** clearly shows that PLGA NP was perfectly hybridized with liposome. Iron NPs (as shown in **Fig. 4C**) with a diameter of 30 nm were encapsulated in PLGA NPs. After hybridization with liposome, PLGA NP including iron NPs were incorporated with a lipid layer (**Fig. 4D**). In consistency with **Fig. 4B**, a lipid layer can be distinctively

observed in iron enclosed lipid-PLGA hybrid NPs. After incubating $2\times10^6$ DCs with 200 μg of iron containing lipid-PLGA hybrid NPs of varying lipid compositions for 90 min, uptake of NPs by DCs was viewed using TEM. As shown in **Fig. 4E-H** (from **Fig. 4E** to **Fig. 4H**, the cholesterol content in lipid layers was 5%, 10%, 15%, and 20%, respectively), DCs internalized different amounts of hybrid NPs depending on the cholesterol concentration. Consistent with the results from confocal imaging and flow cytometry, TEM images of cellular uptake show that more NPs with higher cholesterol content were internalized by DCs. Remarkably, regardless of lipid composition, all the NPs were enclosed inside endosomes after uptake by cells. From an immunological perspective, such a location of NP in DCs is beneficial to trigger immune response, especially for inducing humoral response. In endosomes, antigens can be processed by proteinases into antigenic peptides, which are further presented to T helper cells [20]. It is to be noted that the lipid layer of hybrid NP with 5% cholesterol was no longer detected in NPs after internalization by DCs, but in other hybrid NPs with higher cholesterol content, a lipid layer surrounding NPs could still be observed after endocytosis. It is likely that the lipid layer with higher cholesterol content was stable and able to maintain the core-shell structure during their entrance into DCs.

### 3.4 Stability of hybrid NPs in PBS buffer at 4 °C for 30 days

To assess how cholesterol content could affect long-term stability of hybrid NPs, NPs of varied cholesterol concentrations (5%, 10%, 15%, and 20%) were stored in PBS buffer (pH 7.4, 5 mg/mL) at 4 °C for 30 days, and the size distribution and confocal morphology of the NPs were studied before and after storage. As shown in **Fig. 5 A-D**, size distributions of all the NPs shifted to the right after 30 days of storage, indicating a general trend toward size increase. It appears that the extent of size increase was correlated with cholesterol content in the lipid layer. For example, the initial central peak of all the NPs was around 150 nm, and after storage, it changed to 300 nm, 500 nm, 1500 nm, and 1250 nm for NPs with cholesterol content of 5%, 10%, 15%, and 20%, respectively. The size increase of NPs may result from aggregation or fusion of NPs. This assumption was confirmed by analysis of the confocal image of

NPs after storage. As shown in the magnified confocal image in **Fig. 5D**, many small NPs are distributed around and merging with a NP of much bigger size, suggesting that bigger NPs were formed by fusion of smaller NPs. A closer examination of the confocal images of the stored NP revealed that the number of visible NPs decreased with the decrease in cholesterol content in the lipid layer. It is likely that the lipid layer of hybrid NPs with lower cholesterol concentration was not stable, and might disintegrate from the PLGA core over time of storage. PLGA NPs without the protection from a lipid layer can be hydrolyzed more rapidly compared to those shelled with lipid layer, leading to disappearance of previously visible particles. For example, early study on PLGA degradation showed that the half-life of PLGA structures were less than 4 weeks [21]. The degradation of NPs of lower cholesterol content might result in lower number of visible NPs as well as lead to a reduction in the chance of forming larger NPs. Although NPs with higher cholesterol content were more stable in terms of structural integrity compared to those with lower cholesterol content, the considerable size increase might interfere with antigen delivery. As shown in **Fig. 5E**, analysis of cellular uptake of NPs with 20% cholesterol content demonstrates that 63.9% of the cell internalized newly prepared NPs in 90 min. In contrast, only 26.4% of cells took up the stored NPs, suggesting that long-term stored NPs with higher cholesterol content may not perform ideally as a vaccine carrier unless the fusion effect leading to large size can be minimized.

### 3.5 Minimization of the fusion effect among hybrid NPs through PEGylation

As discussed in previous section, high concentration of cholesterol in the lipid layer was beneficial to maintaining the integrity of the hybrid structure of NP. However, an intact lipid shell increased the chance of fusion between NPs, leading to increased particle size and decreased cellular uptake. Therefore, it is necessary to engineer the high cholesterol content hybrid NPs to be fusion resistant. PEGylation has been reported as one of the most successful strategies to improve the delivery of many therapeutic molecules such as proteins, macro-molecular carriers, small drugs, oligonucleotides, and other biomolecules [22]. PEGylation has also been widely used as a stabilizing process for many NP

formulations, such as dendrimers and liposomes [23]. It is possible that the steric hindrance offered by PEG molecules may mitigate the fusion problem of lipid-PLGA hybrid NPs. Therefore, in this study, hybrid NPs containing 20% cholesterol were incorporated with various molar ratios (10%, 20%, and 30%) of DSPE-PEG(2000) Amine in lipid layer, and size distributions and confocal images of these PEG engineered hybrid NPs were analyzed after 30 days' storage at 4 °C in PBS buffer. As shown in **Fig. 6**, the size distributions of PEGylated NPs remained closer to that of newly made hybrid NPs compared to that without PEG, indicating that PEGylation could markedly reduce the fusion problem of hybrid NPs during storage. Confocal images of NPs in **Fig. 6** also show that no marked size increase were detected among NPs containing DSPE-PEG(2000) Amine compared to newly made NPs. Size distribution of NPs was also related to the concentration of PEG in the lipid layer, and hybrid NPs containing a higher percentage of PEG exhibited less size distribution when compared to newly made NPs.

### 3.6 Influence of PEGylation of hybrid NPs on cellular uptake of NPs

The ultimate goal of introducing DSPE-PEG(2000) amine into the lipid layer was to minimize fusion-caused size increases of NPs, thereby improving uptake of NPs by DCs. To evaluate the effect of PEGylation of NP on cellular uptake, PEGylated NPs after 30 days storage in PBS buffer (5 mg/mL) were mixed with DCs, and internalization of NPs were studied with flow cytometry and confocal microscopy. As shown by flow cytometry data in **Fig. 7**, after 90 min treatment, 26.6%, 58.9%, 54.9%, and 48.3% of the cells internalized NPs with PEG concentration of 0%, 10%, 20%, and 30%, respectively. Confocal microscopic pictures also demonstrate that considerably higher quantities of PEGylated NPs were taken up by DCs compared to non-PEGylated NPs. These results indicate that PEGylation of hybrid NPs could effectively improve cellular uptake of stored NPs. It is very likely that the improved endocytosis of NPs resulted from the relatively unchanged size distribution of PEGylated NPs, because DCs preferably internalize nanoparticles with sizes between 20 nm and 100 nm [24]. However, it should be noticed that among those PEGylated NPs, higher level of PEGylation led to decreased cellular uptake. The percentage

of cells that internalized NPs significantly dropped from 58.9% to 48.3% when PEGlyation level was raised from 10% to 30%. The decreased cellular uptake of NPs with higher PEG concentration implies that PEGylation of NPs is a double-edged sword: on one hand it can stabilize NPs, but on the other hand, it can impede the interaction between NPs and cells, decreasing cellular uptake efficiency.

## *4.* Conclusion

Lipid-PLGA hybrid NPs with various cholesterol contents were fabricated, and a higher content of cholesterol in lipid layer was found to allow slower and more controlled antigen release *in vitro*, facilitate cellular uptake of NPs, and protect the integrity of the hybrid nanostructure. However, concentrated cholesterol in the lipid layer promoted fusion between hybrid NPs, resulting in significant size increase after long-term storage in PBS buffer, which impeded cellular uptake of NPs. To mitigate the fusion effect during storage, hybrid NPs were PEGylated. It was found that PEGylation of hybrid NPs could considerably minimize fusion-caused size increases for NPs of high cholesterol content. Subsequent study on cellular uptake of stored PEGylated NPs demonstrated that PEGylation could significantly increase internalization of NPs compared to non-PEGylated NPs stored for a similar period of time. However, the level of PEGylation has to be cautiously considered, because although higher concentrations of PEG in lipid layesr may improve the long-term stability of hybrid NPs, it also can potentially increase steric hindrance between NPs and cells, undermining cellular uptake efficiency.

## Acknowledgment

This work was financially supported by National Institute on Drug Abuse (R21DA030083 and UO1DA036850).

## References

[1] Mandal B, Bhattacharjee H, Mittal N, Sah H, Balabathula P, Thoma LA, et al. Core-shell-type lipid-polymer hybrid nanoparticles as a drug delivery platform. Nanomedicine. 2013;9:474-91.

[2] Cheow WS, Hadinoto K. Factors affecting drug encapsulation and stability of lipid-polymer hybrid nanoparticles. Colloids Surf B Biointerfaces. 2011;85:214-20.

[3] Wong HL, Bendayan R, Rauth AM, Wu XY. Simultaneous delivery of doxorubicin and GG918 (Elacridar) by new polymer-lipid hybrid nanoparticles (PLN) for enhanced treatment of multidrug-resistant breast cancer. J Control Release. 2006;116:275-84.

[4] Ling G, Zhang P, Zhang W, Sun J, Meng X, Qin Y, et al. Development of novel self-assembled DS-PLGA hybrid nanoparticles for improving oral bioavailability of vincristine sulfate by P-gp inhibition. J Control Release. 2010;148:241-8.

[5] Hu CM, Kaushal S, Tran Cao HS, Aryal S, Sartor M, Esener S, et al. Half-antibody functionalized lipid-polymer hybrid nanoparticles for targeted drug delivery to carcinoembryonic antigen presenting pancreatic cancer cells. Mol Pharm. 2010;7:914-20.

[6] Evjen TJ, Nilssen EA, Fowler RA, Rognvaldsson S, Brandl M, Fossheim SL. Lipid membrane composition influences drug release from dioleoylphosphatidylethanolamine-based liposomes on exposure to ultrasound. Int J Pharm. 2011;406:114-6.

[7] Needham D, Park JY, Wright AM, Tong J. Materials characterization of the low temperature sensitive liposome (LTSL): effects of the lipid composition (lysolipid and DSPE-PEG2000) on the thermal transition and release of doxorubicin. Faraday Discuss. 2013;161:515-34; discussion 63-89.

[8] Ali MH, Kirby DJ, Mohammed AR, Perrie Y. Solubilisation of drugs within liposomal bilayers: alternatives to cholesterol as a membrane stabilising agent. J Pharm Pharmacol. 2010;62:1646-55.

[9] Saito H, Shinoda W. Cholesterol effect on water permeability through DPPC and PSM lipid bilayers: a molecular dynamics study. J Phys Chem B. 2011;115:15241-50.

[10] Yang YY, Chia HH, Chung TS. Effect of preparation temperature on the characteristics and release profiles of PLGA microspheres containing protein fabricated by double-emulsion solvent extraction/evaporation method. J Control Release. 2000;69:81-96.

[11] Hu Y, Zheng H, Huang W, Zhang C. A novel and efficient nicotine vaccine using nano-lipoplex as a delivery vehicle. Hum Vaccin Immunother. 2014;10:64-72.

[12] Kumar MR, Bakowsky U, Lehr C. Preparation and characterization of cationic PLGA nanospheres as DNA carriers. Biomaterials. 2004;25:1771-7.

[13] Chung TH, Wu SH, Yao M, Lu CW, Lin YS, Hung Y, et al. The effect of surface charge on the uptake and biological function of mesoporous silica nanoparticles in 3T3-L1 cells and human mesenchymal stem cells. Biomaterials. 2007;28:2959-66.

[14] Verma A, Stellacci F. Effect of surface properties on nanoparticle-cell interactions. Small. 2010;6:12-21.

[15] Chan JM, Zhang L, Yuet KP, Liao G, Rhee JW, Langer R, et al. PLGA-lecithin-PEG core-shell nanoparticles for controlled drug delivery. Biomaterials. 2009;30:1627-34.

[16] Kirby C, Clarke J, Gregoriadis G. Effect of the cholesterol content of small unilamellar liposomes on their stability in vivo and in vitro. Biochem J. 1980;186:591-8.

[17] Gregoriadis G, Davis C. Stability of liposomes in vivo and in vitro is promoted by their cholesterol content and the presence of blood cells. Biochem Biophys Res Commun. 1979;89:1287-93.

[18] Ito J, Kato T, Kamio Y, Kato H, Kishikawa T, Toda T, et al. A cellular uptake of cis-platinum-encapsulating liposome through endocytosis by human neuroblastoma cell. Neurochem Int. 1991;18:257-64.

[19] Anderson M, Omri A. The effect of different lipid components on the in vitro stability and release kinetics of liposome formulations. Drug Deliv. 2004;11:33-9.

[20] Dudziak D, Kamphorst AO, Heidkamp GF, Buchholz VR, Trumpfheller C, Yamazaki S, et al. Differential antigen processing by dendritic cell subsets in vivo. Science. 2007;315:107-11.

[21] Lu L, Peter SJ, Lyman MD, Lai HL, Leite SM, Tamada JA, et al. In vitro and in vivo degradation of porous poly(DL-lactic-co-glycolic acid) foams. Biomaterials. 2000;21:1837-45.

[22] Milla P, Dosio F, Cattel L. PEGylation of proteins and liposomes: a powerful and flexible strategy to improve the drug delivery. Curr Drug Metab. 2012;13:105-19.

[23] Ryan SM, Mantovani G, Wang X, Haddleton DM, Brayden DJ. Advances in PEGylation of important biotech molecules: delivery aspects. Expert Opin Drug Deliv. 2008;5:371-83.

[24] Bachmann MF, Jennings GT. Vaccine delivery: a matter of size, geometry, kinetics and molecular patterns. Nat Rev Immunol. 2010;10:787-96.

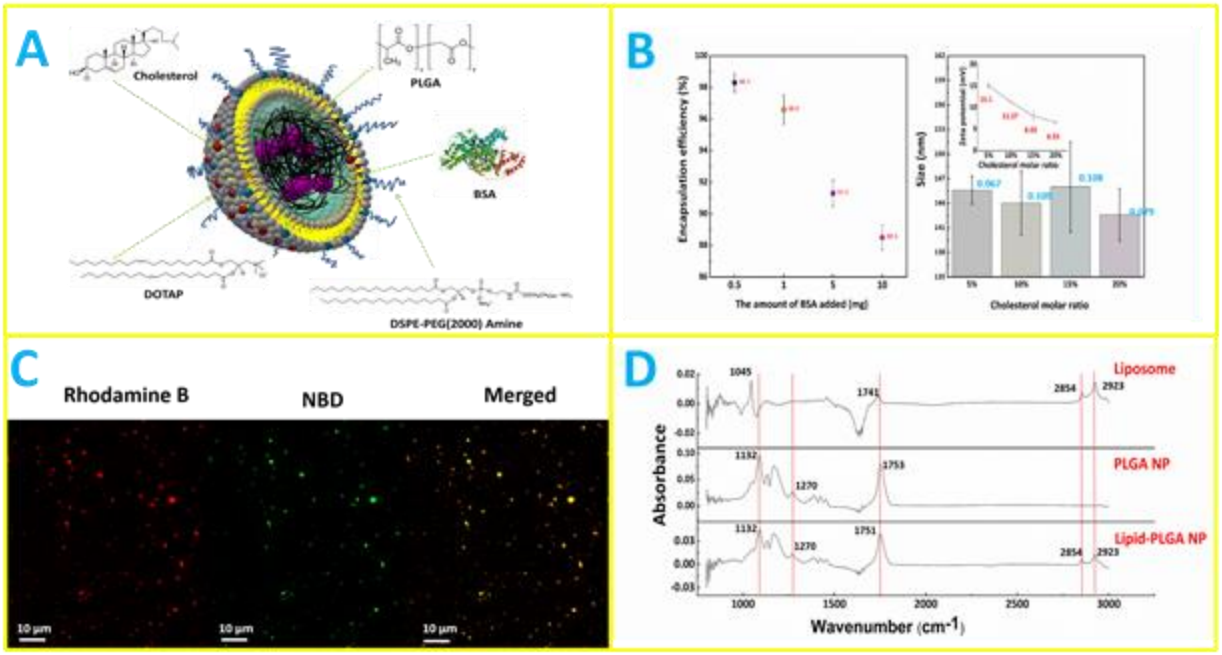


**Figure 1.** Synthesis of lipid-PLGA NPs. (A) A 3D schematic illustration of the structure of lipid-PLGA NPs showing a lipid layer around a BSA core. (B) (Left graph) encapsulation efficiency of BSA at varied amounts (0.5 mg, 1 mg, 5 mg, and 10 mg) by 100 mg PLGA NPs; (right graph) size and zeta potential of lipid-PLGA NPs containing various molar ratios of cholesterol in the lipid layer (5%, 10%, 15%, 20%). (C) Confocal micrograph of lipid-PLGA NPs, in which lipid layer was labeled with NBD PE (green color) and PLGA core encapsulated Rhod B (red color) stained BSA. The merged image shows that PLGA NPs and liposomes were hybridized (D) FTIR spectra of liposome, PLGA NP, and lipid-PLGA NP. Liposomes and hybrid NPs share peaks, demonstrating that the lipid layer was coated onto the PLGA core.

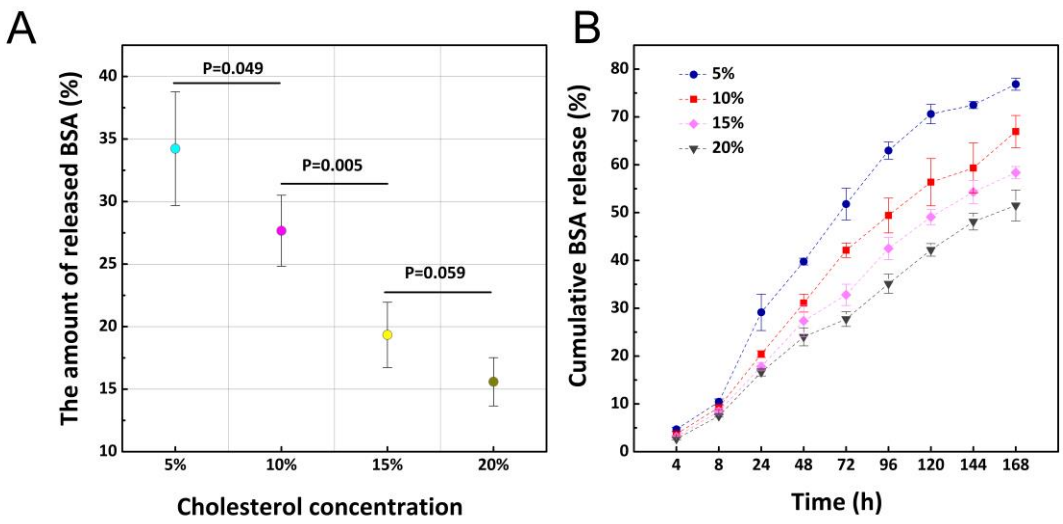


**Figure 2.** Release of BSA from lipid-PLGA hybrid NPs. (A) The release of BSA from hybrid NPs containing various concentrations of cholesterol in lipid layer after incubation for 24h in human serum at room temperature. Higher concentrations of cholesterol decreased BSA release. (B) The release profile of BSA from hybrid NPs, which were suspended in PBS buffer (pH 7.4) at room temperature. After 168 h of incubation in PBS buffer, 51.5% BSA was released from NPs containing 20% cholesterol in its lipid layer. In contrast, 76.8% of BSA was released from NPs with 5% cholesterol, demonstrating a significant impact of cholesterol on retaining antigen in hybrid NPs.

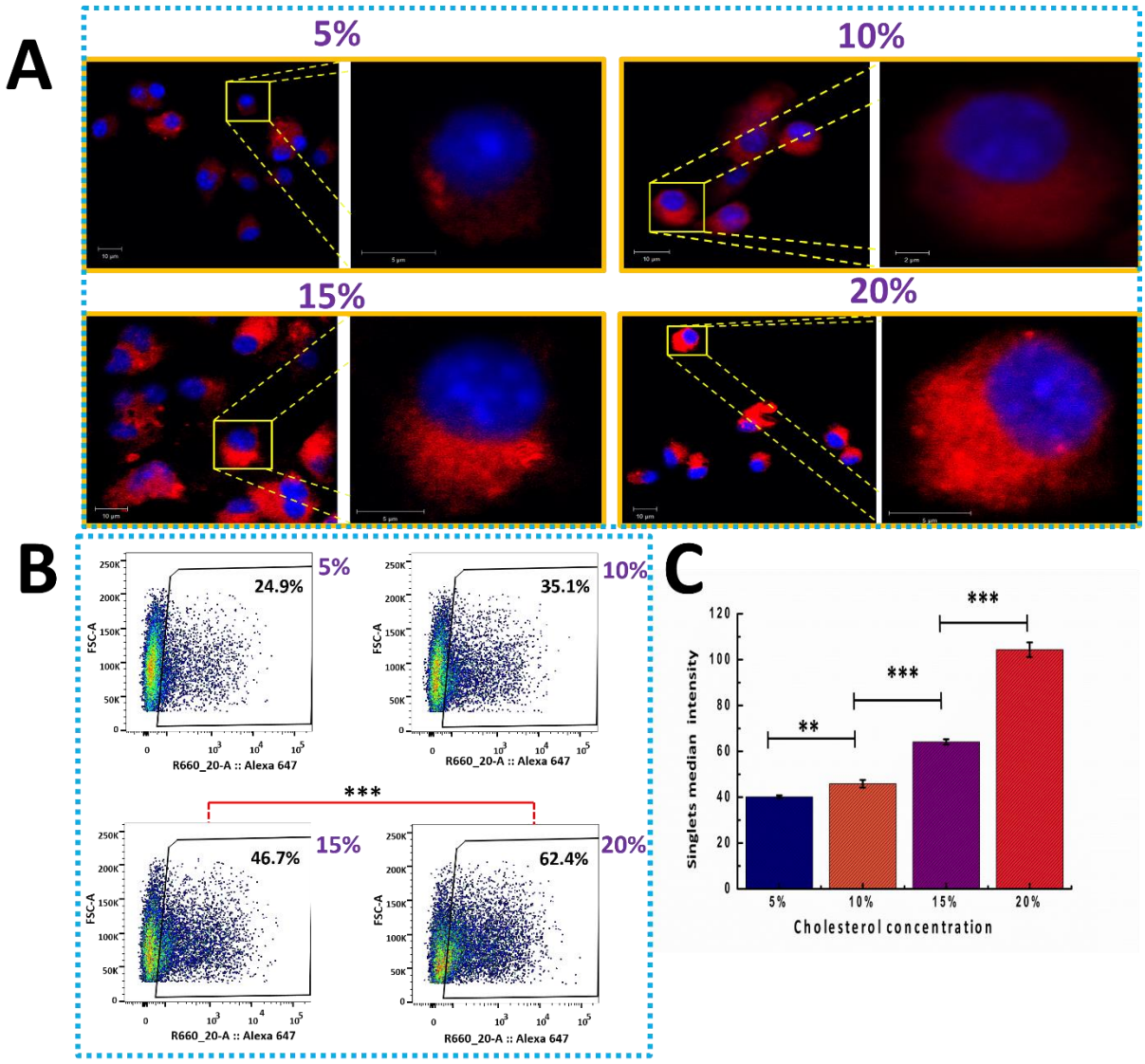


**Figure 3.** Investigation of endocytosis of freshly made hybrid NPs by DCs using CLSM and flow cytometry. Increasing cholesterol concentrations resulted in significantly higher fluorescent intensities in DCs, suggesting that more NPs of higher cholesterol content were internalized. (A) Confocal microscopic image of the uptake of hybrid NPs consisting of various molar ratios (5%, 10%, 15%, and 20%) of cholesterol by DCs. 100 µg of Rhod B stained hybrid NP were incubated with $3\times10^5$ DCs for 5 h. The scale bars in all lower magnification images are 10 µm. (B) Flow cytometry study on the percentage of cells that had taken up the above mentioned hybrid NPs. 200 µg of Alexa Fluor® 647 labeled NPs were cultured with $2\times10^6$ DCs for 90 min. (C) Singlet median intensity of the DCs that had endocytosed hybrid NPs with various molar ratios of cholesterol in lipid layer. ** denotes that P-value is less than 0.05, *** denotes that P-value is less than 0.01.

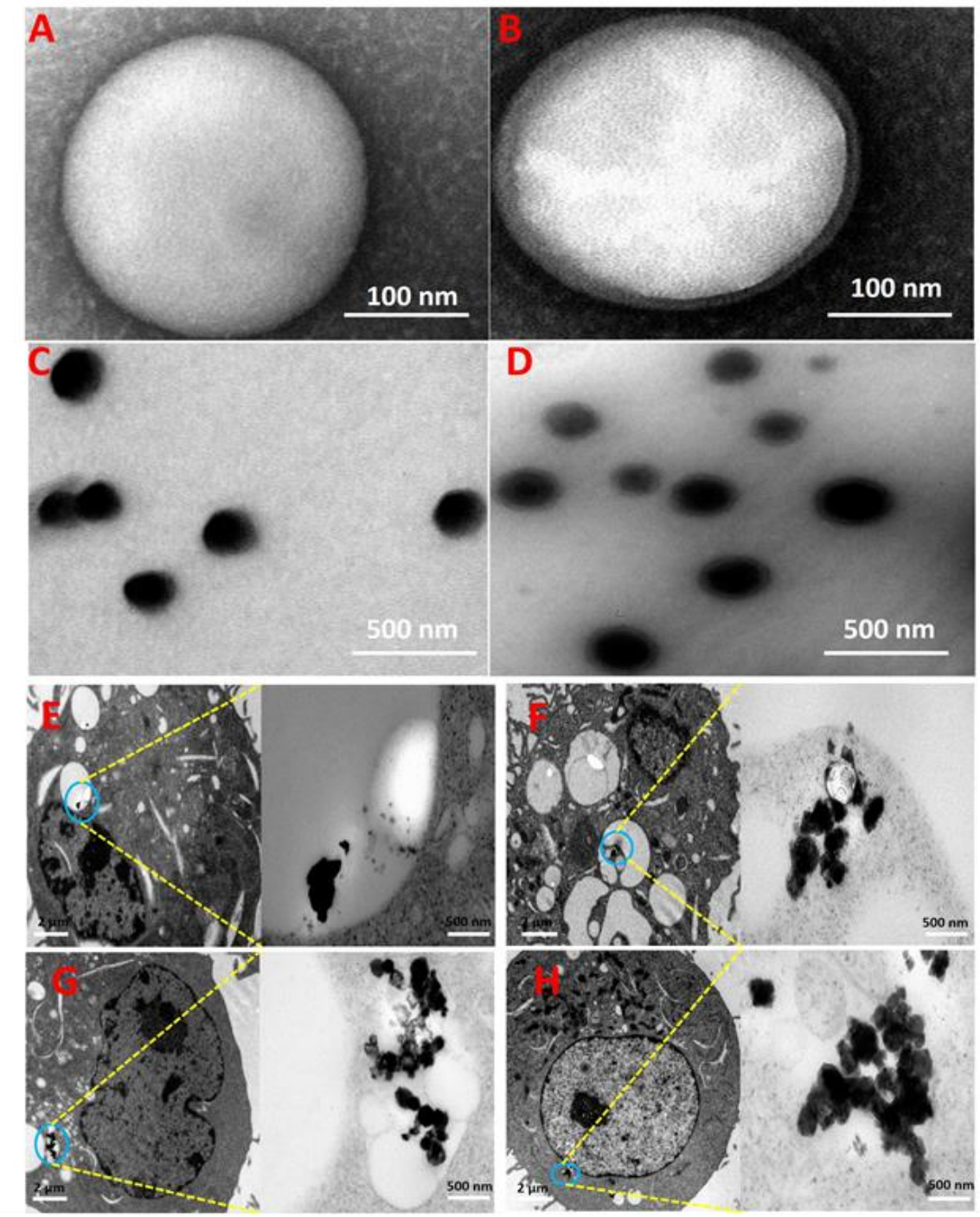


**Figure 4.** TEM images of (A) PLGA NP, (B) Lipid-PLGA hybrid NP, (C) Iron NP, (D) Lipid-PLGA hybrid NP with enclosed iron NP, (E-H) Dendritic cell uptake of iron NP contained lipid-PLGA hybrid NPs, which have different molar ratios of cholesterol (5%, 10%, 15%, and 20%). $2\times10^6$ immature DCs were incubated with 200 µg of hybrid NPs for 90 min. Figure E-H show that DCs internalized more hybrid NPs of higher cholesterol content compared to those of lower cholesterol content.

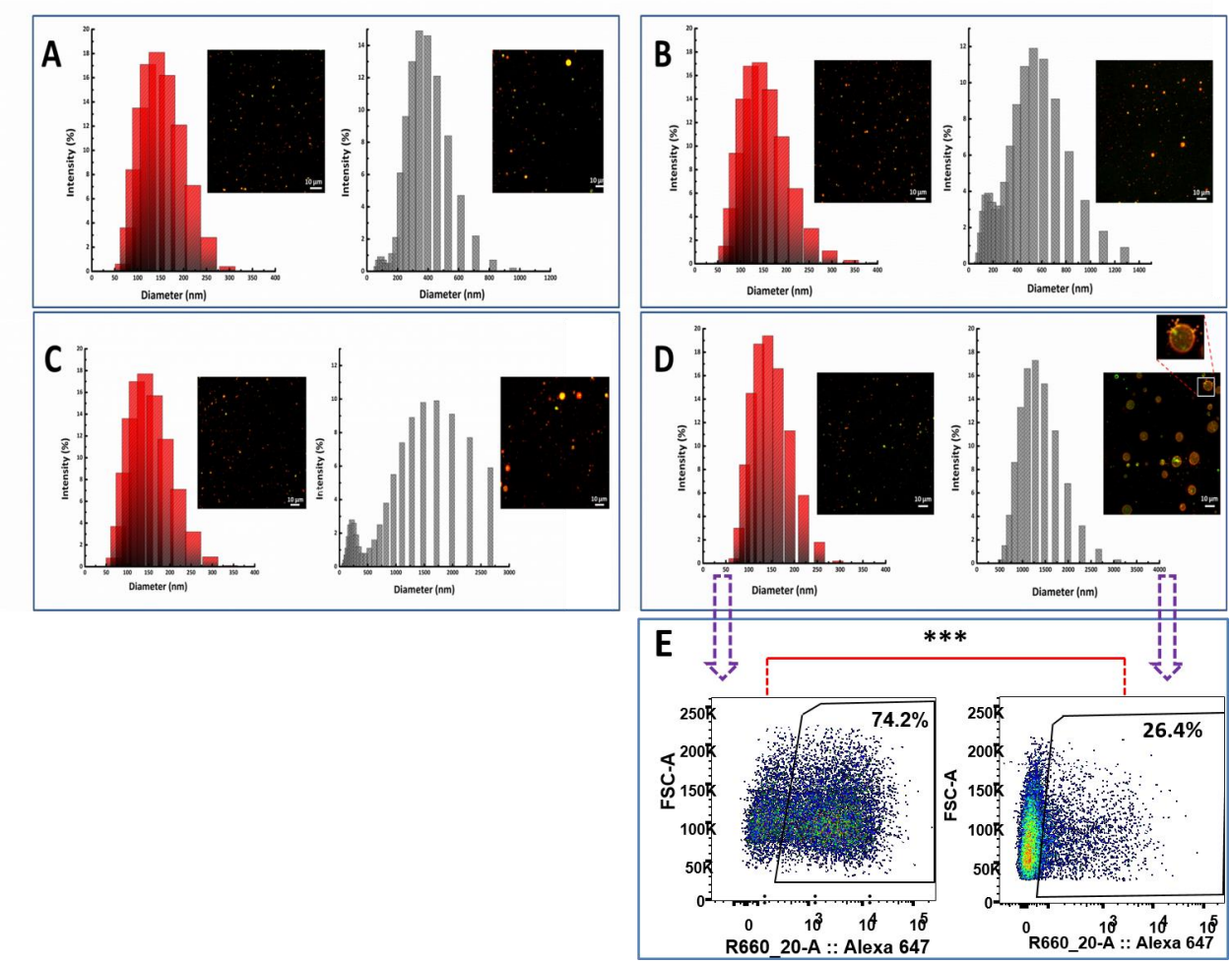


**Figure 5.** Stability of hybrid NPs of different cholesterol content in PBS at 4 °C for 30 days. Size distributions of hybrid NPs were measured before (red columns) and after (grey columns) storage in PBS, and the corresponding confocal images of hybrid NPs were taken (lipid layer of hybrid NPs was labeled with NBD, and PLGA core was labeled with Rhod B). (A) NPs with 5% cholesterol in total lipid content. (B) NPs with 10% cholesterol. (C) NPs with 15% cholesterol. (D) NPs with 20% cholesterol. (E) Cellular uptake of newly prepared NP containing 20% cholesterol and NPs (PLGA core was labeled with Alexa Fluor® 647) stored for 30 days. During storage, hybrid NPs of higher cholesterol content underwent more significant size increase compared to those of lower cholesterol content. Increase in NP size impeded the uptake of NPs by dendritic cells. Scale bars in confocal images represent 10 µm.

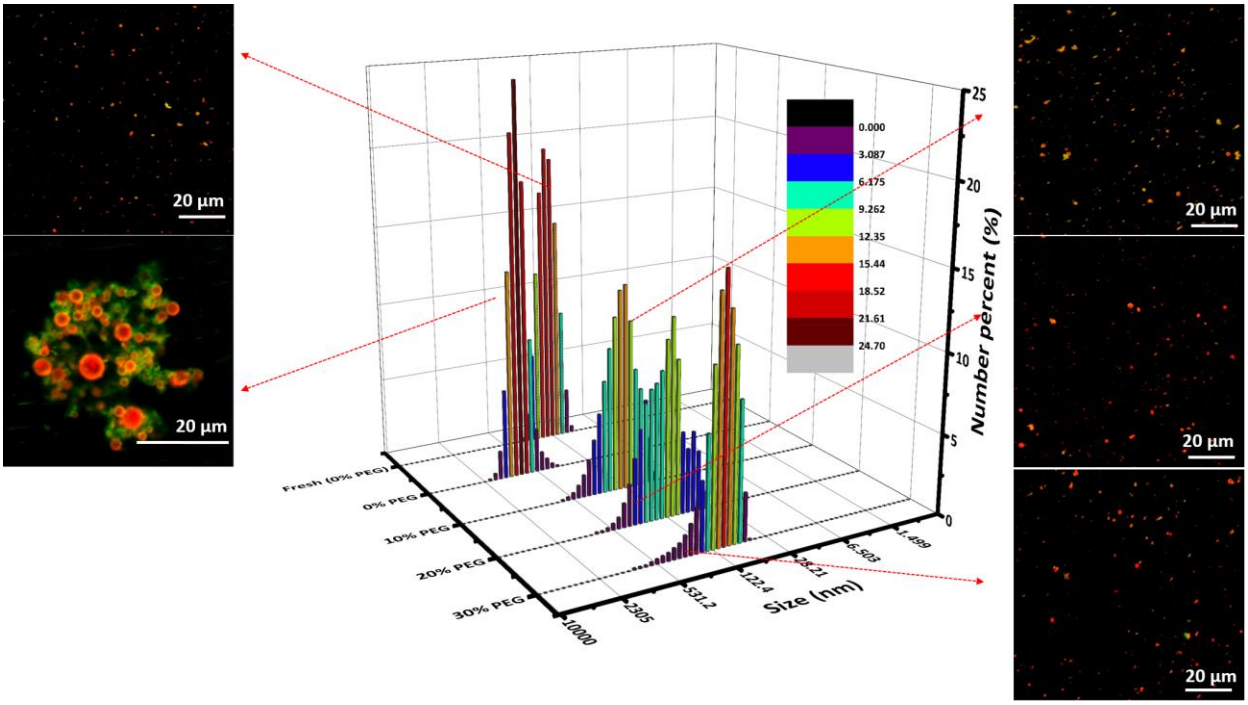


**Figure 6.** Impact of DSPE-PEG (2000) amine on the size distribution of NPs after 30 days' storage at 4 °C. Hybrid NP containing 20% cholesterol in lipid layer were introduced with a range of concentrations (10%, 20%, and 30%) of DSPE-PEG(2000) amine. The pictures on both sides of size distribution are confocal images of NPs labeled with NBD and Rhod B. The colors in confocal images were a result of combination of NBD and Rhod B. After 30 days' storage, no marked size increase were detected among NPs containing DSPE-PEG(2000) amine compared compared to newly made NPs. The scale bars represent 20 µm.

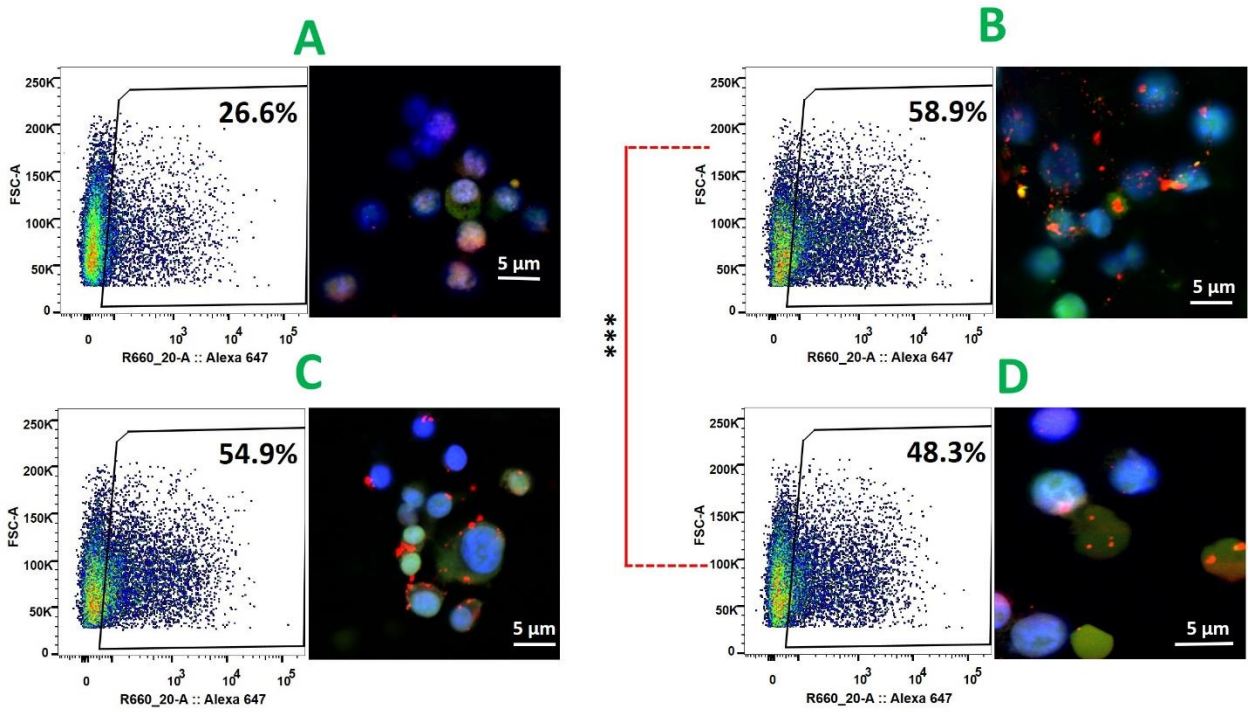


**Figure 7.** Cellular uptake of PEGylated hybrid NPs. Hybrid NPs containing 20% cholesterol and a range concentrations (0%, 10%, 20%, and 30%) of DSPE-PEG(2000) Amine were stored in PBS at 4 °C for 30 days, and cellular uptake of these stored NPs were investigated using flow cytometry and confocal microscope. (A) NPs with 0% PEG, (B) NPs with 10% PEG, (C) NPs with 20% PEG, and (D) NPs with 30% PEG. After 30 days' storage, considerably higher quantities of PEGylated NPs were taken up by DCs compared to non-PEGylated NPs. Scale bar represent 5 µm.

## Chapter VIII: General Conclusions and future directions

The enormous economic loss and tremendous stress on public health caused by tobacco smoking as well as poor effectiveness of current medications necessitate the development of new strategies for smoking cessation. In recent years, nicotine vaccines, acting by producing nicotine specific antibodies to minimize the amount of nicotine that can enter brain during smoking, have emerged as a promising medical intervention against cigarette smoking. Due to the inability of nicotine to induce immune response, the nicotine molecule has to be associated with carriers of bigger mass to produce nicotine specific antibodies. In the past decade, there have been numerous nicotine vaccine candidates evaluated in human clinical trials, including NicVAX®, TA-NIC®, NIC002®, Niccine®, and SEL-068®. Traditional nicotine vaccines using protein-nicotine conjugate as antigen have been extensively studied. However, protein-nicotine conjugate based vaccines have some innate deficiencies, including low immunogenicity, low specificity, and short immune response persistence, all of which render these vaccines ineffective in treating smoking addiction. Currently, nicotine vaccines using nanoparticles as delivery system are believed to be viable designs for overcoming aforementioned disadvantages of conventional nicotine vaccines.

In this study, to facilitate recognition and uptake of nicotine vaccine by immune cells, nicotine-BSA conjugate was linked to nano-sized cationic liposomes. Such a lipoplex based nicotine vaccine demonstrated high antigen loading capacity, high nicotine epitope density, and desirable physiochemical properties, all of which led to significantly stronger immunogenicity than Nic-BSA nicotine vaccine. However, poor stability caused by flocculation and fusion was associated with liposome based delivery system. To improve the stability of liposome based nicotine vaccine, negatively charged nanohorns as scaffold support were incorporated into cationic liposomes via a freeze-thaw method. This nanohorn supported liposome exhibited marked improvement in stability compared to

liposome. A subsequent animal trial showed that nicotine vaccine using nanohorn supported liposome demonstrated significantly higher potency in inducing immune response than cationic liposome based nicotine vaccine. In addition, no clinical signs indicated that this nanohorn supported liposome would cause severe toxicity to animals.

Despite its desirable ability in potentiating immune response, nanohorn supported liposome as vaccine delivery system is still at its infant stage and the cytotoxicity of nanohorns is debatable. Therefore, our subsequent study focused on developing hybrid nanoparticle that can replace nanohorn supported liposome as nicotine vaccine delivery vehicle. Due to its widely accepted good safety profile, PLGA nanoparticles were used to substitute for nanohorns as support for liposome. Preliminary data showed that lipid-PLGA hybrid nanoparticle demonstrated excellent stability in buffers that mimicking both storage conditions and physiological conditions. In addition, uptake rate of hybrid nanoparticles by dendritic cells could be controlled by modulating the surface charge of nanoparticles.

For vaccine delivery, it is desirable to devise a vehicle that can maintain good stability during circulation as well as enable timely antigen release after uptake by immune cells. To fulfill this goal, a hybrid nanoparticle consisting of a PLGA core and a pH sensitive lipid shell was devised. Compared to non-pH sensitive hybrid nanoparticles, in response to low pH challenge, the pH sensitive nanoparticle could allow rapid removal of the lipid shell from the PLGA core, resulting in faster antigen release. The study on uptake of hybrid nanoparticles by dendritic cells demonstrated that pH sensitive nanoparticles could release protein antigens in endosomes of dendritic cells more readily than non-pH sensitive nanoparticles.

Lipid compositions of both cholesterol and DSPE-PEG dictate the surface chemistry of hybrid nanoparticles. This influences nanoparticle stability, antigen release, and internalization by dendritic cells. We found that high content of cholesterol could not only protect the integrity of the hybrid

structure, but also promote the uptake of nanoparticles by dendritic cells. However, high cholesterol content in lipid layer led to increased fusion between nanoparticles during long term storage, resulting in poor uptake of nanoparticle by dendritic cells. Later study found that introducing DSPE-PEG into lipid layer could markedly reduce high cholesterol caused particle aggregation, facilitating nanoparticle uptake by dendritic cells.

In conclusion, using nanoparticles as a vehicle for nicotine vaccine delivery can protect antigen from premature degradation, improve bioavailability of a vaccine to immune system, allow timely antigen release, and permit co-delivery of antigen and adjuvant, leading to enhanced immunogenicity of nicotine vaccine and lengthened immune response persistence.

Based on the findings from this thesis, future work may focus on development of nicotine vaccine using lipid-PLGA hybrid nanoparticle as carrier. In addition, this hybrid delivery system may also be used to construct vaccines against other drugs of abuse, such as cocaine, heroin, and methamphetamine. This hybrid nanoparticle based vaccine may increase bioavailability of vaccine to immune system, allow easy integration of molecular adjuvants to vaccine complex, and minimize immune pathogenicity of nicotine vaccine.

# Appendix A: permission for reproduction of materials from Taylor & Francis publications (reference for Chapter III)

**Permissions**

T & F Reference Number: P032715-08

3/27/2015

Yun Hu

Virginia Tech

hyun86@vt.edu

Dear Yun Hu,

We are in receipt of your request to reproduce your published Open Access article

Yun Hu, Hong Zheng, Wei Huang & Chenming Zhang (2014)

A novel and efficient nicotine vaccine using nano-lipoplex as a delivery vehicle

*Human Vaccines & Immunotherapeutics* 10 (1): 64-72.

DOI: 10.4161/hv.26635

in your dissertation

This permission is all for print and electronic editions.

We will be pleased to grant you permission free of charge on the condition that:

This permission is for non-exclusive English world rights. This permission does not cover any third party copyrighted work which may appear in the material requested.

Full acknowledgment must be included showing article title, author, and full Journal title, reprinted by permission of Taylor & Francis LLC (http://www.tandfonline.com).

Thank you very much for your interest in Taylor & Francis publications. Should you have any questions or require further assistance, please feel free to contact me directly.

Sincerely,

Mary Ann Muller

Permissions Coordinator

Telephone: 215.606.4334

E-mail: maryann.muller@taylorandfrancis.com

530 Walnut Street, Suite 850, Philadelphia, PA 19106  Phone: 215-625-8900  Fax: 215-207-0050

Web: www.tandfonline.com

## Appendix B: permission for reproduction of materials from American Scientific Publishers (reference for Chapter IV)

Dear Yun Hu:

American Scientific Publishers grants permission to re-use whole article of parts in your forthcoming PhD thesis.

Zheng, H.; Hu, Y.; Huang, W.; Villiers, S.; Pentel, P.; Zhang, J.; Dorn, H.; Ehrich, M.; Zhang, C., Negatively charged carbon nanohorn supported cationic liposome nanoparticles: a novel delivery vehicle for anti-nicotine vaccine. Journal of Biomedical Nanotechnology (2014).

Best regards,
H. S. Nalwa
*Publisher*

**Dr. Hari Singh Nalwa | Editor-in-Chief**: **Journal of Nanoscience and Nanotechnology |** Web: www.aspbs.com/jnn
**Editor**: Encyclopedia of Nanoscience and Nanotechnology (25-Volume set) **|** Web: www.aspbs.com/enn
American Scientific Publishers **|** 26650 The Old Road , Suite 208 , Valencia , California 91381-0751 , USA
Phone: (661) 799-7200 **|** Fax: (661) 799-7230 **|** Email: nalwa@aspbs.com **|** Web: www.aspbs.com

## Appendix C: permission for reproduction of materials from SpringerOpen Journal (reference for Chapter V)

**Nano Express**

**In vitro performance of lipid-PLGA hybrid nanoparticles as an antigen delivery system: lipid composition matters**

**Yun Hu**[1], **Marion Ehrich**[2], **Kristel Fuhrman**[3] and **Chenming Zhang**[1*]

*Corresponding author: Chenming Zhang chzhang2@vt.edu

Author Affiliations

[1]Department of Biological Systems Engineering, Virginia Tech, Blacksburg, VA 24061, USA

[2]Department of Biomedical Sciences and Pathobiology, Virginia Tech, Blacksburg, VA 24061, USA

[3]Veterinary Medicine Experiment Station, Virginia Tech, Blacksburg, VA 24061, USA

For all author emails, please log on.

*Nanoscale Research Letters* 2014, **9**:434 doi:10.1186/1556-276X-9-434

The electronic version of this article is the complete one and can be found online at:http://www.nanoscalereslett.com/content/9/1/434

Received: 10 July 2014
Accepted: 21 August 2014
Published: 27 August 2014